# *Electrical characterization of alpha-particle irradiation-induced defects in germanium*

**Abraham Willem Barnard**

**Submitted in partial fulfilment of the requirements for the degree of Magister Scientiae**

**in the**

**Faculty of Natural and Agricultural Sciences**

**Department of Physics**

**University of Pretoria**

**August 2017**

**Supervisor: Prof. W.E. Meyer**

**Co-supervisor: Prof. F.D. Auret**

*To my parents*

*“No one knows what the future holds. That’s why its potential is infinite” ~ Okabe Rintarou*

*“If we all reacted the same way, we’d be predictable and there’s always more than one way to view a situation… It’s simple: overspecialize and you breed in weakness. It’s slow death” ~ Major Motoko Kusanagi*

*“Do what I do. Hold tight and pretend it’s a plan” ~ The Doctor*

*“Don’t waste your time looking back, you’re not going that way ”~Ragnar Lothbrok*

*“A lesson without pain is meaningless. For you cannot gain something without sacrificing something else in return, but once you have overcome it and made it your own…you will gain an irreplaceable fullmetal heart ”~Edward Elric*

# Declaration of Authorship

I, Abraham Willem Barnard, declare this dissertation, which I hereby submit for the degree Magister Scientiae is my original work and has not been submitted by me for any degree at this or another institution.

Signed:_______________________________________________

Date:_________________________________________________

# Acknowledgements

I would like to thank my friends during the time this thesis was written. Without you guys I would have finished this last year.

I would like to thank my supervisor Walter Ernst Meyer for his guidance and expertise in the experimentation field to become one step closer to being true scientist.

I would like to thank my co-supervisor Francois Danie Auret for giving me the opportunity to shadow him in obtaining unique skills in the experimentation field.

# Summary

Recent advances in semiconductor growth techniques have led to the production of high quality Ge that plays a vital role in the fabrication of electrical devices. Germanium (Ge) is mainly used as a detector material being highly sensitive to X-rays, gamma rays and ionizing radiation, and also shows promise for high speed applications. However, the performance of the devices is strongly influenced by radiation damage. Antimony (Sb), being one of the most common dopants in Ge semiconductor devices, forms the well-known Sb-vacancy complex, also known as the E-center, when the fabricated device is exposed to high energy particle radiation.

In this study, the defects induced by high energy alpha-particle irradiation were investigated by means of deep level transient spectroscopy (DLTS). Previous studies found that the DLTS peak traditionally ascribed to the E-center anneals out in two steps, with the first step at room temperature and the second at about 390 K. Possible explanations in the literature for this behavior include interstitials being released by other defects annealing out reacting with the Sb-vacancy. In this study, we have shown that, contrary to previous theories, the DLTS peak that was assigned to the E-center consists of two peaks relating to two defects of similar nature. The peaks were resolved using two techniques: Laplace-DLTS with manual input of regularization parameters and a technique referred to as *subtraction of transients*. It was found that the peak annealing at high temperatures corresponded to the well-known E-center while the peak annealing at lower temperatures was a new defect which was denoted the E'.

Using these techniques, it was shown that, although the two defects had very similar emission characteristics (DLTS signatures: E-center was determined to have an ionization enthalpy of 0.0370±0.005 eV with an apparent capture cross section of $7.9 \times 10^{-15}$ cm$^2$ while the corresponding values for the E' were 0.0375±0.005 eV and $6.2 \times 10^{-15}$ cm$^2$). Other properties of the defects differed significantly, for instance the true capture cross sections at $T \rightarrow \infty$ were $2.2 \times 10^{-15}$ cm$^2$ and $1.0 \times 10^{-13}$ cm$^2$ respectively and the capture barriers were 0.043 eV and 0.092 eV. The annealing activation energy of the E-center was 1.05 eV and that of the E' was 0.73 eV with frequency factors of $2.5 \times 10^9$ s$^{-1}$ and $2.7 \times 10^8$ s$^{-1}$ respectively.

Furthermore, the study showed that the defects had significantly different introduction kinetics, mainly a linear introduction rate for the E-center and the E' introduced quadratically and being dependent on the introduction and presence of another defect.

It is believed that the evidence presented in this study provides conclusive proof for the existence of an up to now unobserved defect in Ge which has up to now been confused with the well-known E-center.

# Contents

**1 INTRODUCTION ........ 1**
1.1 GE VERSUS SI ........ 1
1.2 GE CRYSTAL STRUCTURE AND GROWTH ........ 2
1.3 APPLICATION ........ 3
1.4 SB-VACANCY (E-CENTRE) ........ 3
1.5 DISSERTATION LAYOUT ........ 4
**2 BACKGROUND THEORY ........ 5**
2.1 SEMICONDUCTOR DEFECTS ........ 5
*2.1.1 Point, line, plane and bulk defects ........ 5*
*2.1.2 Deep- and shallow-level defects ........ 7*
*2.1.3 Radiation induced defects in Ge ........ 8*
2.2 METAL-SEMICONDUCTOR INTERFACE ........ 10
*2.2.1 The ideal case ........ 10*
*2.2.2 Reverse and forward bias ........ 12*
2.3 DEEP-LEVEL TRANSIENT SPECTROSCOPY ........ 13
*2.3.1 Capacitance signal generation ........ 14*
*2.3.2 DLTS signal processing ........ 17*
*2.3.3 Laplace DLTS (L-DLTS) ........ 19*
2.4 ARRHENIUS' LAW ........ 19
*2.4.1 Annealing activation energy ........ 20*
*2.4.2 Activation energy for electron emission ........ 21*
*2.4.3 Capture cross-section ........ 21*
2.5 DEPTH PROFILES ........ 23
2.6 INTRODUCTION KINETICS ........ 26
**3 EXPERIMENTAL TECHNIQUES ........ 31**
3.1 SCHOTTKY DEVICE FABRICATION ........ 31
*3.1.1 Germanium ........ 31*
*3.1.2 Silicon ........ 32*
*3.1.3 Resistive thermal evaporation (RTE) ........ 32*
3.2 MEASUREMENT EQUIPMENT AND TECHNIQUES ........ 33
*3.2.1 Investigating closely spaced peaks by means of L-DLTS ........ 33*
*3.2.2 DLTS setup ........ 40*
3.3 CV CHARACTERIZATION ........ 41
*3.3.1 Free carrier concentration ........ 41*
3.4 DLTS CHARACTERIZATION ........ 41
*3.4.1 Concentration ........ 41*
*3.4.2 Annealing profiles ........ 42*
*3.4.3 Annealing kinetics ........ 42*
*3.4.4 Introduction profiles ........ 43*
*3.4.5 Conventional DLTS ........ 44*

*3.4.6 Depth profiles* ... *44*
*3.4.7 Depth profiles of samples annealed under reverse and zero bias* ... *44*
*3.4.8 Determining the activation energy and apparent capture cross-section (finger print)* ... *45*
*3.4.9 True capture cross-section* ... *45*
**4 EXPERIMENTAL RESULTS** ... **47**
4.1 INTRODUCTION ... 47
*4.1.1 Previous investigations of E and E'* ... *47*
*4.1.2 Vacancies induced by alpha particle irradiation* ... *47*
4.2 RESULTS ... 48
*4.2.1 Free carrier density* ... *48*
*4.2.2 Annealing profiles* ... *48*
*4.2.3 Conventional DLTS* ... *50*
*4.2.4 Annealing activation energy* ... *50*
*4.2.5 Introduction profiles* ... *52*
*4.2.6 Depth profile* ... *52*
*4.2.7 Activation energy & apparent capture cross-section ("DLTS finger print")* ... *53*
*4.2.8 True capture cross-section* ... *54*
*4.2.9 E' in Si* ... *56*
**5 CONCLUSION** ... **87**
5.1 SUMMARY ... 87
5.2 FUTURE RESEARCH ... 89
**6 REFERENCES** ... **91**

# List of Tables

Table 5.1: Summary of electrical properties obtained through experimentation. .......................................88

# List of Figures

Figure 1.1: Model of a cubic unit cell of Ge showing the crystal structure (Barron and Smith, 2008)........ 2

Figure 2.1: Simple illustration of different point defects found in semiconductor crystals (Kopeliovich, 2012)........................................................................................................................... 6

Figure 2.2: Simple diagrams representing (left) edge dislocation and (right) screw dislocation (de Juan, Cortijo and Vozmediano, 2010). ......................................................................................... 7

Figure 2.3: A model of the development of vacancy paths and clusters due to high energy particles. (Top right) Model of atomic displacement in a crystal lattice (Meroli, 2012). .......................................... 9

Figure 2.4: The formation of the Schottky barrier between a metal contact and n-type semiconductor. In (A) the metal and semiconductor are isolated in vacuum conditions. In (B) they are electrically connected. In (C) they are separated by a narrow gap. In (D) they are in perfect contact with each other. (Montanari, 2005)......................................................................................................... 11

Figure 2.5: The Schottky barrier between a metal and n-type semiconductor in perfect contact with each other and place under (A) reverse bias and (B) forward bias (Montanari, 2005). ........................... 13

Figure 2.6: Diagram representing the different simple devices that generate a capacitance signal used in DLTS (Silvaco, 2014)............................................................................................................. 15

Figure 2.7: The basic procedure of a DLTS cycle and process of obtaining a DLTS spectrum as a function of temperature................................................................................................................. 17

Figure 2.8: Left: Capacitance transients with change in temperature. Right: Signal obtained from transients (Wei, 2015)........................................................................................................................ 18

Figure 2.9: Diagram showing (a) DLTS spectra with different rate window conditions and (b) the Arrhenius obtained from the maxima ................................................................................................. 21

Figure 2.10: The effect of changing the filling pulse width on the DLTS spectrum as would be required for the determination of the capture cross-section..................................................................... 22

Figure 2.11: (a) Energy band diagram for a Schottky diode under a quiescent reverse bias. (b) Solid line shows the corresponding charge distribution and dashed lines show the charge distribution right after the pulse which relaxes back to the solid line (Drawn after Zohta and Watanabe, 1982). ............... 25

Figure 2.12: DLTS transient obtained during depth profiling. From left to right we have the pulse applied to the Schottky diode, its corresponding depletion width being filled and the signal obtained through DLTS and L-DLTS measurments.......................................................................................... 26

Figure 2.13 Simulations of Equations 2.42 (Defect 1 with linear introduction rate) and 2.46 (Defect 2 with introduction rate linearly dependent on that of defect 2) with the expected summation that would be observed. Defect 1 would exhibit a linear introduction and Defect 2 would exhibit a quadratic growth. ......................................................................................................................................... 28

Figure 2.14 Simulations of equations 2.48 and 2.49 with the expected summation that would be observed. Defect 1 would exhibit an exponential rise to a maxima while Defect 2 would initially exhibit exponential growth before transforming into a linear introduction. ....29

Figure 3.1: Schematic diagram of the resistive evaporation setup used to deposit AuSb ohmic and Pd Schottky contacts. ....32

Figure 3.2: Top and side view of the fabricated metal-semiconductor devices. ....33

Figure 3.3: Measured capacitance transients spaced further than the resolution limit of L-DLTS (a) and the combined transient with their relative emission spectrums (b). ....36

Figure 3.4: (a) Two measured capacitance transients with emission rates 275 $s^{-1}$ and 380 $s^{-1}$, spaced closer than the usual resolution limit of L-DLTS and the summation of their capacitance transients. (b) L-DLTS spectra of the individual transients as well as the summed transient with and without manual input of regularization parameters. ....37

Figure 3.5: The effect of manual input of Contin regularization parameters on the separation of the closely spaced peaks shown in Figure 3.4. ....38

Figure 3.6 Manuel input of contin regularization parameters for a single emission spectrum peak used in Figure 3.4. ....39

Figure 3.7: Block diagram of DLTS and L-DLTS experimental setup ....41

Figure 4.1: TRIM simulation of 100nm Pd on 200 µm Ge exposed to 15000 alpha particles with 5.4 MeV energy. ....48

Figure 4.2: C-V measurement of a Pd-Ge Schottky diode under a reverse bias of -5 V to -0.2 V ....49

Figure 4.3: Isochronal annealing profile of a DLTS peak corresponding to the E-centre of a sample irradiated at 270 K then immediately measured and annealed for 15 minute intervals with increasing 10 K steps (black dots). The same measurement performed on a sample that was left at room temperature for several weeks after irradiation, annealed for 15 minute annealing periods with increasing 25 K steps (red dots). ....49

Figure 4.4: Conventional DLTS after room temperature irradiation ....51

Figure 4.5: Conventional DLTS showing the isothermal annealing of defects first at 330 K and then at 425 K. ....51

Figure 4.6: Depth profiles of a 270 K alpha-particle irradiated sample subjected to 330 K isothermal annealing, first under a reverse bias of -3 V for 90 minutes and then later without any applied bias. ....53

Figure 4.7 Peak height versus the pulse width (filling pulse duration) at different temperatures of a sample irradiated at 273 K and then annealed at 330 K for 1 hour. ....55

Figure 4.8 Peak height versus the pulse width (filling pulse duration) at different temperatures of the E' obtained through the subtraction of transient method. ....55

Figure 4.9: Arrhenius obtained for the capture cross-section of the E-centre, E' and the combination of their emission rates. Dashed lines represent the confidence intervals for each true capture cross-section. ........ 56

# List of Abbreviations and Acronyms

| | |
|---|---|
| DLTS | Deep-level transient spectroscopy |
| L-DLTS | Laplace deep-level transient spectroscopy |
| SNR | Signal to noise ratio |
| CMOS | Complementary metal-oxide-semiconductor |
| MOS | Metal-oxide-semiconductor |
| MOSFET | Metal-oxide-semiconductor field-effect transistor |
| CV | Capacitance-Voltage |
| IV | Current-Voltage |
| SBD | Schottky barrier diode |
| RTE | Resistive thermal evaporation |

# 1 INTRODUCTION

Germanium (Ge), atomic number 32 and in Group IV on the periodic table, is seen as the grandfather of semiconductor materials that paved the road to semiconductor transistor and integrated circuit developments. The material was first discovered by Winkler in 1866, approximately 66 years after the discovery of silicon (Si) (Discovery of a New Element by Clemens Winkler, 1886). In 1948, the first point contact transistor was fabricated in Bell labs consisting of a Ge slab that had a plastic wedge pressing two gold foils into it. Since then the fabrication technique for transistors improved drastically and Ge was overtaken by Si in the semiconductor industry. This was mainly due to the ability of Si to form a stable oxide. However, due to the low effective masses of charge carriers in Ge, it has again been considered as an alternative to Si for complementary metal-oxide semiconductor (CMOS) devices and fast switching transistors (Claeys and Simoen, 2007).

## 1.1 Ge versus Si

Si is the most used semiconductor material in a USD 335 billion industry of today's society (Rosso, 2016). Ge has its pros and cons when comparing the electrical properties to that of Si. Ge has a small band gap of 0.66 eV compared to Si with a band gap of 1.12 eV. This allows Ge to absorb light with longer wavelengths in the infrared spectrum. Ge has the unfavourable property of low quality oxide formation ($GeO_2$) where Si easily forms a high quality surface layer of oxide ($SiO_2$). For Ge, a different oxide layer has to be grown in order to manufacture oxide related devices. Bulk and pure Ge cost approximately 120 USD and 360 USD per 100 g respectively. However, bulk and pure Si are much cheaper costing 0.14 USD and 5.4 USD per 100 g respectively (Stewart, 1996). This, with the easily formed oxide layer, lead to the choice of Si being used. The electron Hall mobility at 300 K, however, was found to be 3900 $\frac{cm^2}{Vs}$ for Ge and 1600 $\frac{cm^2}{Vs}$ for Si. The hole mobility at 300 K for Ge is 1900 $\frac{cm^2}{Vs}$ and for Si is 430 $\frac{cm^2}{Vs}$. This property alone makes Ge a possible competitor for fast switching devices. Due to its narrower band gap, Ge has a larger intrinsic carrier concentration than Si, approximately $10^{13}$ cm$^{-3}$ vs $10^{10}$ cm$^{-3}$ at 300 K (Palmer, 2014). This allows for a

much smaller forward voltage bias in a p-n junction. However, it results in a higher reverse bias leakage current and limits the maximum working temperature of devices.

## 1.2 Ge crystal structure and growth

The Ge crystal structure can be described as a tetrahedral crystal lattice. This structure is commonly referred to as the diamond structure: Two inter-penetrating face centred cubic lattices that are displaced along the body diagonal by a translation of $\frac{a_0}{4}(1,1,1)$ (Patterson and Bailey, 2010). The lattice parameter $a_o$ for Ge is 0.565791 nm with the distance to the nearest neighbouring atom being 0.245 nm.

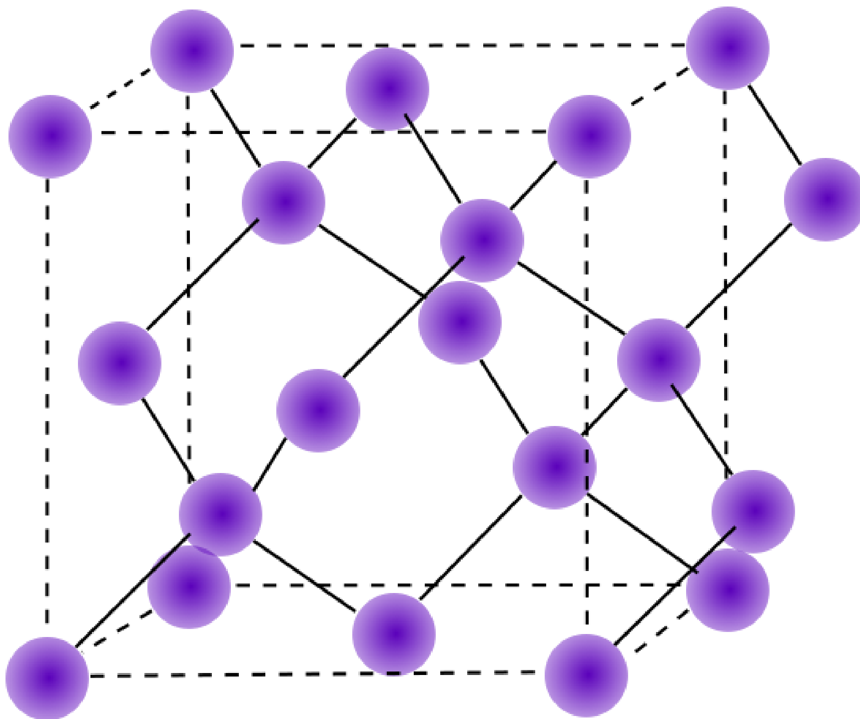

**Figure 1.1: Model of a cubic unit cell of Ge showing the crystal structure (Barron and Smith, 2008).**

Bulk semiconductor crystals are commonly obtained by slowly cooling molten material. However, this yields undesirable poly-crystalline material since crystals will grow in different orientations at different locations. There are two main methods of growing single bulk crystals, mainly Czochralski and Bridgman.

Production of Czochralski Ge requires high purity Ge melted in a crucible. Dopant impurities such as antimony, phosphor, arsenic or boron are added to the molten Ge to change it either into n-type or p-type material. A seed crystal that is specifically orientated is placed at the end of a rod that is dipped in the molten material. The seed crystal is then slowly pulled up from the molten material while being rotated. The temperature gradient and the speed at which it is rotated and pulled determines the size of the crystal (Nishinaga, 2015).

Bridgman-Stockbarger Ge single crystals are grown using a similar technique: It involves melting the material in a container with a seed crystal on the one side of the container. The material is then cooled from the one side of the container where the seed is located. This will form a single crystal with the same orientation as the seed. The process is either done vertically or horizontally while the crucible is rotated to stir the molten material (Scheel, Capper and Rudolph, 2011).

## 1.3 Application

Ge is generally used in the production of solid state electronics and in metallurgy. The wavelength of light associated with the bandgap energy is in the near infrared, which allows the production of current when light of this wavelength is shone on Ge diodes. These diodes are used as photo detectors to detect near-infrared light for telecommunications. Since germanium is transparent to infrared (IR) radiation absorbed by Si, Ge is often used to make IR lenses, which also filter out visible light (Moskalyk, 2004). For a single junction, Si will make a more efficient solar cell due to its larger band gap leading to a higher voltage output. However, in multi-junction solar cells, Ge is used as the bottom layer of a stack of solar cells. This allows the Ge to absorb the longer wavelengths of the infrared spectrum that passes through the upper layers. High purity Ge is mainly used in detectors for gamma radiation. Lithium doped Germanium detectors need to be cooled to 77 K during use to minimise leakage current, and need to be kept at low temperature for best stability, however in some cases, radiation damage may be annealed out by heating the detector for a few days. In crystal radios, the lower forward bias of Ge allows for greater signal and headphones to perform better than with Si. Due to the lower capacitance, Ge diodes can be used in radio frequency circuits with lower voltage needs.

## 1.4 Sb-vacancy (E-centre)

In many radiation induced environments where electronics are used, the electrical properties of semiconductors are constantly changing. The amount of change in their behaviour is highly dependent on the fluence and type of radiation they are exposed to. The main effect of radiation (alpha, beta, gamma, etc.) on the structure of the bulk of the semiconductor is the introduction of vacancies, electron hole pairs and charging effects (Iniewski, 2011). Ge doped with Sb shows the presence of $E_{0.37}$ (0.37 eV below the conduction band) after exposure to radiation. The introduction rate of this defect increases with Sb concentration. The peak was observed to anneal out in two stages shortly after irradiation. A minor fraction of this peak first anneals out at room temperature after which the concentration remains essentially constant. The majority of the peak, however, anneals out at approximately 400 K. This majority peak was identified to be a vacancy captured by a Sb substitutional defect. The minor fraction annealing out at room temperature was initially believed to be due to the release of interstitial atoms caused by the dissociation of interstitial complexes that combined with the trapped vacancy (Fage-Pedersen, Larsen and Mesli, 2000). However, in this study, it is shown that it is actually a second defect, which is named the E' in this thesis. The electrical

properties of this E’ are described in Chapter 4 of this paper. The properties will be compared to those of the Sb-vacancy complex the hope of identifying the defect itself.

## 1.5 Dissertation layout

- Chapter 2 will cover the background theory on the formation of the Schottky diode for the ideal case. The relevant theory for characterization of the electrical properties of traps near the junction of the Schottky diode for experimental practices are summarized.
- Chapter 3 will discuss the experimental techniques used for the characterization of the electrical properties with their relevant conditions used for identification of the E-centre and E’ properties.
- Chapter 4 will present and discuss the results obtained.
- Chapter 5 will conclude the study and describe future work.

# 2 BACKGROUND THEORY

The formation of a potential barrier occurs at the interface of a metal in contact with a semiconductor material when the work function of the metal is greater than the electron affinity of the n-type semiconductor material. The potential barrier forms for p-type material under the opposite conditions. Defects introduced in the semiconductor change the performance of these devices, especially on smaller scales. Laplace DLTS (L-DLTS) is used to determine the electrical characteristics of defects in semiconductors. This chapter explains the formation of metal-semiconductor junctions for the ideal case with a brief introduction on the types of defects found in semiconductors. A brief explanation of DLTS and the improved technique of high resolution L-DLTS is also covered.

## 2.1 Semiconductor defects

Imperfections in crystal lattices such as a missing, additional, misplaced or foreign atom causing a discontinuity in the lattice repetition are known as defects. These defects are introduced either during the growth of the semiconductor material or during fabrication of devices. Defects change the local electrical properties of the material. These changes often cause energy states in the band gap of the semiconductor.

### 2.1.1 Point, line, plane and bulk defects

A point defect can be described as any local modification to the crystal matrix that results in a deviation from the lattice periodicity (Lannoo and Bourgoin, 1981). These defects are formed either by introducing foreign atoms into the lattice or by removing atoms that are in fixed lattice positions.

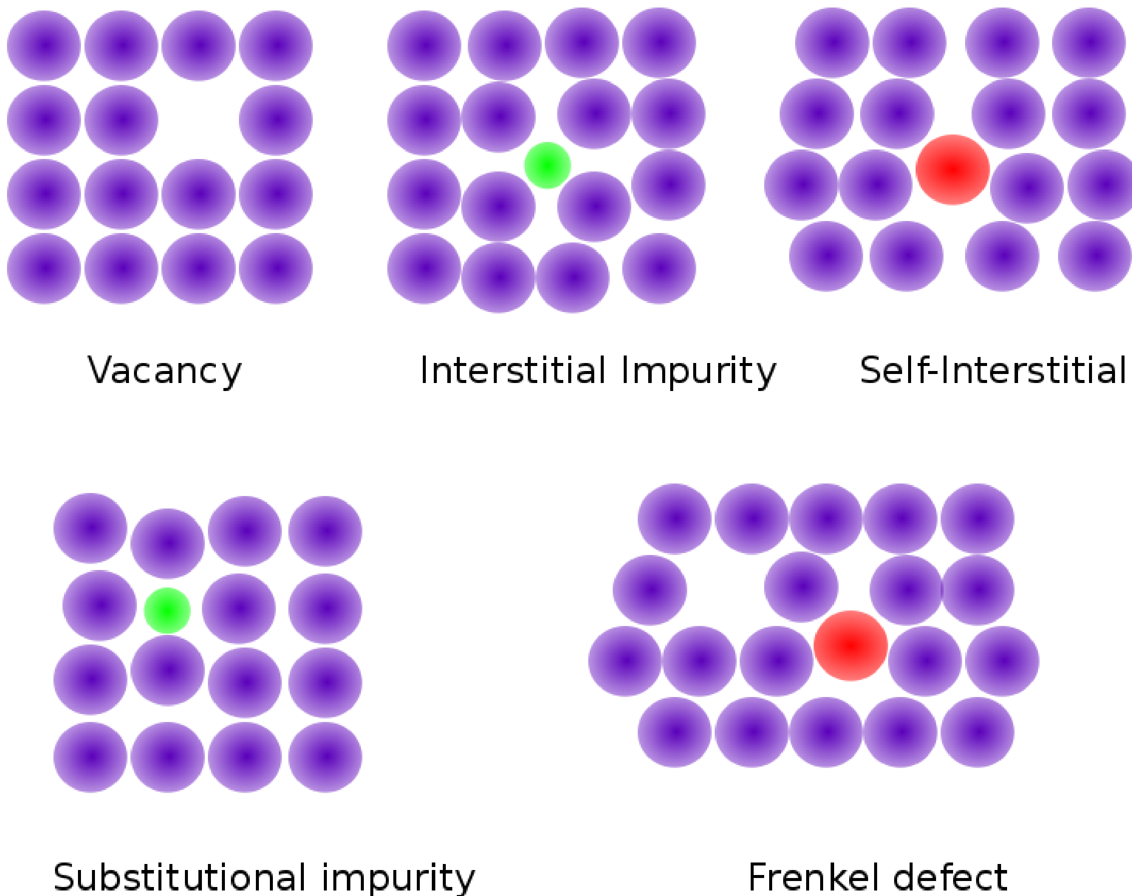


**Figure 2.1: Simple illustration of different point defects found in semiconductor crystals (Kopeliovich, 2012).**

The simplest point defects are shown in Fig 2.1 and summarized below:

- **Vacancy** – A site in a crystal lattice position that has a missing atom.
- **Interstitial impurity** – A foreign atom occupying a site where an atom would not normally appear.
- **Self-interstitial** – A crystal lattice atom occupying a site where an atom would normally not appear.
- **Substitutional impurity** – A foreign atom occupying a crystal lattice position.
- **Frenkel defect** – A vacancy near a self-interstitial defect, usually the one responsible for creating the vacancy site.

Line (one-dimensional) defects are present when there is an entire row of lattice points deviating from the perfect arrangement (de Juan, Cortijo and Vozmediano, 2010). Dislocations are generally caused by applying stress. There are two main types of dislocations, mainly screw dislocation and edge dislocation.

- **Edge dislocation** – Half a plane of atoms are inserted into the uniform crystal lattice.

- **Screw dislocation** – This is formed when one part of the crystal lattice undergoes shearing and is shifted relative to the other part of the lattice. Around the dislocation line, the atomic planes form a spiral surface.

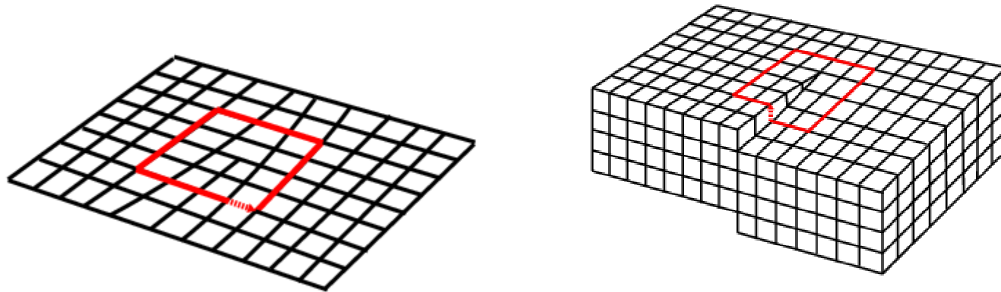

**Figure 2.2: Simple diagrams representing (left) edge dislocation and (right) screw dislocation (de Juan, Cortijo and Vozmediano, 2010).**

A planar (two-dimensional) defect is formed when there is a distortion across a plane in a perfect crystal. This defect can take the form of a grain boundary or stacking fault (Williams and Carter, 2009).

- **Grain boundary** – This is the formation of a boundary between two crystal grains. This can be seen as the rotation about a specific axis of one of the crystal lattices. Depending on the axis rotation direction this can be either tilt boundary or twist boundary. Tilt boundary is the rotation around the axis, parallel to the boundary plane and twist boundary is the rotation around the axis, perpendicular to the boundary plane.
- **Stacking** – This is a distortion in the stacking sequence and can either form a stacking fault or a twin region. A stacking fault is a deviation of the stacking sequence, for example ABABCABAB. A twin boundary is the formation of mirrored symmetric stacking in the sequence, for example ABCABCBACBA.

Bulk (three-dimensional) defects are volume distortions in the crystal lattice. These can be pores, inclusions, cracks, voids or precipitates. Voids could be considered as clusters of vacancies and precipitates are clusters of impurities.

## 2.1.2 Deep- and shallow-level defects

The electronic properties of semiconductors are controlled by introducing impurity atoms to make the semiconductor conducting or be a conducting type (n-type or p-type). The impurities are introduced via a process known as doping or ion implantation. The levels induced by these defects are classified as either deep or shallow depending on the localisation of their wave functions and not necessarily their energy. Shallow defects have energy states close to the band edges, the wave function associated with the level is

not localised (usually spread out over several lattice parameters) and the defect is usually well described by the hydrogen model. States caused by deep-level defects are much more localised and are usually deeper in the valence band. Traps will capture either a hole or an electron.

Shallow levels are easily ionised by thermal energy to release carriers into the semiconductor. To form n-type material, the material is doped with donors atoms, which "donate" electrons to the conduction band leaving a positively charged ionized donor. In Group IV semiconductors, these are usually Group V elements. To form p-type material, the opposite is done, i.e. the material is doped with acceptor atoms, which introduces "holes" in the valance band.

Deep-level defects usually bind electrons more strongly and interfere with electrical transport and other electrical properties of semiconductors. They also act as recombination centres allowing holes and electrons to recombine, thereby decreasing minority carrier lifetime and increasing the noise in transistors and photodiodes (Poole, 2004).

### 2.1.3 Radiation induced defects in Ge

High energy particles, commonly referred to as radiation, induces damage in semiconductor materials introducing various defects. The minimum energy required to displace an atom in a crystal lattice to form a stable Frenkel pair is known as the threshold displacement energy $E_D$. For Ge, the average threshold energy for formation of Frenkel pairs over all lattice directions was calculated to be 23±5 eV using density functional theory. The threshold energies for <100> and <111> were found to be 19.5±1.5 eV and 11.5±1.5 eV respectively (Holmström, Nordlund and Kuronen, 2010). When high energy particles transfer energy greater than the threshold energy during a collision, it may result in the formation of a single vacancy-interstitial (Frenkel) pair. If the Ge atom receives enough energy, it can collide with other Ge lattice atoms and produce another vacancy. Most Frenkel pairs are closely situated allowing many of them to repair. These regions of disorder are known as defect clusters which have a high local defect density. The properties of semiconductor devices tend to be more critically affected by the clusters than by point defects.

Kinchin and Pease (1955) derived an estimate on the number of atoms displaced $N(E)$ in a solid as

$$N(E) = \frac{E}{2E_D} \tag{2.1}$$

where $E$ is the ion energy. This holds for both equal and unequal masses of both the ion and lattice atoms. It was pointed out by Sigmund that the assumptions for hard-sphere scattering and elastic collisions can be eliminated. The equation is then modified to be

$$N(E) = \frac{\xi\, V(E)}{2\, E_D} \tag{2.2}$$

where depending on the form of the scattering potential, $\xi$ is a factor less than 1 and energy not lost to electron excitation is $\boldsymbol{V}(E)$. It was calculated by Sigmund that $\xi$ is ~0.8.

Sigmund (2006) calculated the upper limit of the number of displaced atoms by neglecting the loss of defects by replacement collisions and using a power-law approximation to the Thomas-Fermi cross-section:

$$N(E) = \frac{6E}{\pi^2 U} ln\left(1 + \frac{U}{E_D}\right). \tag{2.3}$$

When an atom leaves a lattice site, the binding energy lost is given by $U$. The displacement model given by Bauerlin (1962) shows $E_D = 4E_b$ where $E_b$ is the bond energy. If $U = E_D$, Equation 2.3 will then reduce to

$$N(E) = \frac{0.42\, E}{E_D} \tag{2.4}$$

which is similar to Equation 2.1. However, this is based on the fact that each displaced atom has to break four bonds. When one considers the cluster regions they will break on average only two bonds which raises $N(E)$ by a factor of 2. The number of displaced atoms is linearly proportional to the energy of the incident particle regardless of the theoretical approach (Mayer, 1970).

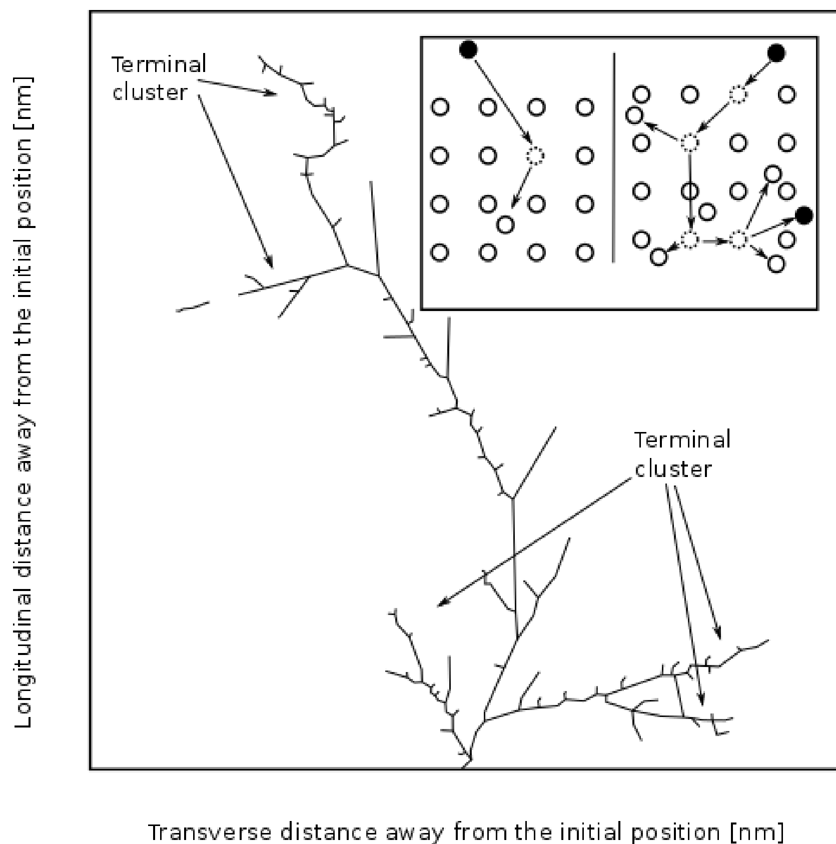


**Figure 2.3: A model of the development of vacancy paths and clusters due to high energy particles. (Top right) Model of atomic displacement in a crystal lattice (Meroli, 2012).**

## 2.2 Metal-semiconductor interface

The Schottky model describes the formation of a potential barrier at the interface between a metal and a semiconductor. The rectifying properties of metal-semiconductor junctions are classified as either ohmic or Schottky. Schottky contacts are rectifying contacts which allow current flow in one direction only while ohmic contacts are non-rectifying contacts that allow current flow freely in both directions. Only the case for n-type semiconductor will be discussed. The formation of the potential barrier in *p*-type occurs similarly (Schroder, 2006).

### 2.2.1 The ideal case

A potential barrier is formed when a metal comes into contact with a semiconductor material at the interface of these two materials. In the case of the formation of a potential barrier for n-type semiconductor material, the Fermi level of the metal is lower than the Fermi level of the corresponding semiconductor. In Figure 2.4 diagram (A), the electrically neutral, isolated metal and semiconductor energy-band diagram is shown. In isolation, the Fermi level positions ($E_F$) of the metal and semiconductor are generally different. Here $e\phi_m$ represents the metal work function, $e\phi_s$ the work function of the semiconductor and $e\chi_s$ the electron affinity of the semiconductor with $e$ as the electronic charge. The electron affinity is the amount of energy released when an electron is added to the material which is the difference between the energy levels of the conduction band ($E_C$) and the vacuum level (the energy of an electron at rest just outside the surface of the material). The work function is the minimum amount of energy required to remove an electron from a material which is the difference between the Fermi level and vacuum level. $E_V$ represents the top of the valence band and $E_C$ the bottom of the conduction band (Sze and Kwong, 2006). In the case depicted in Figure 2.4, the work function of the metal is greater than the electron affinity of the semiconductor, which leads to the formation of a Schottky contact.

Now suppose we electrically connect the metal and the semiconductor with a thin wire. Instantaneously after the connection is made between the two materials, electrons will start to flow from the semiconductor to the metal due to the difference in Fermi-level. As the electrons flow from the metal, the electrostatic potential of the metal lowers, i.e. the electron potential energy increases, therefore all the energy levels are raised. Due to the transfer of electrons there is a negative charge build up on the surface of the metal and a positive charge on the semiconductor surface. The positive charge of the semiconductor is the result of donor atoms with a lack of electrons. Since there is a finite concentration of donors, this region devoid of electrons, called the depletion region, stretches up to a significant depth below the surface of the semiconductor. In contrast, the metal can easily accommodate a very high concentration of electrons, and the charge concentration on the metal is effectively limited to the surface.

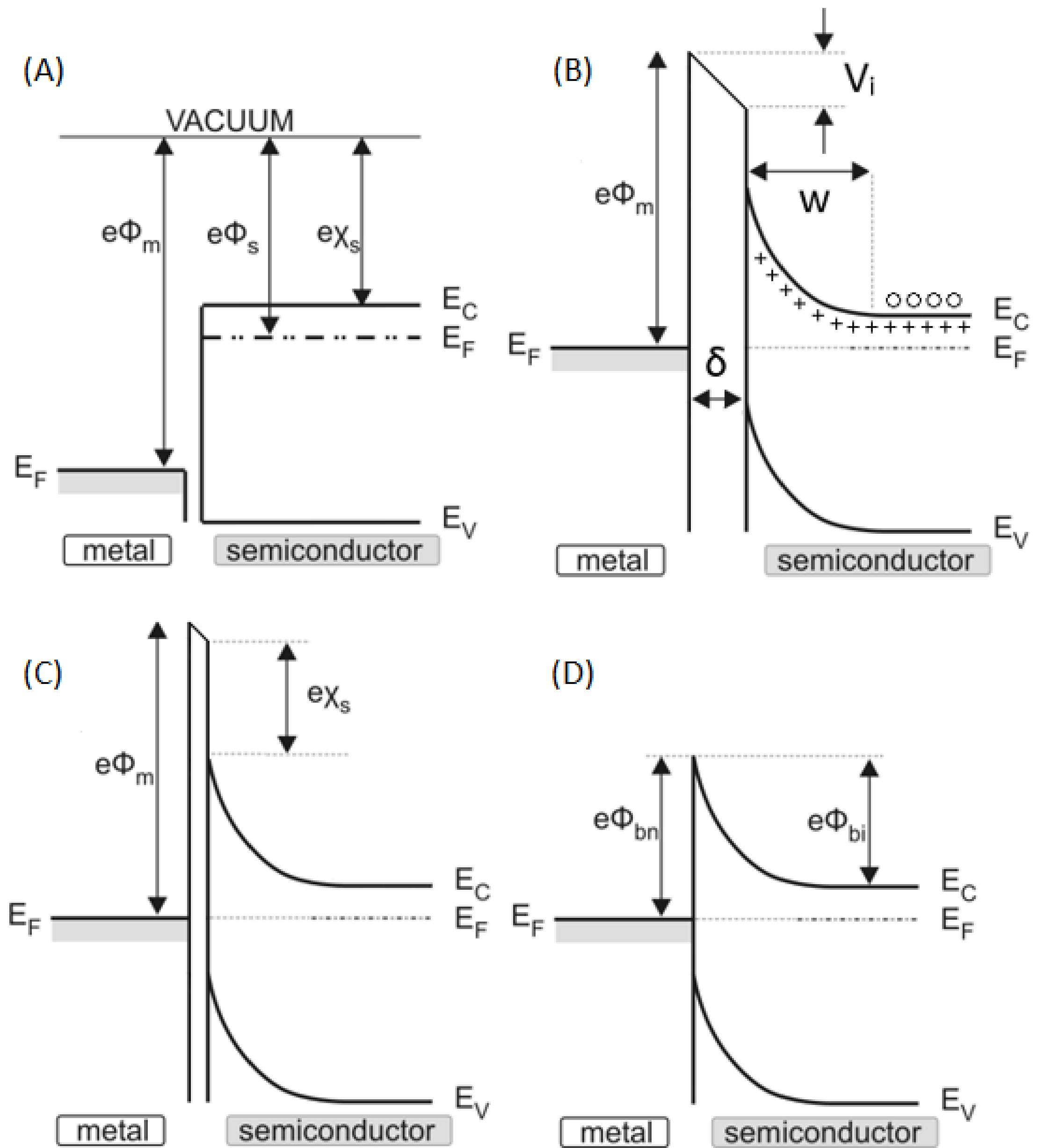


**Figure 2.4: The formation of the Schottky barrier between a metal contact and n-type semiconductor. In (A) the metal and semiconductor are isolated in vacuum conditions. In (B) they are electrically connected. In (C) they are separated by a narrow gap. In (D) they are in perfect contact with each other. (Montanari, 2005).**

This build-up of charges continues until the Fermi levels in the two materials are equal and causes an electric field in the gap ($\delta$ is the distance between the metal and semiconductor) between the two materials due to the vacuum levels not being the same anymore. The field causes the formation of a depletion region with width *w* which can be seen in Figure 2.4 (B). This is due to the electrons in the conduction band of the semiconductor being repelled by the field.

In Figure 2.4 (C), $V_i$ represents the electrostatic potential difference between the surfaces of the two materials (difference between the two vacuum levels). If the gap between the metal and the semiconductor decreases, it results in an increase in the electric field in the gap, but the electric field remains finite. The energy difference between the two vacuum levels thus decreases which can be seen from

$$E = q\Delta V. \tag{2.5}$$

When the two bodies are almost in contact, ($\Delta V$ is practically zero) there is a very thin potential barrier separating the two surfaces. This barrier is thin enough for electrons to easily pass through it by means of tunnelling.

When ideal contact is made as seen in Figure 2.4 (D) (i.e $\delta = 0$) the barrier due to the vacuum is completely disregarded and the electrons will only experience the potential barrier due to the bending of the bands. The potential barrier is then equal to the difference between the metal work function and the semiconductor electron infinity which is given as

$$e\phi_b = e(\phi_m - \chi_s). \tag{2.6}$$

The diffusion potential, which is the barrier height relative to the conduction band in the neutral semiconductor, is given by

$$\phi_{bi} = \phi_b - (\phi_s - \chi_s) \tag{2.7}$$

when no bias is applied to the system (Sze and Kwong, 2006).

## 2.2.2 Reverse and forward bias

When no bias is applied, the system will be in a dynamic equilibrium where the rate at which electrons transfer from the semiconductor to the metal is equal to the rate of electrons transferring from the metal to the semiconductor. If we now place the Schottky contact under reverse bias (i.e. a voltage is applied to the system with semiconductor positive and the metal negative) the Fermi level of the semiconductor is lowered relative to the metal. We can see from Figure 2.5 (A) that there is a further bending of the conduction and valance bands which shows an increased barrier height experienced by the electrons in the semiconductor. The barrier height experienced by the electrons in the metal is unaltered by the effects of the biasing. The energy distribution of electrons in the conduction band of the semiconductor may be assumed to follow Boltzmann's law and only electrons with sufficient energy will be able to transfer from the semiconductor to the metal. This means the net number of electrons transferring to the metal will steadily decrease with increased applied reverse bias. The net number of electrons transferring to the semiconductor remains the same. This results in a net current flow of electrons from the metal to the semiconductor.

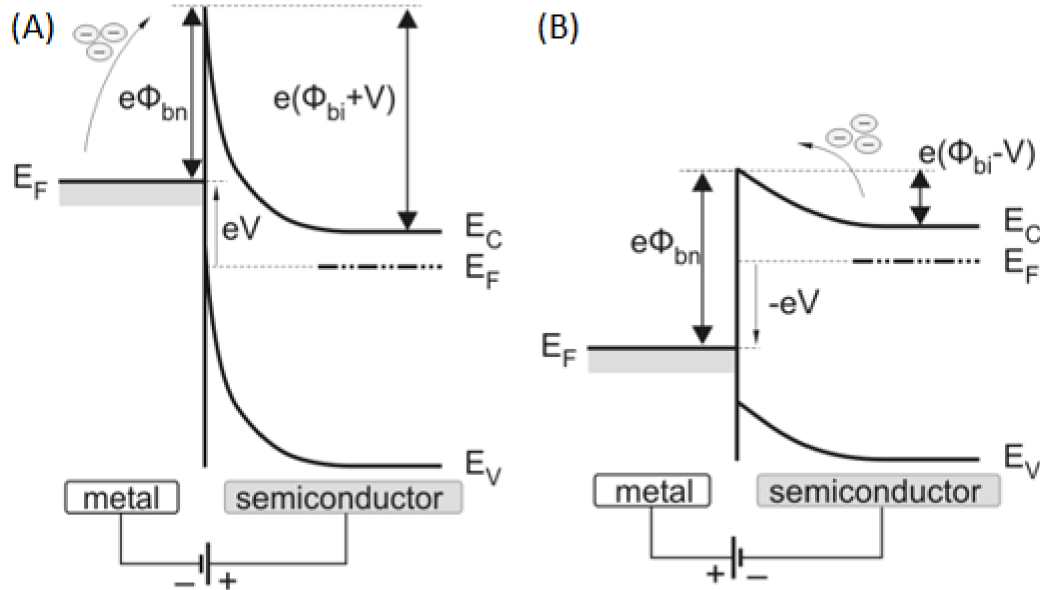


**Figure 2.5: The Schottky barrier between a metal and n-type semiconductor in perfect contact with each other and place under (A) reverse bias and (B) forward bias (Montanari, 2005).**

The magnitude of the reverse bias applied is limited as a dielectric breakdown will occur when the maximum field in the semiconductor is surpassed. This reverse bias is known as the break down voltage, which is the largest reverse voltage that may be applied to the system without it experiencing an exponential increase in the current flow. This can cause irreversible damage to the diode and degrade the rectification properties of the Schottky barrier.

When the system is placed under forward bias (i.e. a voltage is applied to the diode with the semiconductor negative and the metal positive) the Fermi level of the semiconductor shifts to a higher position relative to the metal. The barrier experienced by the electrons in the metal remains unaltered and therefore does not affect the net flow of electrons into the semiconductor. The electrons in the semiconductor experience a smaller barrier allowing a greater net flow into the metal. The barrier in the semiconductor decreases with increasing forward bias resulting in a rapidly increasing net flow of electrons from the semiconductor into the metal with increasing bias (Streetman, 1990).

## 2.3 Deep-level transient spectroscopy

DLTS is an experimental technique that measures the capacitance of a Schottky diode, p-n junction or metal oxide semiconductor (MOS) junction to characterise deep level impurities in semiconductors. This technique was introduced by D.V. Lang in 1974 as a high frequency (megahertz) capacitance transient thermal scanning technique. The capacitance of the junction is used to observe the change in the charge state of a deep level. This technique is able to distinguish between minority and majority carrier traps. Using this technique it is possible to establish the concentration, energy, capture rates and other fundamental

parameters of defects in the material. The ionisation enthalpy and the apparent capture cross section of the defect are referred to as the "finger prints" of a defect, and are used in identifying the defects.

### 2.3.1 Capacitance signal generation

The technique can be applied to any Schottky device, p-n junction device or a MOS device. In Figure 2.6 a simple circuit diagram is shown for measuring these different devices and where their depletion region would typically lie. A similar emmission transient is observed for all three devices.

When changing the voltage across the metal-semiconductor junction it results in a corresponding change in the width of the depletion region. As the depletion width changes, the capacitance observed changes similarly as described in Section 2.2.2. This change in width results in a change in capacitance due to the number of free carriers changing on both sides of the junction. This change is due to junction and diffusion capacitance. Junction capacitance, dominant under reverse bias conditions, contributes to this change due to the change in the depletion width. Diffusion capacitance, dominant under forward bias conditions, contributes to the change due to the change in minority carrier concentrations.

Consider a junction formed by a metal and n-type semiconductor material. When the system is in a steady state there is no net flow of electrons between the two materials and within the depletion region the hole and electron densities are negligible. The relationship between the density of filled traps $n_T$ and total density of deep states $N_T$ has been determined to be

$$e_p n_T = (e_n + e_p) N_T \tag{2.8}$$

where $e_n$ is the electron emission rate and $e_p$ is the hole emission rate (Shockley and Reed, 1952). This can be rewritten in terms of the density of filled traps under a steady state.

$$n_T = \left(\frac{e_n + e_p}{e_p}\right) N_T \tag{2.9}$$

If we now disturb the system, the total charge of the depletion region either increases or decreases resulting in a change in the capacitance.

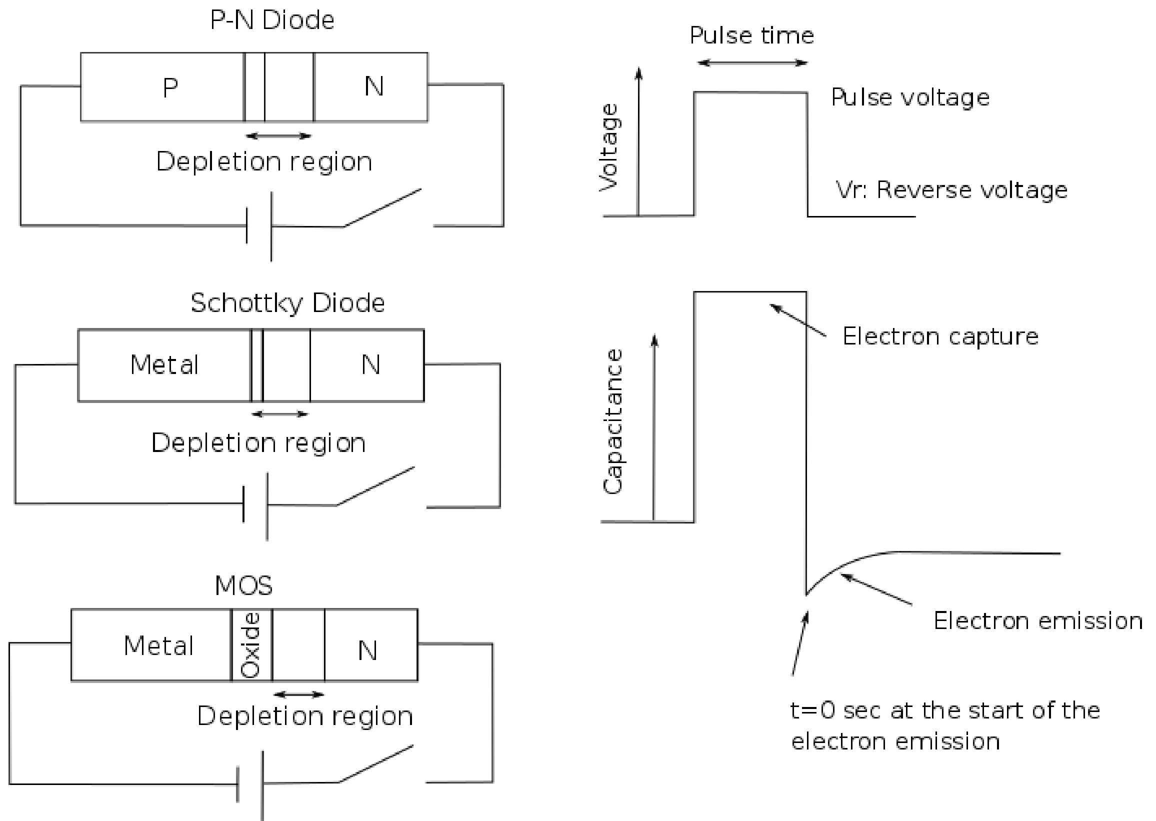


**Figure 2.6: Diagram representing the different simple devices that generate a capacitance signal used in DLTS (Silvaco, 2014).**

The DLTS scan cycle for obtaining the capacitance transient is shown in Figure 2.7. The Schottky as seen in Figure 2.7(a) is in an inactive state under a reverse bias $V_R$. The traps in the depletion region are assumed to be empty during this time. In Figure 2.7(b) a filling pulse (majority carrier pulse) is used to reduce the reverse bias to zero causing the depletion width to decrease and allowing electrons to be captured by the deep levels. If the re-emission of electrons is neglected, the rate of density of traps being filled can be written as

$$\frac{dn_T}{dt} = c_n(N_T - n_T) \tag{2.10}$$

where $c_n$ denotes the capture time constant of the defect for electrons. If the time of the filling pulse being applied is long enough$\left(t \gg \frac{1}{c_n}\right)$, then all the traps will be filled and $n_T = N_T$.

The bias is then restored to its former level, as seen in Figure 2.7(c) which results in a sharp drop in the capacitance to a minimum value caused by the electrons trapped in the depletion region. Since the system is put back into a steady state under a reverse bias of $V_R$, the traps start thermally emitting the trapped electrons and $n_T$ varies with time. The rate of density of traps emitting electrons can then be written as:

$$\frac{dn_T}{dt} = e_p N_T - (e_n + e_p) n_T. \tag{2.11}$$

The solution of this is given by

$$n_T(t) = \frac{e_p}{e_n + e_p} N_T + \frac{e_n}{e_n + e_p} N_T e^{-(e_n + e_p)t}, \qquad t \geq 0. \tag{2.12}$$

The density of filled traps thus decrease exponentially with a time constant:

$$\tau = \frac{1}{e_n + e_p}. \tag{2.13}$$

If we consider the case for an electron emitting centre i.e. $e_n \gg e_p$, the solution reduces to

$$n_T(t) = N_T e^{(-e_n t)}. \tag{2.14}$$

The amplitude of the transient will give a measure of the trap concentration. The emission rate of electrons is then described by the time constant:

$$\tau = \frac{1}{e_n}. \tag{2.15}$$

The capacitance of a Schottky diode can be considered to be the same as that of a parallel plate capacitor:

$$C = \frac{\varepsilon A}{w} \tag{2.16}$$

where *w* is the depletion width given by

$$w = \sqrt{\frac{2\varepsilon(V_b - V)}{q {N^*}_d}}. \tag{2.17}$$

Here $V$ is the applied bias, $V_b$ the built-in voltage, ε the permittivity of the semiconductor, A the junction area and ${N^*}_d = N_D - n_T$.

If we assume $n_T \ll N_D$, the width of the depletion region will not change much during the emission of the traps. In this situation the emission of carriers is described by the exponential decay function seen in Equation 2.14. The capacitance can then also be described as an exponential decay,

$$C(t) = C_\infty + \Delta C e^{-\lambda t}. \tag{2.18}$$

With some expansion from Equation 2.17 at a reverse bias $V_R$ one can get:

$$C(t) = C_0 - C_0 \frac{n_T}{2N_D} \tag{2.19}$$

where $C_0$ is the steady-state capacitance at bias $V_R$.

This is then rewritten as

$$C(t) = C_0 - C_0 \frac{N_T}{2N_D} e^{-\frac{t}{\tau}} \tag{2.20}$$

when the time variation of $n_T$ is taken into consideration. This shows that the concentration and emission rates can be determined from the observed change in capacitance due to a pulsing bias (Kosyachenko, 2015).

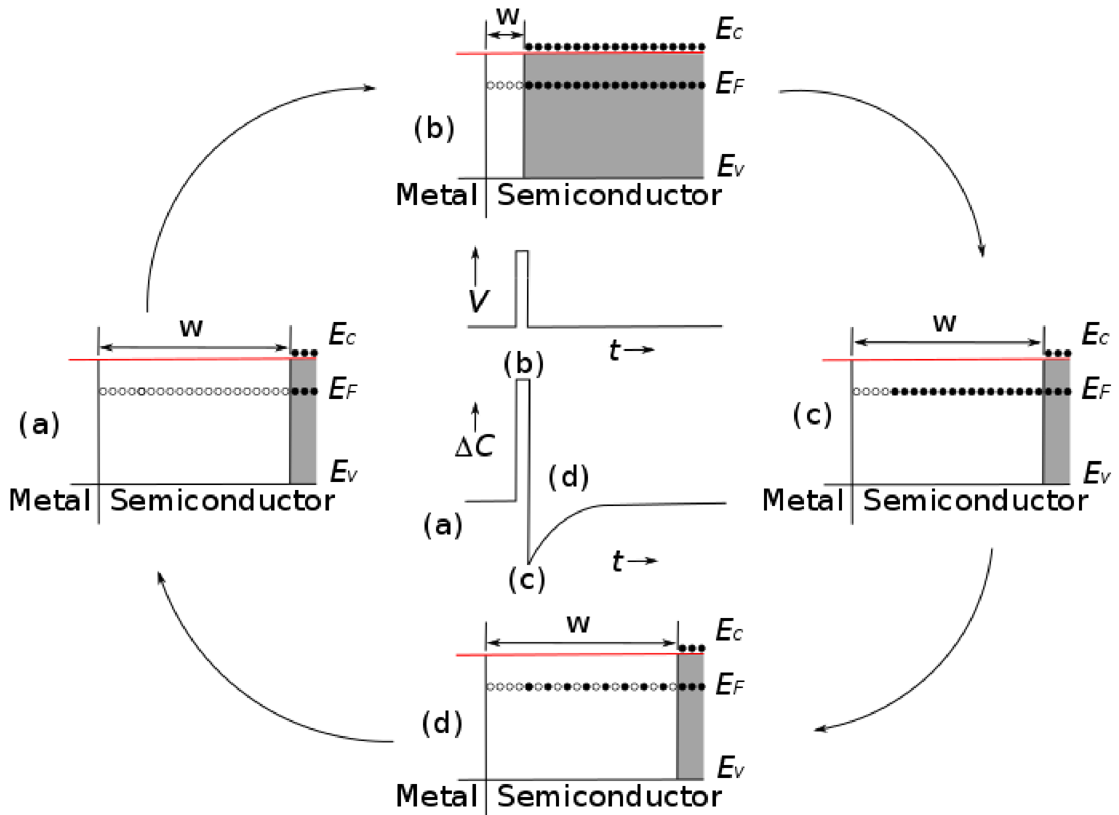


**Figure 2.7: The basic procedure of a DLTS cycle and process of obtaining a DLTS spectrum as a function of temperature (Lang, 1974).**

## 2.3.2 DLTS signal processing

The sample is held at a constant temperature and bias, then a filling pulse is applied to obtain the capacitance transient according to Equation 2.20. The original conventional DLTS technique is known as a fixed rate window temperature scan which is the fundamental technique in determining signals. The importance of this technique is setting up the rate window, which will allow the apparatus to give an output only when the transient generated is within this rate window. The rate window is best described as a time filter, where an output signal is only generated when the time constant of the transient coincides with the centre of the time window of the filter. This system allows the Schottky diode to be repeatedly excited while varying the temperature, in order to obtain a temperature dependent graph. The maximum output is proportional to the amplitude. One of the most common ways of obtaining this time filter is using a dual-gate boxcar average.

The boxcar has its two gates set to $t_1$ and $t_2$ and measures the capacitance at those times. The difference between these measured capacitances is then the DLTS signal $S(T)$. From this definition and Equation 2.20 we get

$$S(T) = C(t_1) - C(t_2) = C_0 \frac{N_T}{2N_D}\left(e^{-\frac{t_1}{\tau}} - e^{-\frac{t_2}{\tau}}\right). \tag{2.21}$$

The difference in capacitance as a function of temperature results in the formation of a bell curve seen in Figure 2.8. From Equation 2.21 one can see that there is a maximum $S$(T) for some time constant $\tau_{max}$. To determine the shape of $S(T)$ we can consider a very rapid transient which is represented by a high temperature transient and a very slow transient represented by a low temperature transient (see Figure 2.8). For the very fast transient, the change in capacitance occurs before the first gate resulting in both gates measuring the same capacitance. Since $C(t_1) = C(t_2)$, from Equation 2.21 $S(T) = 0$. If we consider the very slow transient then a negligible change will occur between the two gates i.e. $C(t_1) \approx C(t_2)$ and thus $S(T) = 0$ again. From this one can see that there is some $S(T)_{max}$ for a transient with a time constant $\tau_{max}$ between these two transients. By differentiating Equation 2.21 with respect to $t$ we can determine $\tau_{max}$. This gives:

$$\tau_{max} = \frac{t_1 - t_2}{ln\left(\frac{t_1}{t_2}\right)}. \tag{2.22}$$

Substituting Equation 2.22 into Equation 2.21 we can determine $S_{max}$ as:

$$S(T)_{max} = C_0 \frac{N_T}{2N_D}\left(exp\left(\frac{-ln\left(\frac{t_2}{t_1}\right)}{\frac{t_2}{t_1} - 1}\right) - exp\left(\frac{\frac{t_2}{t_1} ln\left(\frac{t_2}{t_1}\right)}{\frac{t_2}{t_1} - 1}\right)\right). \tag{2.23}$$

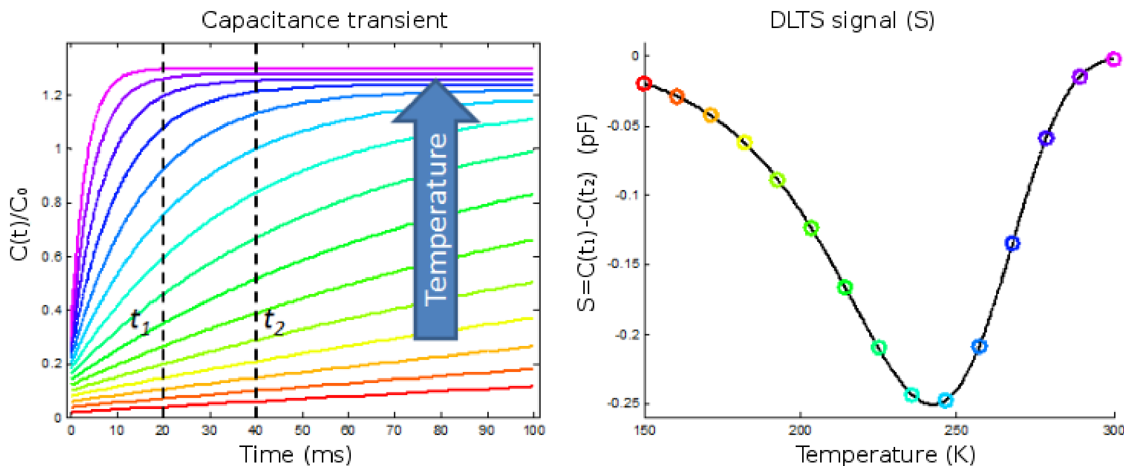


**Figure 2.8: Left: Capacitance transients with change in temperature. Right: Signal obtained from transients (Wei, 2015).**

It can now be seen that $S_{max}$ is proportional to the defect centre concentration $N_T$ and that the peak height is dependent on the ratio of $t_1$ and $t_2$ rather than their absolute values (Kosyachenko, 2015).

Over large temperature ranges, information on the levels that are present and their respective concentrations can be obtained. By changing the rate window, information on the thermal activation energies can be obtained. The major limitation of conventional DLTS is, however, the resolution of the technique. Defects that have similar emission properties would be too closely spaced for identification.

## 2.3.3 Laplace DLTS (L-DLTS)

In contrast to the conventional DLTS method of measuring transients as a function of temperature, L-DLTS measures the transient at a fixed temperature and analyses the transient mathematically by means of a numerical inverse Laplace transform. The inverse Laplace transform technique is very sensitive to noise, therefore the average of a large number of transients is taken to improve the signal to noise ratio (SNR). L-DLTS was introduced by Dobaczewski in 1994 based on the assumption that the observed transient may in general consist of a sum of transients with a spectrum of emission rates

$$f(t) = \int_0^\infty F(s)e^{-st}ds. \tag{2.24}$$

Here $f$(t) is the recorded transient and $F$(s) is the spectral density function. The spectrum of emission rates can be obtained by performing inverse Laplace transform on the function $f(t)$. It should be noted that the numerical inversion of a Laplace transform of a real function is an “ill posed” problem (Dobaczewski *et al.*, 1994), therefore great care has to be taken to ensure validity of the results. The accuracy of these emission rates is highly dependent on the SNR of the transient. This is influenced by the number of averages, the quality of the sample, the equipment used and other external influences. Single peaks or multiple peaks can be obtained for single or multiple exponential transients or a continuous broad spectrum with little fine structure if the spectrum is continuous (Dobaczewski, Peaker and Nielson, 2004). In contrast to conventional DLTS, with L-DLTS the area under each emission rate peak is directly related to the defect concentration. This technique can routinely accurately distinguish multiple emission rates more than a factor of 6 apart.

# 2.4 Arrhenius’ law

It is common knowledge that reaction rates increase with increasing temperature. The Arrhenius equation was proposed by Svante Arrhenius in 1889 by combining the Boltzmann distribution law and the concepts of activation energy (Laidler, 1987). This approach is useful for calculating activation energies. The Arrhenius equation is written as

$$k = Ae^{-\frac{E_\propto}{k_B T}} \tag{2.25}$$

where $k$ is the rate constant, $A$ the frequency factor, $k_B$ the Boltzmann constant, $T$ the absolute temperature and $E_\propto$ is the activation energy (Moore, 1987).

### 2.4.1 Annealing activation energy

During isothermal annealing at a set temperature $T$, the concentration of defects which anneal per given time period $\frac{dN_T(t)}{dt}$ is a function of the concentration of defects at time $t, f(N_T)$. That said the relationship can be written as:

$$\frac{dN_T}{dt} = -Kf(N_T) \tag{2.26}$$

where $K$ is the annealing rate constant. If we assume $f(N_T) = N_T$ then the annealing kinetics will be first order. If we now solve Equation 2.26 with this assumption the concentration at any given time will be

$$N_T(t) = N_T(0)e^{-k(T)t}. \tag{2.27}$$

$N_T(0)$ is the initial concentration before annealing, $t$ is the total annealing time and $k$(T) is the temperature dependent annealing rate constant, which is given by Equation 2.25 (Mikelsen et al., 2005). This means that, during the isothermal annealing process, the defect concentration follows an exponential decay.

Rewriting Equation 2.27:

$$ln\left(\frac{N_T(t)}{N_T(0)}\right) = -k(T)t, \tag{2.28}$$

it follows that the data can be plotted as the natural logarithm of the normalized concentration versus time, to get a straight line with a negative gradient. From Equation 2.28, it can easily be seen that the gradient of this line will be the annealing rate constant for that specific temperature. Equation 2.25 can be rewritten as:

$$ln[k(T)] = ln\ (A) - \frac{E_\propto}{k_B T}. \tag{2.29}$$

Using the annealing rate constants determined for each temperature and plotting them on an ln[k($T$)] versus $T^{-1}$ plot another linear plot will be obtained, if it is a first order reaction. Using the gradient of this graph, the annealing activation energy can be calculated and using the $y$-intercept, the frequency factor can be determined. This activation energy is the energy barrier that needs to be overcome in order to remove a single defect from the system. The annealing mechanism determines the frequency factor which is roughly related to the frequency of attempts to overcome the barrier and may give an indication as to whether the defect undergoes diffusion, recombination, dissociation or complex formation (Bourgoin and Lannoo, 1983).

### 2.4.2 Activation energy for electron emission

Two important methods for determining the emission rate in order to calculate activation energy is conventional DLTS and L-DLTS. The conventional method requires multiple scans across a large temperature region using different emission rate windows. Recall from Equation 2.22 and 2.23 that $S(T)_{max}$ is the maximum peak height at $\tau_{max}$. The temperature scan is repeated with different $t_1$and $t_2$ settings to change the rate window. The temperature at which the trap emits carriers at that rate window is thus obtained at each $T_{max}$ where each $S(T)_{max}$ is. The emission rate, $e$, can be calculated for each peak. These points are used in a semi log graph with $\log\left(\frac{e}{T^2}\right)$ vs $\frac{1}{T}$ from which a linear plot is obtained. These plots are seen in Figure 2.9. Using the gradient the activation energy can be obtained and the apparent capture cross-section can be obtained from the $y$-intercept. Using modern software, it is, however, possible to run a scan with multiple rate windows, reducing the number of scans required.

Using L-DLTS the activation energies may be determined using similar method. The method requires isothermal measurements at different temperatures at which the emission rate is measured. The emission rates and their respective temperatures are plotted and processed the same way as with the conventional DLTS. L-DLTS is able to identify multiple traps that have similar emission rates that cannot be identified by the conventional DLTS method.

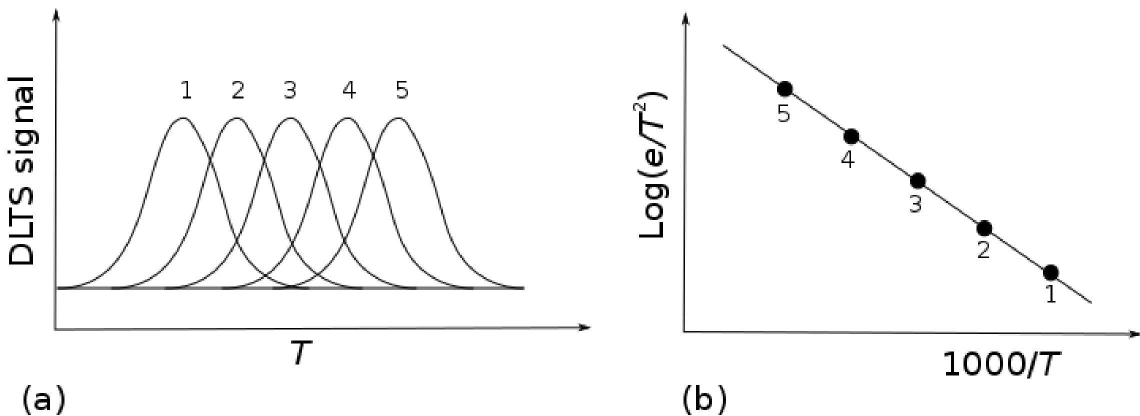


**Figure 2.9: Diagram showing (a) DLTS spectra with different rate window conditions and (b) the Arrhenius obtained from the maxima**

### 2.4.3 Capture cross-section

Capture cross-section is an important parameter in identifying a defect centre. The Arrhenius plot from Section 2.4.2 can be extrapolated to 1/T = 0 to obtain the capture cross-section. This capture cross-section, referred to as the apparent capture cross-section, $\sigma$, may not correspond to the true capture cross-section because:

- Due to the long range of the extrapolation, a slight error in the extrapolation could lead to an order of magnitude error.

- The capture cross-section might be temperature dependent, as would be the case if a capture barrier were present.

The true capture cross-section can be directly measured by determining the concentration of filled defects as a function of filling pulse width. The peak height will increase as the filling pulse width is increased until a maximum height is reached. This maximum peak height is due to all the defect centres being completely filled by a single pulse. An example of the results of such a measurement is shown in Figure 2.10 where only the filling pulse length is varied between each measurement.

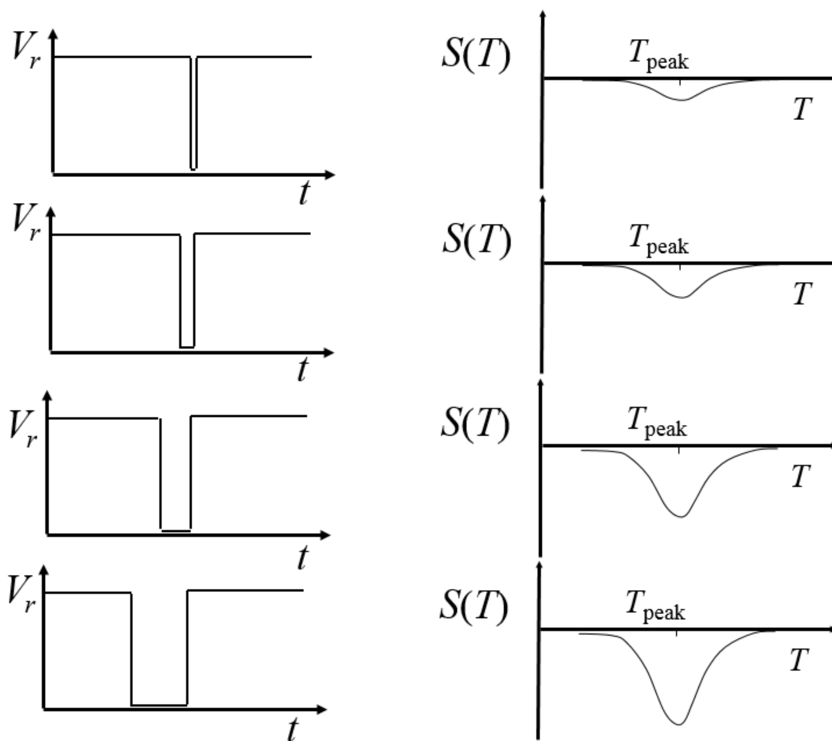


**Figure 2.10: The effect of changing the filling pulse width on the DLTS spectrum as would be required for the determination of the capture cross-section.**

The peak height *S* is related to the filling pulse width $t_{pulse}$ by:

$$S = S_{\infty}\left(1 - e^{\frac{-t_{pulse}}{\tau}}\right) \tag{2.30}$$

where $S_{\infty}$ is the maximum peak height as obtained for a very long filling pulse. To simplify this for experimental purposes Equation 2.30 can be rewritten in terms of capacitance measurements

$$\Delta C(t_{pulse}) = \Delta C_{\infty}\left(1 - e^{\frac{-t_{pulse}}{\tau}}\right). \tag{2.31}$$

The theoretical shape of the plot of $\ln[\Delta C(\infty)/\Delta C(\infty)-\Delta C(t_p)]$ vs $t_{pulse}$ is a S-shaped curve. The steep maximum slope gives $1/\tau$.

$$\sigma_T = \frac{1}{\tau n \langle v_{th} \rangle} \tag{2.32}$$

where $n$ is the number of free carriers during the capture process, which can be determined from C-V measurements. $\langle v_{th} \rangle$ is the thermal velocity of the electrons and can be calculated from:

$$\langle v_{th} \rangle = \sqrt{\frac{8Tk_B q}{\pi m_e}} \tag{2.33}$$

where $T$ is the temperature at which the measurements are done, $m_e$ is the electron effective mass of the material and q is the charge of an electron. To determine the capture cross-section, $\sigma_T$ is measured across a wide temperature range. The natural logarithm of these values are plotted as a function of $1/T$ to determine the capture cross-section. This calculation works well for the capture cross-section of majority carriers. The capture cross-section for minority carrier may also be determined by applying an injection pulse, but the calculations are more complicated due to the concentration of electrons or holes being a function of the current during the injection pulse (Zhao, Schlesinger and Milnes, 1987).

# 2.5 Depth profiles

Equation 2.19 was used to calculate the concentration of deep levels, $N_T$, as a function of depth. However, this has been shown to be an approximation (Lang, 1979). In certain situations such as thin film measurements, this equation may result in some serious errors in determining $N_T$ for a majority carrier trap. For a more accurate calculation we assume an n-type semiconductor with the same shallow donors $N_D$ as previously and at an energy level $q^{-1}E_T$ we have $N_T$ deep donors where $q$ is the absolute electronic charge. Placing the Schottky diode under a quiescent reverse bias, the depletion layer is the region defined by $0 \leq z \leq w$ in Figure 2.11. The layer $0 \leq z \leq w - \lambda$ is the region in which the electronic states of the deep level are above the Fermi level, and will eventually empty. The depletion layer width relates to the capacitance

$$C = \frac{\varepsilon A}{w} \tag{2.34}$$

which is the high frequency junction capacitance where $\varepsilon$ is the dielectric constant. The plane where the deep-levels cross the bulk Fermi level $q^{-1}E_F$ is denoted by $w - \lambda$. We can calculate $\lambda$ from

$$\lambda = \left(\frac{2\varepsilon(E_F - E_T)}{q^2 N_D}\right)^{\frac{1}{2}}. \tag{2.35}$$

In order to start profiling the distribution of the deep levels, the region being profiled must be filled with electrons. Experimentally this is done by applying a forward bias $V_+$ superimposed on a quiescent reverse bias, reducing the resultant reverse bias during the pulse ($V_p = V - V_+$). This results in a depletion width of

reduced width. The depletion width as a function of pulse height is shown in Figure 2.12 where the depletion width increased as a function of increased applied pulse resulting in more defects being filled and consequently an increase in peak height. In a Schottky diode with a constant defect density, there will be a linear relationship between the depletion width filled and the signal ($\Delta C/C$) observed. It is important to note that when a smaller positive pulse is used, the depth resolution of the depth profile is increased, however this is limited by the Debeye length.

Immediately after applying a pulse, electrons will fill defects in the region $w_p - \lambda \leq z \leq w - \lambda$. By double integration of the Poison's equation in the depletion region and the region filled with electrons after the applied pulse, the sum of the built in voltage $V_D$ and quiescent negative bias is given by

$$V + V_D = \int_0^{w_p - \lambda_p} N_T(z) \cdot z\, dz + \int_0^{w_0} N_D(z) \cdot z\, dz. \tag{2.36}$$

where, $w_p$ and $\lambda_p$are the values of $w$ and $\lambda$ during the applied pulse and $w_0$ is the depletion width during the pulse. This charge distribution relaxes with time to

$$V + V_D = \int_0^{w - \lambda} N_T(z) \cdot z\, dz + \int_0^{w} N_D(z) \cdot z\, dz. \tag{2.37}$$

Combining these two equations it follows that

$$\int_w^{w_0} N_T(z) \cdot z\, dz = \int_{w_0 - \lambda_0}^{w - \lambda} N_D(z) \cdot z\, dz \tag{2.38}$$

With the assumption that $\Delta C(0)$ is small in comparison to $C$, $N_D(z)$ slowly varies as a function in the range of $w \leq z \leq w_0$ and $N_{T(z)}$ slowly varies in the range $w_p - \lambda_p \leq z \leq w - \lambda$ and it follows from Equations 2.34 and 2.38 that

$$\frac{N_T(w_m - \lambda_m)}{N_D(w)} = \frac{1}{\left(\frac{w - \lambda}{w}\right)^2 - \left(\frac{w_p - \lambda_p}{w}\right)^2} \tag{2.39}$$

with

$$w_m - \lambda_m = \frac{1}{2}\left[(w - \lambda) - \left(w_p - \lambda_p\right)\right]. \tag{2.40}$$

This equation reduces to Equation 2.19 when the conditions $\frac{\lambda}{w} \ll 1$ and $\frac{(w_p - \lambda_p)}{w} \ll 1$ are met. However if Equation 2.19 is used instead of 2.40 for the case where $\frac{\lambda}{w} \ll 1$ is not true, $N_T$ reduces by a factor of $\left(1 - \frac{\lambda}{w}\right)^2 - \left(\frac{w_p}{w} - \frac{\lambda_p}{w}\right)^2$. Therefore even in the cases of homogenous doped samples, $N_T(z)$ appears to become lower as z approaches the surfaces for Equation 2.19 (Zohta and Watanabe, 1982).

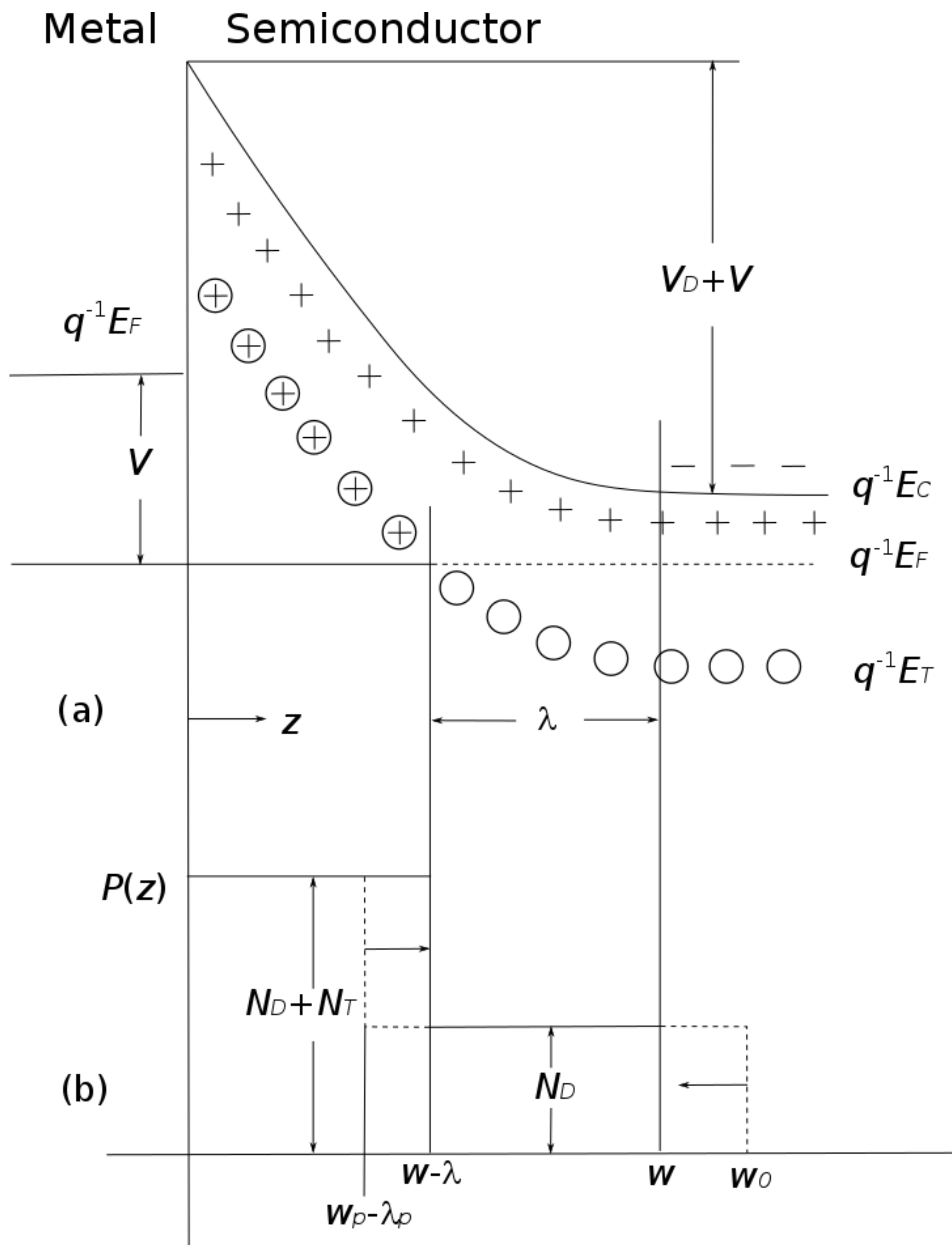


**Figure 2.11: (a) Energy band diagram for a Schottky diode under a quiescent reverse bias. (b) Solid line shows the corresponding charge distribution and dashed lines show the charge distribution right after the pulse which relaxes back to the solid line (Drawn after Zohta and Watanabe, 1982).**

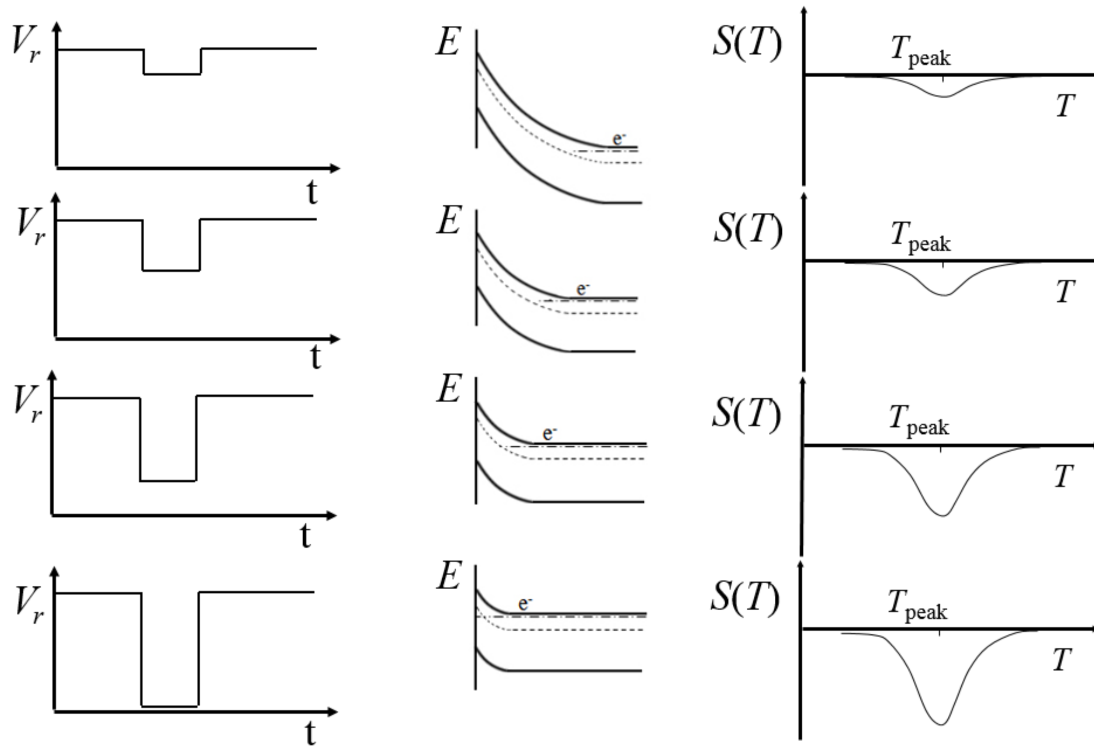


**Figure 2.12: DLTS transient obtained during depth profiling. From left to right we have the pulse applied to the Schottky diode, its corresponding depletion width being filled and the signal obtained through DLTS and L-DLTS measurments.**

## 2.6 Introduction kinetics

Introduction kinetics describe the introduction rate of a defect as well as the influence caused by other defects present in the system on this rate. Three theories will be taken into consideration to address possible outcomes of the introduction rates of the E-centre and E'.

**Zeroth order reaction** – In this case, the introduction rate is independent of the concentration of other radiation-induced defects present. The introduction rate of the defect does not change with increasing concentration of other radiation induced defects. The Zeroth order reaction rate law is:

$$rate = \frac{dN_{T,1}(t)}{dt} = k_1 \tag{2.41}$$

where $N_{T,1}$(t) represents the concentration of Defect 1 at a particular time and $k_1$ is the constant introduction rate. Using integration the above equation is rewritten as

$$N_{T,1}(t) = N_{T,1}(0) + k_1 t \tag{2.42}$$

with $N_{T,1}(0)$ as the initial concentration which can be set to zero if no defects are present at the start of the experiment. In the case of radiation induced defects, the concentration is only dependent on the exposure time to a constant irradiation flux (or fluence rate).

**First order reaction** – Here the introduction rate of the defect, which we will refer to as Defect 2, is linearly dependent on the concentration of another defect, Defect 1. First we will assume that Defect 1 follows the introduction rate shown in Equation 2.41, with Defect 2 following an introduction rate linearly dependent on the concentration of the first defect. The first order reaction rate law can be written as follows:

$$rate = \frac{dN_{T,2}(t)}{dt} = N_{T,1}(t)k_2 \tag{2.43}$$

where $k_2$ is the introduction rate constant of Defect 2 and $N_{T,1}(t)$ is the concentration of Defect 1 present in the system. Integrating this we get:

$$\int dN_{T,2}(t) = \int N_{T,1}(t)k_2 dt \tag{2.44}$$

$$\int dN_{T,2}(t) = k_2 \int \left(N_{T,1}(0) + k_1 t\right) dt \tag{2.45}$$

$$N_{T,2}(t) = k_2 N_{T,1}(0)t + \frac{1}{2}k_1 k_2 t^2 + N_{T,2}(0) \tag{2.46}$$

If we assume that the initial concentration of both defects is zero (i.e $N_{T,1}(0)=N_{T,2}(0)=0$), Equation 2.46 can be simplified to:

$$N_{T,2}(t) = \frac{1}{2}k_1 k_2 t^2. \tag{2.47}$$

Equation 2.42, Equation 2.46 and the summation of these two equation have been modelled in Figure 2.13.

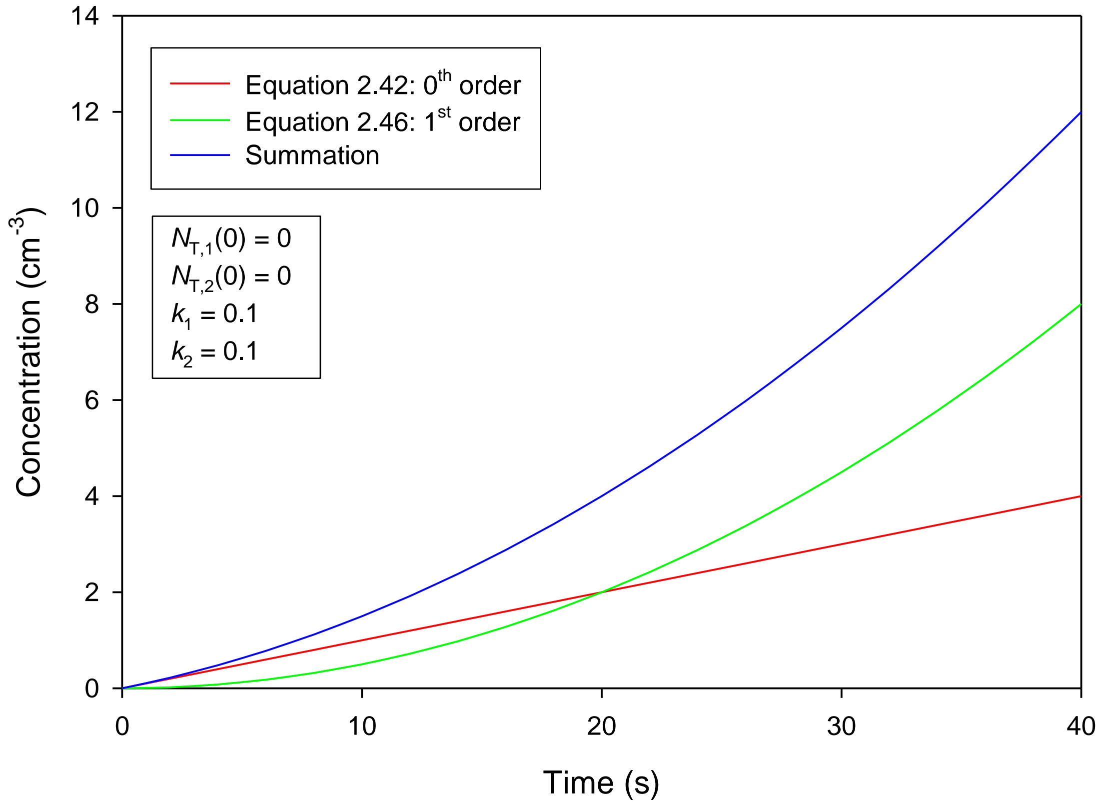


**Figure 2.13 Simulations of Equations 2.42 (Defect 1 with linear introduction rate) and 2.46 (Defect 2 with introduction rate linearly dependent on that of defect 2) with the expected summation that would be observed. Defect 1 would exhibit a linear introduction and Defect 2 would exhibit a quadratic growth.**

**First order introduction with removal of defects:** This model is similar to the previous model, except that the reduction in concentration of Defect 1 due to the formation of Defect 2 is taken into account. The model assumes the linear introduction rate for Defect 1 as seen in Equation 2.42. Assuming that Defect 2 is formed by the reaction of another radiation induced defect with Defect 1, then the introduction rate for Defect 2 is however, dependent on the concentration of Defect 1 while consuming Defect 1 during the formation of Defect 2. The introduction rate of Defect 2 after annealing Defect 1 will require further modification of Equation 2.42. The new relationship can be written as:

$$N_{T,1}(t_{n+1}) = N_{T,1}(\mathrm{t}_n) + k_1 t - dN_{T,1}(t_{n+1}) \tag{2.48}$$

where d is the fraction of Defect 1 converted to Defect 2 during annealing. The concentration of Defect 2 will then follow the new relationship described as:

$$N_{T,2}(t_{n+1}) = N_{T,2}(0) + N_{T,2}(t_n) + dN_{T,1}(t_n). \tag{2.49}$$

Equation 2.48, Equation 2.49 and the summation of these two equation have been modelled in Figure 2.14.

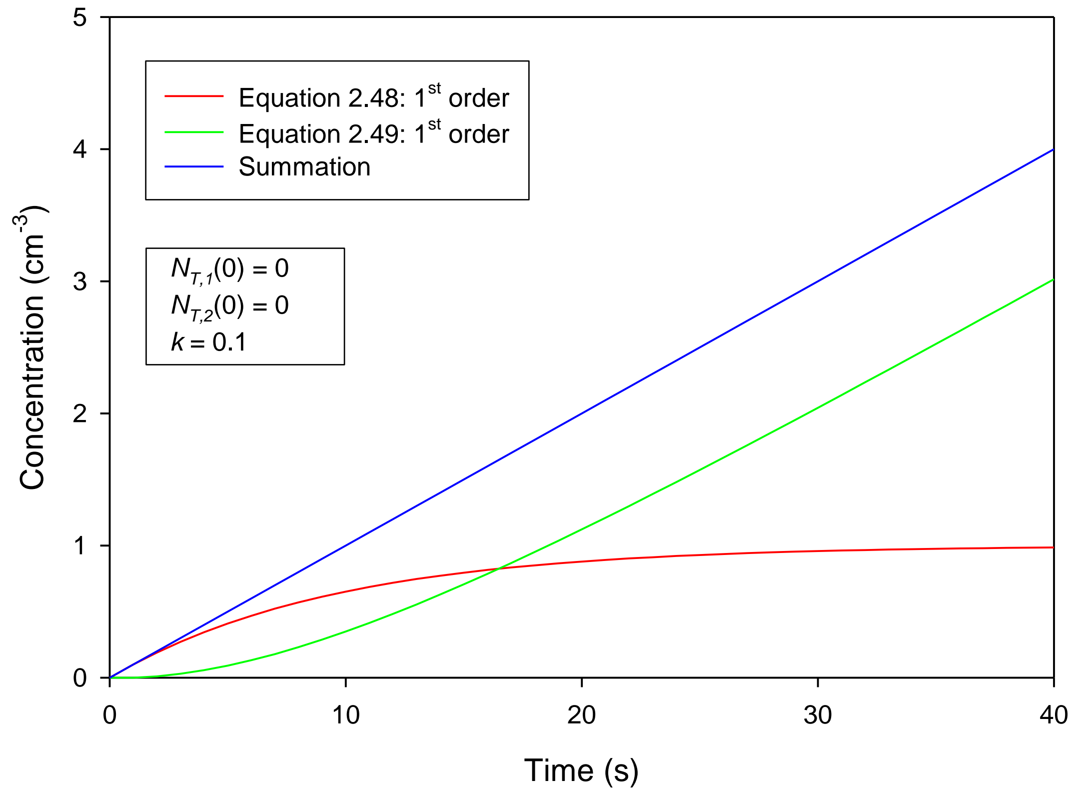


**Figure 2.14 Simulations of equations 2.48 and 2.49 with the expected summation that would be observed. Defect 1 would exhibit an exponential rise to a maxima while Defect 2 would initially exhibit exponential growth before transforming into a linear introduction.**

# 3 EXPERIMENTAL TECHNIQUES

In this chapter the experimental techniques and apparatus that were used will be discussed. A brief summary of the cleaning process of n-type Si and Ge will be given as well as a brief background theory on the setup of the equipment.

## 3.1 Schottky device fabrication

### 3.1.1 Germanium

Bulk grown n-type Ge supplied by Umicore with <100> crystal orientation was used. The samples were doped with Sb and had a free carrier concentration of $2\times10^{15}$ cm$^{-3}$. Before fabrication of the metal-semiconductor device, the samples had to be cleaned. Any organic contamination on the samples was removed using a three step degreasing process involving trichloroethylene, isopropanol and methanol. The samples were placed successively in each of the above mentioned chemicals for 5 minutes at room temperature in an ultrasonic bath. The samples were then etched in a solution of hydrogen peroxide (30%) mixed with deionized water (1:5) for one minute. Each sample was blown dry with nitrogen gas before being mounted on a metal evaporation mask for making Ohmic contacts. Ohmic contacts were made by depositing 1000 Å AuSb (0.6% Sb) at a rate of 1 Å/s on the back of the sample in a vacuum of $1\times10^{-6}$ mbar. The samples were then annealed at 620 K for 10 minutes in an argon environment flushed at 0.1 litres per minute to convert the AuSb Schottky contact to an ohmic contact.

The samples then underwent the same degreasing and etching process before being mounted on a Schottky contact mask. Schottky contacts were made by depositing 1000 Å Pd at a rate of 1 Å/s on the front of the samples in a vacuum of $1\times10^{-6}$ mbar.

## 3.1.2 Silicon

The Si samples underwent the same degreasing process as the Ge previously mentioned. The etching process, however, consisted of dipping the samples in hydrofluoric acid (40%) periodically for approximately 20 seconds before drying off with nitrogen. AuSb (0.6% Sb) Ohmic contacts and Pd Schottky contacts were used for the experiments. More information on the type of Si wafers that were used is discussed in Chapter 4.

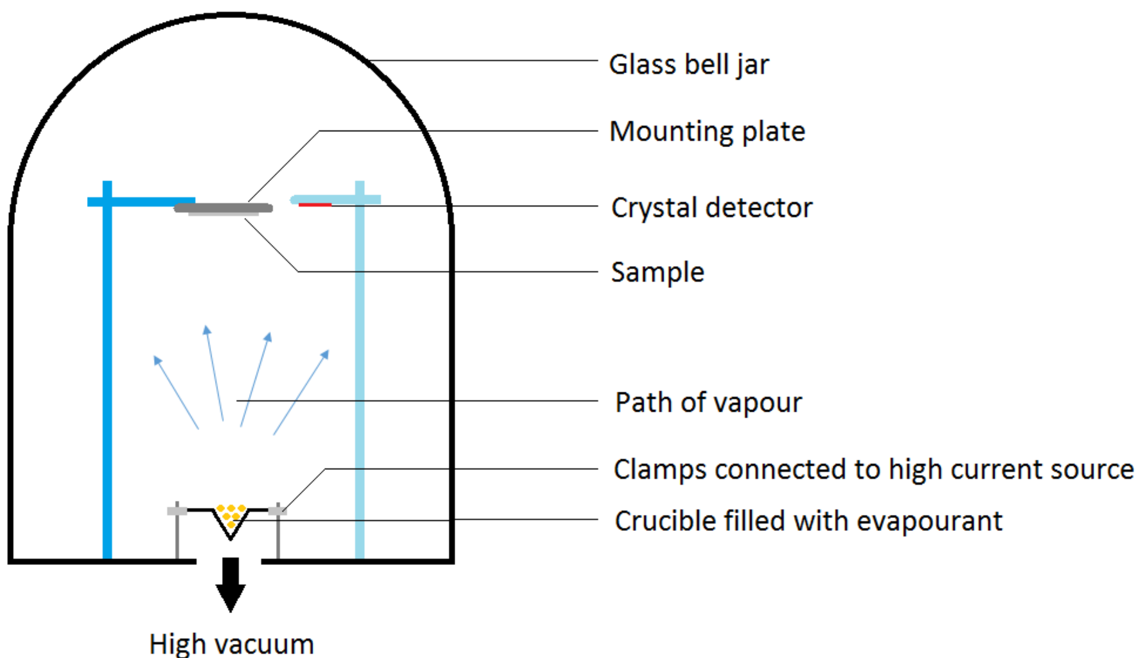


**Figure 3.1: Schematic diagram of the resistive evaporation setup used to deposit AuSb ohmic and Pd Schottky contacts.**

## 3.1.3 Resistive thermal evaporation (RTE)

The schematic of the RTE setup can be seen in Figure 3.1 which consists of a glass bell jar, mounting plate, crucible, crystal thickness monitor and high vacuum pumps. RTE is one of the most commonly used techniques for metal deposition. A large current is sent through the filament crucible that has a finite electrical resistance to carry out heating of the deposition material. The solid material (in the case of this thesis would be AuSb or Pd) is indirectly heated to high enough temperature to undergo evaporation. A thin film is formed on the substrate when condensation occurs. When a material undergoes evaporation it will experience collisions with remnant gas molecules inside the chamber resulting in a fraction of the material being lost. At 25 °C the mean free path at pressures $10^{-4}$ and $10^{-6}$ mbar is approximately 45 and 4500 cm respectively. The distance between the crucible and the mounted sample is approximately 30 cm

therefore requiring pressures of at least $10^{-5}$ mbar or lower for deposition. One of the requirements for RTE is a good vacuum to prevent contamination during deposition.

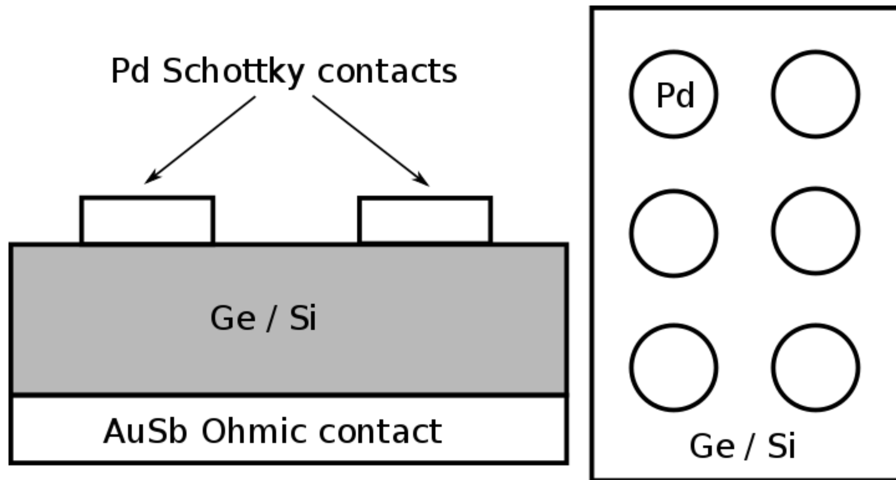


**Figure 3.2: Side and Top view of the fabricated metal-semiconductor devices.**

# 3.2 Measurement equipment and techniques

## 3.2.1 Investigating closely spaced peaks by means of L-DLTS

The first technique used for investigating closely spaced peaks will be referred to as *subtraction of transients*. The process involves the following:

- The capacitance transient of a sample containing the two different defects with closely spaced emission rates is measured.
- One of the two defects is then removed by means of annealing or, in the case of metastable defects, one of the peaks may be removed by transforming the defect to another state.
- The capacitance transient representing only the remaining defect is then subtracted from the initial transient (containing contributions from both defects). The emission rate obtained from the new capacitance transient represents the defect that was previously removed from the system.

This technique is illustrated experimentally in Article 3 (page 71).

The second technique involves using manual input of regularization parameters to the L-DLTS analysis routine. The regularization parameter determines how easily the inversion algorithm will split a broad single peak into two (or more) single peaks. Manual regularization parameters were used to allow the inversion routine (Contin) to take into consideration the possibility of 2 or more closely spaced peaks.

L-DLTS analysis is made under the assumption that the capacitance transient is composed of a spectrum of exponential decay functions. In this section, the ability of the technique to resolve two transients with closely spaced emission rates is discussed. In order to make the data as realistic as possible, experimental

data, consisting of two single transients with different emission rates was used. The two transients with differing emission rates were produced by measuring the same sample at different temperatures. The final transient was the summation of these two single-emission-rate transients.

In Figure 3.3 (a) two capacitance transients were measured with emission rates spaced far enough apart to be easily resolved by L-DLTS. These capacitance transients were added together to make a resultant transient. The emission rates obtained for the individual capacitance transients were 278.2 $s^{-1}$ and 1996.7 $s^{-1}$, spaced a factor 7 apart (see Figure 3.3 (b)). The emission rates of the peaks obtained by L-DLTS from the resultant transient varied by less than 1% from that of the individual transients.

In Figure 3.4 (a) two separate capacitance transients were recorded that were spaced close enough to not be resolved by standard L-DLTS. The two transients were added together to make a resultant transient. The emission rates obtained from the individual capacitance transients were 278.2 $s^{-1}$ and 392.5 $s^{-1}$, spaced a factor 1.4 apart (see Figure 3.4 (b)). However, the emission rate obtained from the resultant transient was 334 $s^{-1}$ showing no signs of the transient consisting of two exponential decays with different emission rates. With manual input of regularization parameters it was possible to split the peak into two constituent peaks. However, the area under the peaks ($\Delta C$) obtained from the resultant transient using regularization parameters differ from that of the peaks obtained from the constituent transients. However, the sum of the areas remained constant.

The resultant capacitance transient from Figure 3.4 was used to explore the effect of different regularization parameter inputs to the L-DLTS inversion routine. The results obtained are show in in Figure 3.5:

- With a regularization parameter of $10^{-2}$, no peak splitting was observed, similar to what was seen with automatic determination of parameters.
- With a regularization parameter from $10^{-3}$ to $10^{-4}$, the peak partially splits. In practice, with repeated measurements, the emission rates would vary due to external factors such as noise, causing the peaks to split to a greater or lesser extent.
- With a regularization parameter in the range of $10^{-5}$ to $10^{-7}$, the peak was successfully split into two distinct peaks with emission rates comparable to that of the peaks observed for the single transients. In practice, with repeated measurements the peaks continued to give the very similar emission rates with the regularization parameter varying over a wide range.
- With regularization parameters of $5 \times 10^{-8}$ or less, the peak splits into multiple false peaks. In practice, with repeated measurements, these peaks vary in position and amplitude.

In general, it was found that there was a large range of the regularization parameters where successful splitting occurred with emission rates consistent between repeated measurements. Multiple external factors need to be taken into consideration when the regularization parameters are selected:

- The noise of the measured transient. The more noise the measured transient had, the smaller the regularization parameter required to split the peaks. (I.e. low noise led to easier splitting of the peaks.)
- The position of the emission rate peak. The closer the peak is to the centre of the emission spectrum measurable by L-DLTS, the easier the peak splits.
- The relative magnitude of the single capacitance transients. If the two transients are of similar size, peak splitting occurs more easily.
- The number of exponential decay components in the transient. The greater the number of exponential decay functions in the transient, the more complicated the peak splitting becomes.
- The ratio between the emission rates. The closer the two emission rates observed are to each other, the smaller the regularization parameter required for splitting becomes.

In Figure 3.6 the same regularization parameters used on the resultant transient in Figure 3.5 were used on the capacitance transient of the single emission rate peak of 392.5 $s^{-1}$ from Figure 3.4. The peak in this case experienced no signs of splitting with change in regularization parameters. However, the peak broadened and narrowed with negligible change to the emission rate and $\Delta C$.

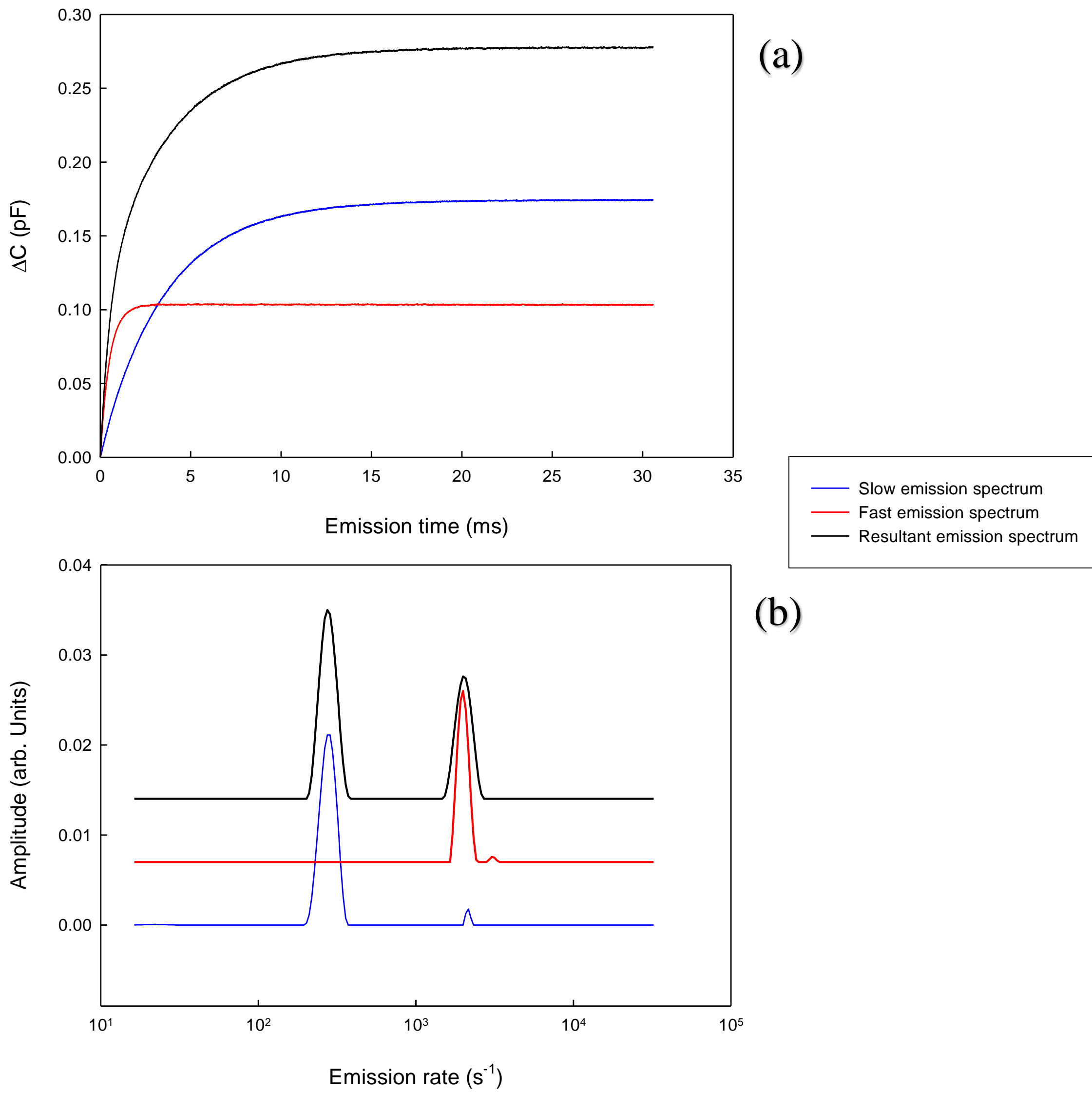


**Figure 3.3: Measured capacitance transients spaced further apart than the resolution limit of L-DLTS (a) and the combined transient with their relative emission spectrums (b).**

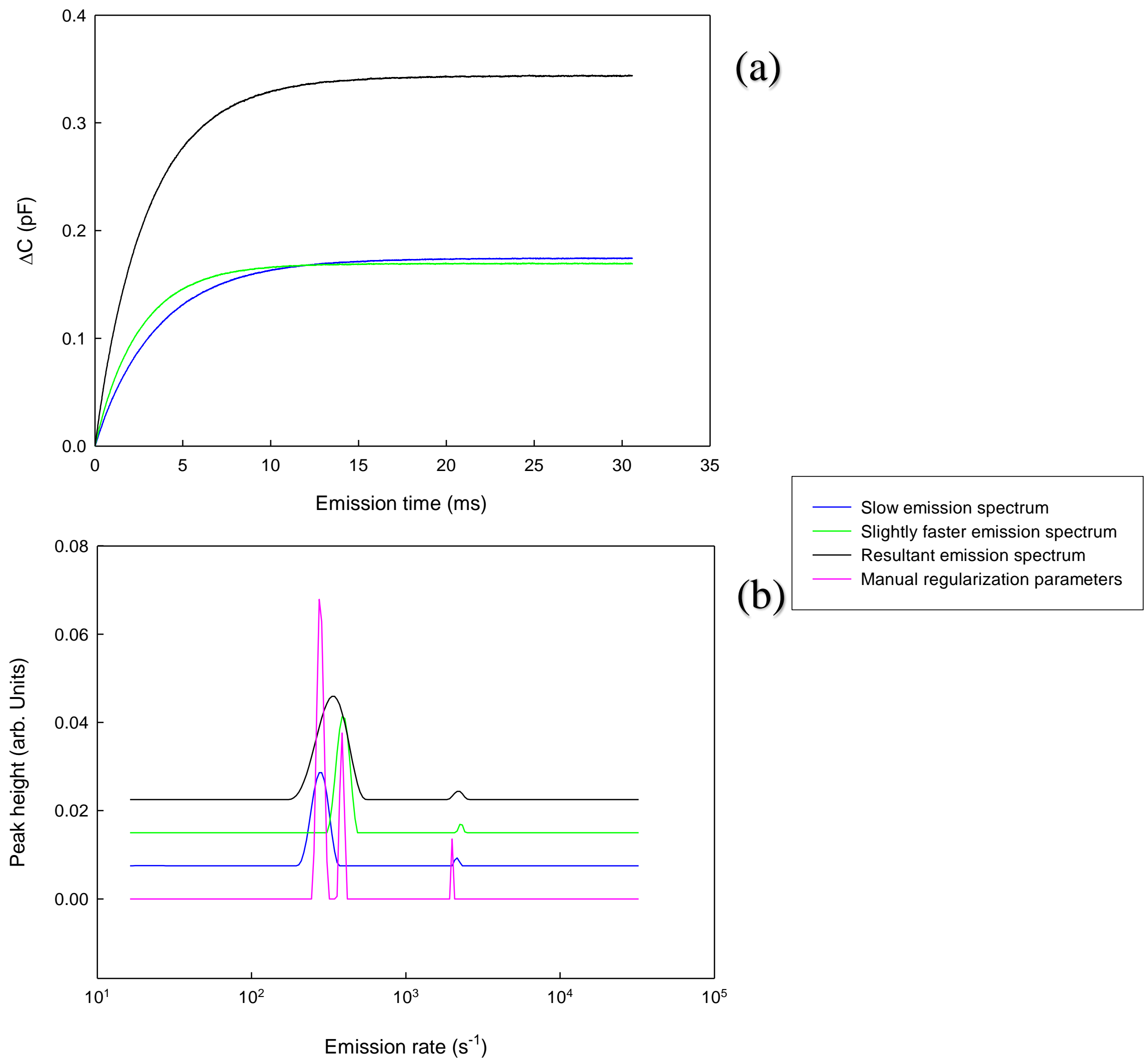


**Figure 3.4: (a) Two measured capacitance transients with emission rates 275 $s^{-1}$ and 380 $s^{-1}$, spaced closer than the usual resolution limit of L-DLTS and the summation of their capacitance transients. (b) L-DLTS spectra of the individual transients as well as the summed transient with and without manual input of regularization parameters.**

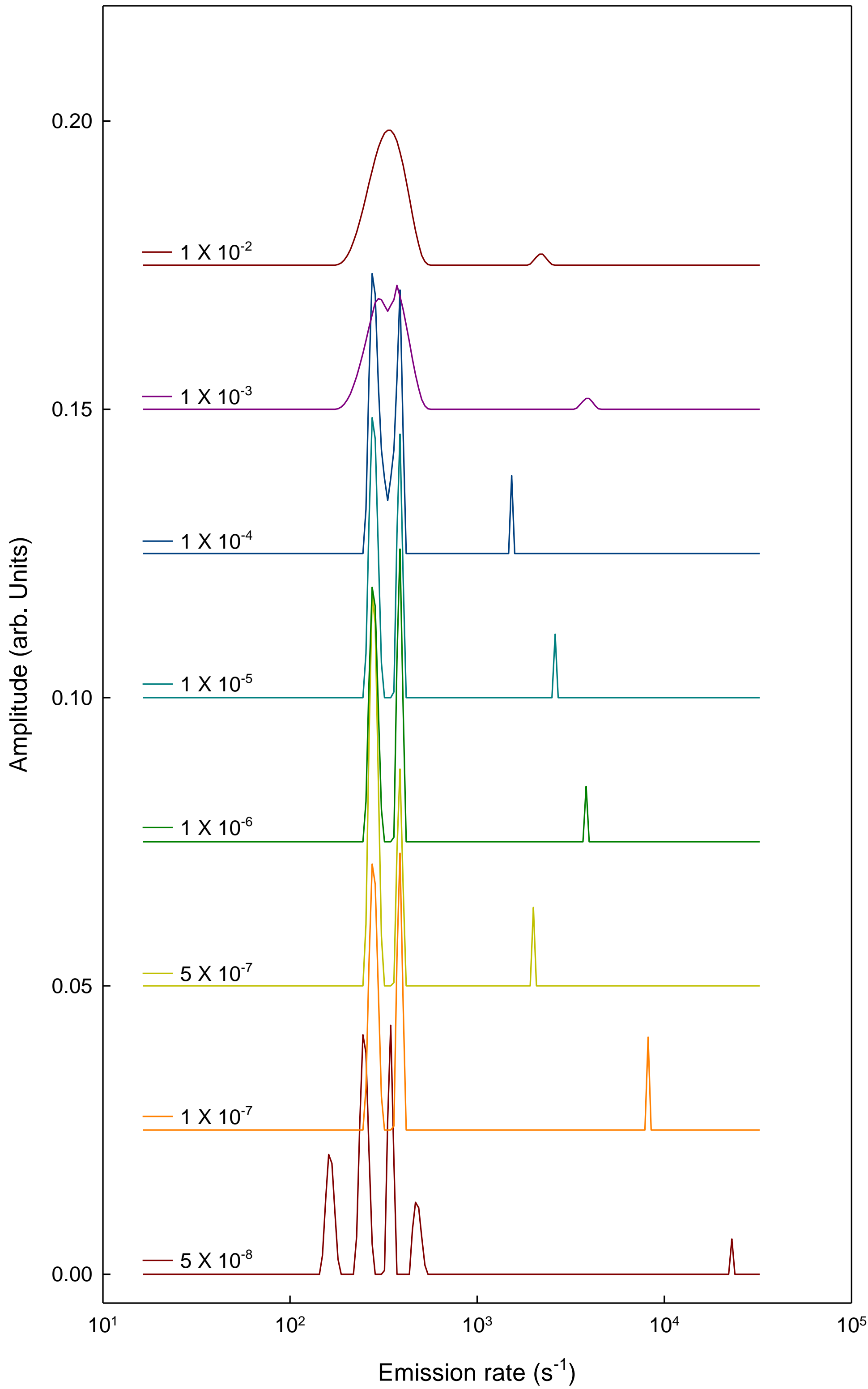


**Figure 3.5: The effect of manual input of Contin regularization parameters on the separation of the closely spaced peaks shown in Figure 3.4.**

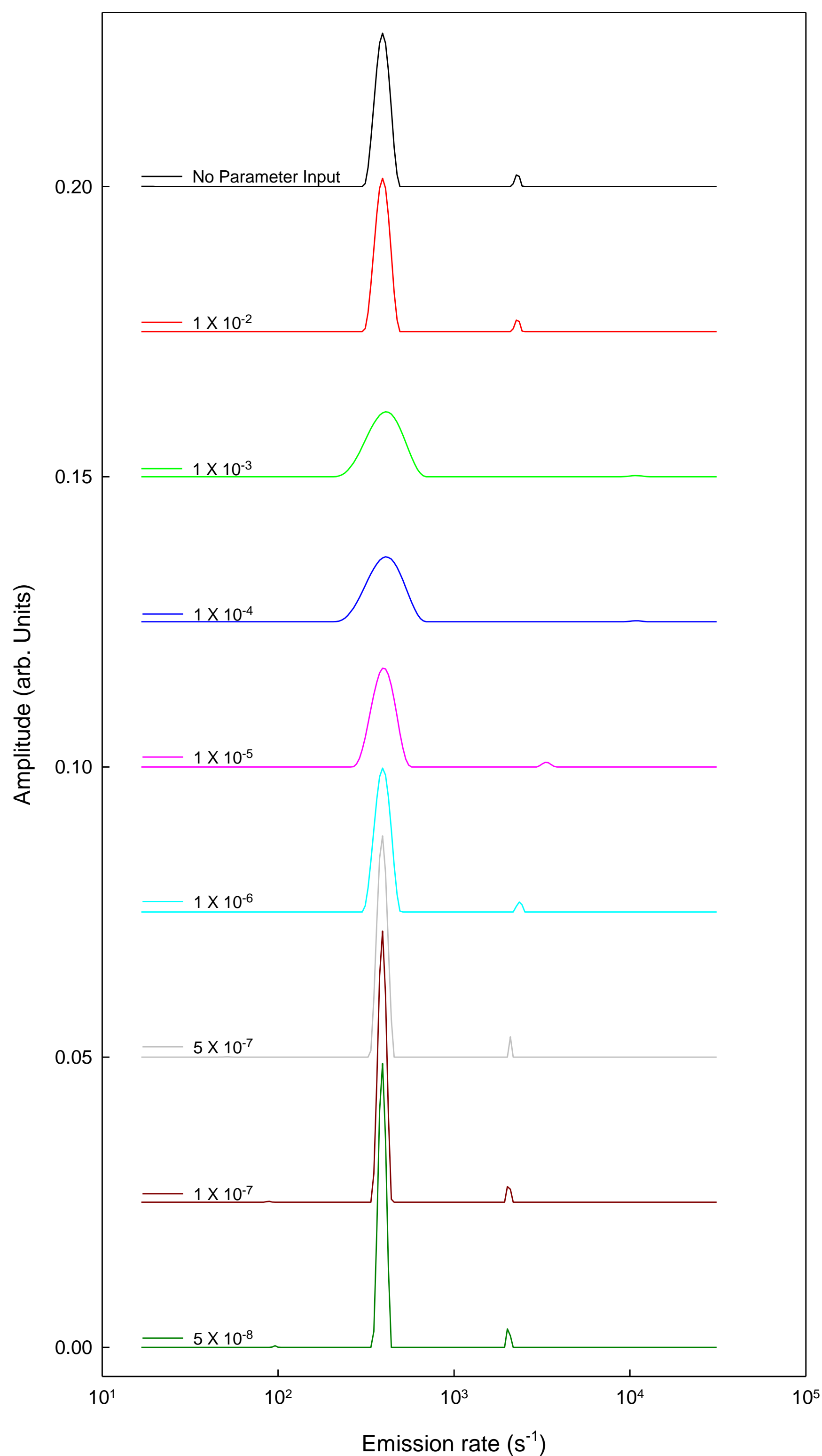


**Figure 3.6 Manuel input of contin regularization parameters for a single emission spectrum peak used in Figure 3.4.**

## 3.2.2 DLTS setup

The DLTS system was comprised of the following equipment:

- **Boonton model 7200 capacitance meter** - This is a high speed instrument with high precision used to measure capacitance in semiconductors.
- **Lakeshore 340 temperature controller** - This device stabilizes the temperature of the sample being observed. Using a PID loop, it controls the current passing through the heater while observing the temperature. With the correct settings, the controller can stabilize the temperature to within 0.02 K to 0.005 K.
- **Variable capacitor or offset box** - This is connected to the “diff” terminals of the Boonton, and used to reduce the capacitance observed by subtracting a constant capacitance. This allows the capacitance transient to fit in the more sensitive 2 pF scale of the Boonton which can read a capacitance in the range −3 pF to 3pF. The offset capacitor may introduce noise to the system.
- **Insulating sapphire disk** - This insulates the sample electrically from the cold finger of the cryostat, while keeping good thermal contact. The disk is soldered to the tip of the cold finger and indium foil is placed on top of the disk for thermal and electrical contact to the sample.
- **Laplace card** – Converts the analogue signal from the capacitance meter to digital data for processing by the personal computer (PC) and produces trigger pulses for the pulse generator (arbitrary wave form generator).
- **Agilent 33220A Arbitrary Wave Form Generator** – This is an external pulse generator that applies the required quiescent reverse bias and filling pulse.
- **Vacuum pump** – The system is placed under a vacuum for insulation and to prevent condensation.
- **Closed cycle helium cryostat** - This is used to cool the system down to temperatures as low as 15 K.

Figure 3.7 shows a block diagram of the system for measuring DLTS. The sample is placed on indium foil which is isolated from the system by a sapphire disk. Two probes are used, one is directly placed on the Schottky contact and the second is placed on the Ohmic contact. In the case of the samples made as described by Figure 3.2, the second probe is placed on the indium to make contact with the ohmic contact at the back of the sample. The contact on the sample serves the dual purpose of also keeping the sample in close mechanical contact with the cold finger to ensure good thermal conduction.

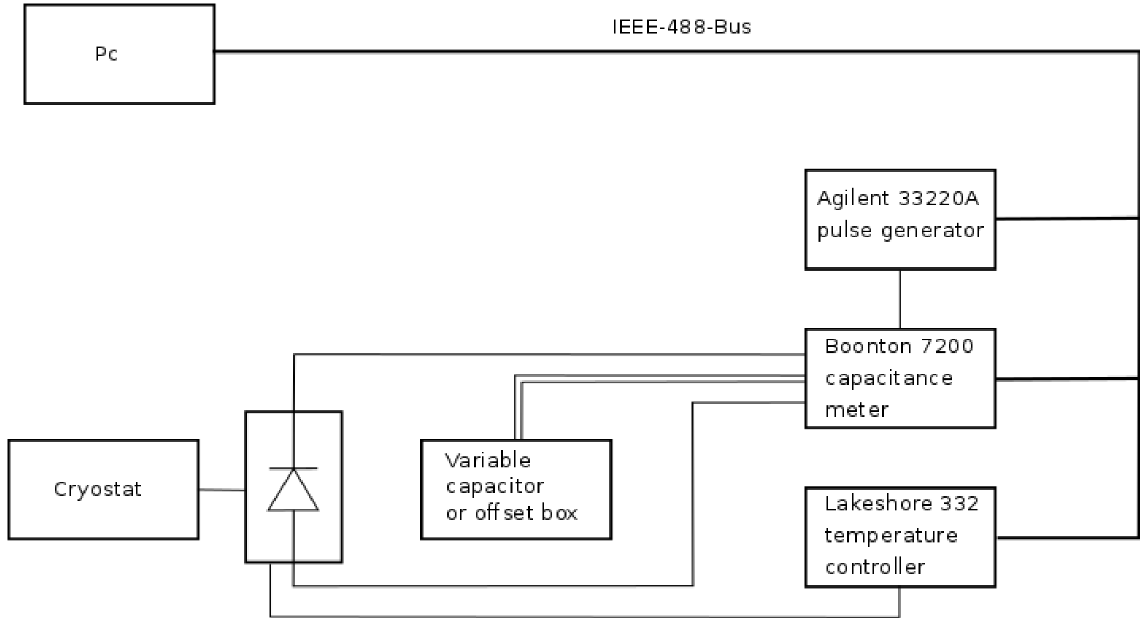


**Figure 3.7: Block diagram of DLTS and L-DLTS experimental setup**

# 3.3 CV characterization

## 3.3.1 Free carrier concentration

Charge carriers are particles that are free to move. They carry electrical charges in electronic conductors. Examples of these particles would be holes and electrons. Electric fields can exert a force on the free carriers in a conducting medium resulting in a net motion through the medium which constitutes an electric current. The free carrier concentration is obtained through a capacitance measurement as a function of the applied bias (C-V measurement). This relationship is plotted as a $C^{-2}$ versus $V$ function with a slope equal to

$$\frac{C^{-2}}{V} = \frac{2}{qK_s\varepsilon_0 A^2 N_D}. \tag{3.1}$$

Here $q$ is the electron charge, $K_s$ the dielectric constant, $N_D$ is the charge carrier concentration, $\varepsilon_0$ the permittivity of free space and $A$ is the area of the Schottky diode (Hartmut and Sadrozinski, 2007).

# 3.4 DLTS characterization

## 3.4.1 Concentration

Introduction and annealing profiles require an understanding of the concentration of defects. To determine the defect concentration we assume that all the defects in the depletion region are filled by the filling pulse $n_T = N_T$. Equation 2.19 can then be rewritten as:

$$N_T = \frac{2\Delta C}{C_0} N_D. \tag{3.2}$$

The defect concentration $N_D$ can be determined from C-V measurements. $C_0$ is the stabilized capacitance at a set bias and $\Delta C$ is the change in capacitance after the filling pulse has been removed.

### 3.4.2 Annealing profiles

Annealing is a technique in which the physical or chemical properties of a material are altered through heat treatment. In the semiconductor industry this technique is generally used to diffuse dopant atoms into substitutional positions in the crystal lattice. It is also used to remove radiation induced defects in the material caused, for instance, by implantation. Both result in drastic changes in electrical properties of the material. There are two main types of annealing profiles, namely isochronal and isothermal. Isochronal annealing is the process during which the sample is annealed at increasing temperatures for fixed periods of time. Isothermal annealing involves annealing the sample at a fixed temperature with increasing time.

Isochronal annealing is used here to identify the temperatures at which the E' and E-centre defects anneal. This gives a temperature range in which the one can be annealed out without affecting the other. Isothermal annealing is used to identify the annealing activation energies and frequency factors of both defects. It is also used to determine the time period that is required to anneal out the E' at a set temperature to study the properties of the E-centre.

### 3.4.3 Annealing kinetics

Isothermal annealing profiles are used to determine the annealing activation energies and determine if the defect undergoes migration, recombination, complex formation or complex dissociation. When a single defect concentration $N_T$ is observed and the defect anneals out by means of a first order process, the concentration can be written as an exponential decay:

$$N_T(t) = N_T(t)e^{-c(T)t} \tag{3.3}$$

where $c(T)$ defines the constant decay rate for a set temperature.

The two defects E' and E-centre have indistinguishable L-DLTS signals, therefore the observed concentration was assumed to be the sum of the concentrations of the two defects. It is assumed that both defects anneal with first order kinetics, and that the defects anneal out in two stages. The concentration of the observed peak will eventually reduce to a set concentration representing the second stage defect concentration. With this we can assume the second defect concentration to be constant and write the new relationship as:

$$N_T(t) = A + N_T(t)e^{-c(T)t}. \tag{3.4}$$

The concentration of the second defect is represented by A and the first defect follows the relationship of a single defect with a first order decay. In the case of the E' and E-centre, it has been found that the E' anneals out at much lower temperatures than the E-centre. Equation 3.3 will be used to determine the activation energy and frequency factor for the E-centre and Equation 3.4 will be used for E'.

The Ge samples were first irradiated at 270 K with alpha particles from an $^{241}$Am source with no external applied bias for 60 minutes under a vacuum of $10^{-3}$ mbar. Laplace DLTS was used to observe the change in the capacitance at 200 K at 97 kHz using 3000 samples and 6000 averages under a reverse bias of -2 V and the filling pulse level set to 0 V. For the concentration profiles Equation (4.1) was used. The E' isothermal profiles were measured over the temperature range 300 K to 325 K in 5 K intervals. Each profile was measured using 15 minute annealing intervals until a 'stabilized' concentration was reached. The E-centre isothermal profiles were measured under the same conditions but over the temperature range 415 K to 435 K until a constant concentration was observed.

Using SigmaPlot (SigmaPlot, 1996), best fit lines can be plotted for the concentration versus time measurements. Here the non-linear least-squares curve fitter supplied with SigmaPlot employing the Levenberg-Marquardt method was used. The main advantage of this technique is that it correctly weighs the errors in the experimental data. The best fit for the E-centre is the 'single, 2 parameter' exponential decay which is represented by Equation (3.3). For the E' the 'single, 3 parameter' exponential decay which is represented by Equation (3.4) can be used.

### 3.4.4 Introduction kinetics

The emission rates of the two defects are virtually indistinguishable making the approach to determining the introduction rates slightly different to usual methods.

Firstly, the introduction rate of the E-centre was determined. This profile was made by first irradiating the sample at room temperature and then taking a concentration measurement for the sum of the two defects with L-DLTS. The sample was then annealed at 330 K for 60 minutes to remove the E' before another concentration measurement was done which yielded the concentration of the E-centre. These steps were repeated until a threshold concentration of approximately 10% of the carrier density was achieved. A second introduction profile was also measured where the sample was not annealed between irradiations. This profile determined the concentration of the sum of the two defects that were introduced. The introduction rate of the E' was then determined from the difference between the two concentrations. For the introduction of the E and E', three theories using the theoretical models described in section 2.6 were considered.

The first theory assumes there are two defects (E-centre and E'). The introduction of the E-centre is independent of the concentration or introduction of the other defects. However, the E' is introduced at a rate using the E-centre as a catalyst. The E-centre will undergo zeroth order introduction and the E' will undergo first order reactions as described by Equations 2.42 and 2.46.

The second theory assumes the linear introduction rate for the E-centre as assumed previously. Assuming that the E’ is formed by the reaction of another radiation induced defect with the E-centre, then the introduction rate for the E’ is however dependent on the concentration of the E-centre while consuming the E-centre during the annealing of the E’. The introduction rate of the E-centre after annealing the E’ will then be modelled after Equation 2.48, a first order introduction with removal of defects. It then follows that the E’ will follow Equation 2.49, a first order introduction from the consumption of another defect.

The third theory involves three defects, mainly the E-centre, E’ and an third unobservable defect (Defect 3). The E-centre would experience a linear introduction rate as seen by Equation 2.48 ($1^{st}$ order). The E’ is assumed to have an introduction rate dependant on the consumption of present Defect 3 concentration. The E’ would undergo a first order introduction from the consumption of another defect as described by Equation 2.49, while Defect 3 will undergo a first order introduction with removal of defects, described by Equation 2.48.

### 3.4.5 Conventional DLTS

Conventional DLTS was used to survey the electrically active defects that are present in the material. A scan was done before irradiation to determine if the sample was free from electrically active defects. All radiation induced defects were then identified after exposure to alpha particle radiation. The sample was exposed to alpha particle radiation at 270 K, then the DLTS scan was recorded from 270 K to approximately 20 K. The sample was then isothermally annealed at 330 K for 15 minute intervals to remove the E’. After the $E_{0.37}$ peak stopped decreasing in height, the sample was isothermally annealed at 425 K for 15 minute intervals to remove the E-centre.

### 3.4.6 Depth profiles

The sample was placed under a revers bias of -8 V. The filling pulse level was varied from -7.5 V to 0 V in increments of 0.5 V using L-DLTS at a sampling rate of 97 kHz, with 6000 samples, averaged 3 000 times. Subtraction of transient method was used to determine the depth profile of the E’.

### 3.4.7 Depth profiles of samples annealed under reverse and zero bias

A reduction in the annealing rate of the E’ was observed when the sample was placed under a reverse bias during annealing. Isothermal depth profiles were taken using the same measuring conditions as above for the depth profiles. The sample was annealed repeatedly under a reverse bias of -3 V at 330 K. After the depth profile stabilized, the bias was removed and further isothermal annealing followed.

### 3.4.8 Determining the activation energy and apparent capture cross-section (finger print)

The L-DLTS process described in Section 2.4.2 was used to determine the activation energies of the E-centre and E' using both techniques described in section 3.2.1. Pd-Ge Schottky diodes were irradiated at 270 K with alpha particles from a $^{241}$Am source with no external applied bias. L-DLTS was performed at a sampling rate of 97 kHz with 6000 samples, averaged 10000 times under a reverse bias of -2 V and a filling pulse of 0 V. Directly after irradiation, the full measurement was done over the temperature region 188 K to 212 K with 3 K increments. For the subtraction of transient method, a second full set of measurements were done after the samples were annealed at 330 K for 1 hour with no external applied bias.

### 3.4.9 True capture cross-section

The capture cross-section was determined using the L-DLTS process described in section 2.4.3 and the subtraction of transient method described in Section 3.2.1. The L-DLTS measurements were performed at 97 kHz under a reverse bias of −5 V and measuring filling pulse of 0 V with a subtraction filling pulse of −2 V. The filling pulse duration was varied from 1 μs to 0.1 s over a temperature range of 196 K to 212 K with 4 K increments. The number of samples and averages varied due to temperature dependency. The first set of capture cross-section measurements was done directly after irradiation. The second set of measurements was done after the samples were annealed at 330 K for 1 hour to give the capture cross-section of the E-centre. Using the subtraction of transient method, the capture cross-section of the E' was determined from the two sets of data.

# 4 EXPERIMENTAL RESULTS

## 4.1 Introduction

### 4.1.1 Previous investigations of E and E'

The E-centre (a vacancy paired with a group V donor atom) is one of the dominant defects induced by high energy irradiation in Group V-doped Ge. The structure and electrical properties of the E-centre are previously well understood. The dominant deep level trap observed in proton or electron irradiated Sb-doped Ge crystals have been observed to have an activation energy for electron emission of 0.37 eV. This has been identified to be related to the Sb-vacancy complex in previous studies by Nyamhere et al. (2000) where the peak was observed in Ge:Sb but not in Ge:O samples.

### 4.1.2 Vacancies induced by alpha particle irradiation

An $^{241}$Am source was used to irradiate samples with alpha particles with energies of approximately 5.4 MeV for the experiments. TRIM simulations (Ziegler, Biersack and Littmark, 1983) for the alpha particle penetration in a Pd-Ge Schottky with a 100 nm thick contact are shown in Figure 4.1. The alpha particles penetrate up to depths of 19.4 $\mu$m in the Ge layer. In this material, DLTS measurements only observed up to approximately 2 $\mu$m beneath the junction. This means the end of range damage will not be observed by DLTS measurements, and the damage produced in the sampled region should mostly be due to isolated vacancies and interstitials.

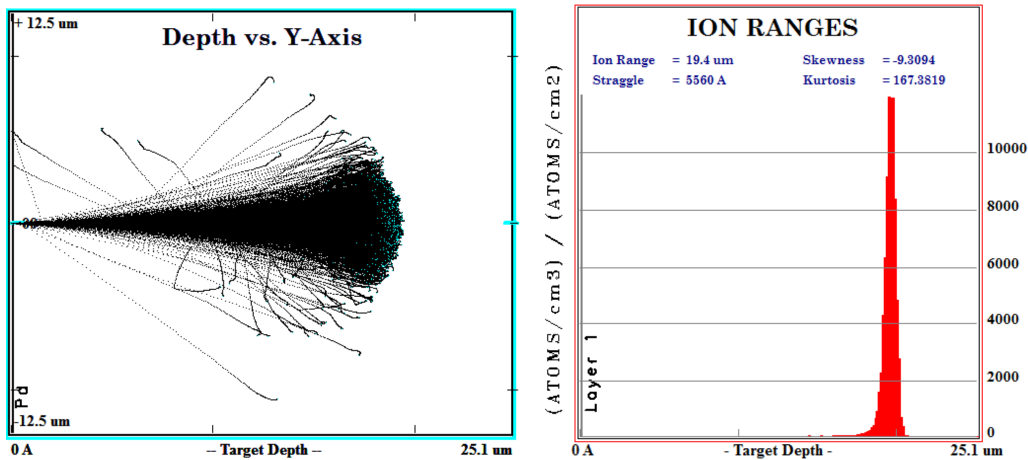


**Figure 4.1: TRIM simulation of 100nm Pd on 200 µm Ge exposed to 15000 alpha particles with 5.4 MeV energy.**

## 4.2 Results

### 4.2.1 Free carrier density

The C-V measurement obtained from the Pd-Ge Schottky diode of approximately 0.6 mm in diameter can be seen in Figure 4.2. Using Equation 3.1 the free carrier concentration was calculated to be approximately $2 \times 10^{15}$ cm$^{-3}$.

### 4.2.2 Annealing profiles

The first annealing profile that showed signs of a second defect with similar emission properties as the E-centre was an isochronal annealing profile directly after irradiation, shown in Figure 4.3 (black dots). In this profile, a peak appearing where the E-centre was expected, showed an initial decrease of concentration at room temperature (~300 K) which then stabilised and only started to anneal out at approximately 390 K. A similar annealing profile, performed a few weeks after irradiation, showed only a single annealing step. The higher annealing temperature corresponded with that observed for the E-centre, and, in this study, it is proposed that the peak annealing at lower temperature is due to a different defect, which has been called the E’.

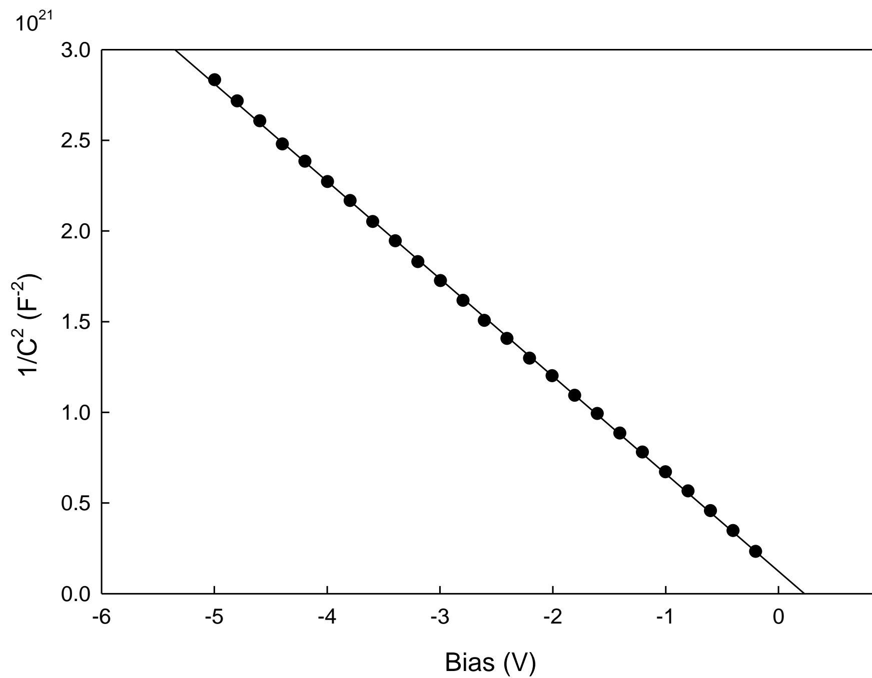


**Figure 4.2: C-V measurement of a Pd-Ge Schottky diode under a reverse bias of -5 V to -0.2 V**

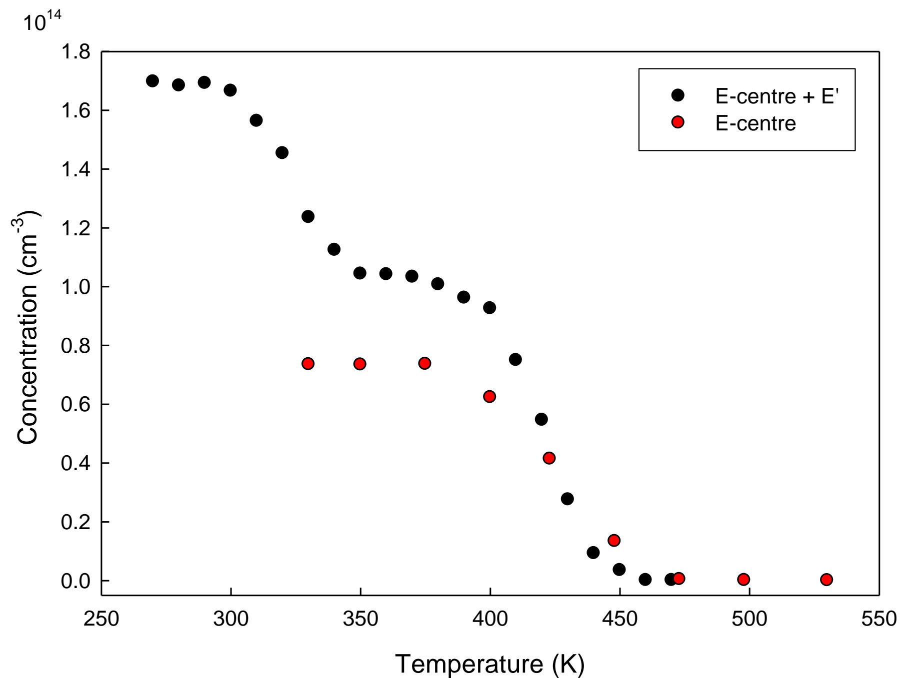


**Figure 4.3: Isochronal annealing profile of a DLTS peak corresponding to the E-centre of a sample irradiated at 270 K then immediately measured and annealed for 15 minute intervals with increasing 10 K steps (black dots). The same measurement performed on a sample that was left at room temperature for several weeks after irradiation, annealed for 15 minute annealing periods with increasing 25 K steps (red dots).**

The isothermal annealing profiles obtained for the E’ in Article 1 were found to follow first order kinetics described by Equation 3.3. This means the rate of annealing of the E’ is directly proportional to its concentration, leading to an exponentially decaying concentration as a function of time.

In order to observe different contributions of the two defects, it was necessary to have a procedure to remove all E’ reasonably fast, without influencing the E centre significantly. In Article 1 the optimal isothermal annealing procedure for removal of the E’ was found to be annealing 60 minutes at 330 K or 40 minutes at 340 K.

### 4.2.3 Conventional DLTS

Conventional DLTS measurements were done on the sample immediately after irradiation at room temperature (300 K) and at 270 K. At room temperature, 5 distinct peaks were observed as seen in Figure 4.4, but irradiating at 270 K only introduced 3 distinct peaks. The two peaks $E_{0.15}$ and $E_{0.20}$ made their appearance after the sample had been annealed at 330 K with $E_{0.37}$ reducing in height. Further annealing at 330 K showed no further increase in the two peaks but the $E_{0.37}$ decreased further to a constant height as seen in Figure 4.5. Once the sample started annealing at 425 K, the heights of all defects present started to decrease approximately exponentially, until there was barely any visible peak to observe. Previous investigations of $E_{0.15}$ and $E_{0.20}$ had shown that their introduction is time dependent and that they are introduced sometimes up to 2 weeks after irradiation (Nyamhere, 2009).The first and second annealing phase of the $E_{0.37}$ did not correspond to the introduction of new defects.

### 4.2.4 Annealing activation energy

The Arrhenius plots obtained for the E-centre and E’ from the isothermal annealing profiles can be seen in Article 4. The annealing activation energies for the E-centre and E’ were determined to be approximately 1.05 eV and 0.73 eV with pre-factors $2.05\times10^{9}$ $s^{-1}$ and $2.05\times10^{8}$ $s^{-1}$ respectively. This suggested that both defects underwent an annealing process of similar nature, which is best described as annealing by means of dissociation.

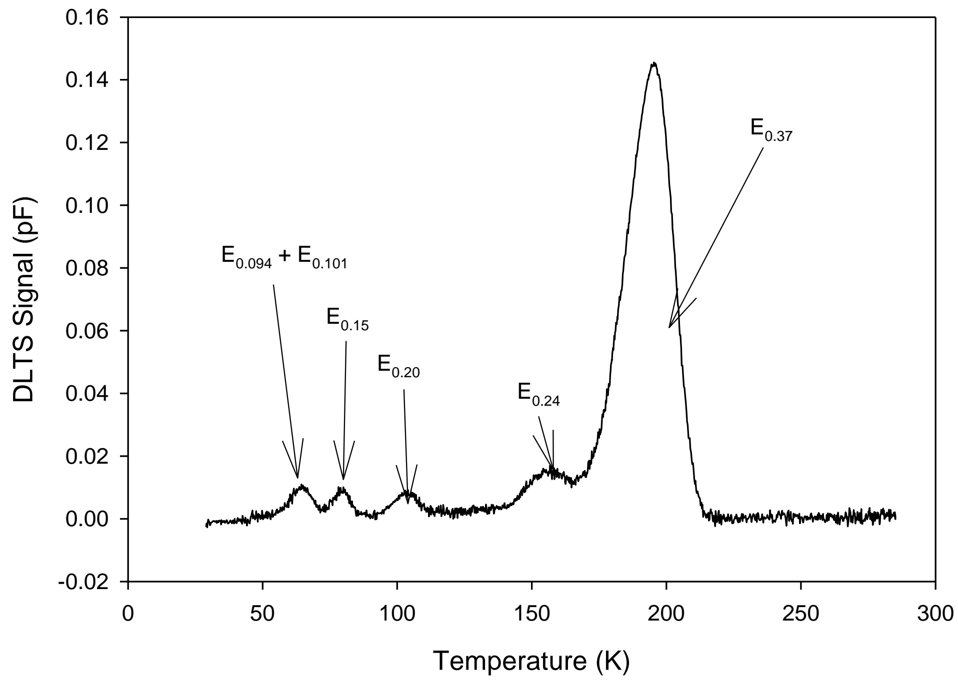


**Figure 4.4: Conventional DLTS after room temperature irradiation**

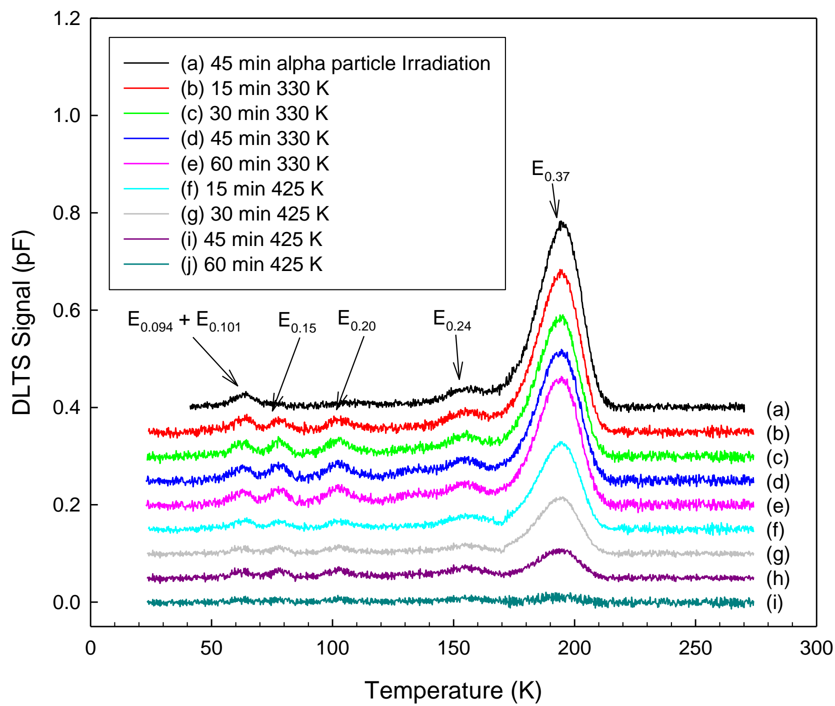


**Figure 4.5: Conventional DLTS showing the isothermal annealing of defects first at 330 K and then at 425 K.**

## 4.2.5 Introduction profiles

In Article 1 the introduction profiles of the E-centre and the E' were determined. The individual concentrations of the two defects were determined by annealing out the E' after each irradiation period. The component that did not anneal out was assumed to be due to the E-centre and the reduction observed after annealing was attributed to the E'. The introduction of the E-centre as a function of irradiation time was linear, as described by Equation 2.42. Therefore, we deduced that the E-centre had a zeroth order introduction rate and only depended on the exposure time of a constant fluence of alpha radiation. In contrast, the introduction rate of the E' seemed to be highly dependent on the concentration of the E-centre. The concentration of the E' induced after each irradiation increased with available E-centre concentration already present. The E' introduction profile was found to fit $1^{st}$ order described by Equation 2.46 and $1^{st}$ order with removal of defects described by Equation 2.49. In Article 1 the combined introduction rate best fit the model shown in Figure 2.13, strongly suggesting that he E' follows the model described by Equation 2.46. This E-centre might therefor be used as a type of catalyst for the introduction of the E' during irradiation. Further experimentation will be required to remove external factors, such as room temperature annealing during irradiation, before concrete conclusion can be drawn. More information about future experimentations will be discussed in Chapter 5 section 2.

## 4.2.6 Depth profile

### 4.2.6.1 Annealing

In Article 3 the depth profiles of the E-centre and E' were investigated. The E' was annealed out at 330 K which revealed a uniform concentration of the E-centre below the junction. Using the subtraction of transient method, the depth profile for E' was obtained, which was also uniform. Since the alpha particles penetrate the sample to much greater depths than the 2 microns observed by DLTS, These profiles suggest that neither of the defects are surface related defects.

### 4.2.6.2 Annealing under bias

Here, unlike the previous depth profile that was observed in Article 3, the sample was placed under a reverse bias during the first set of isothermal annealing's. It was observed that, under a reverse bias, the E' experienced a slower annealing rate than unbiased. The sample, of which the depth profile is shown in Figure 4.6, was irradiated at 270 K to retain as much E' as possible for observation. The depth profile for the annealing under −3 V bias showed approximately uniform annealing beneath the junction to a set concentration.

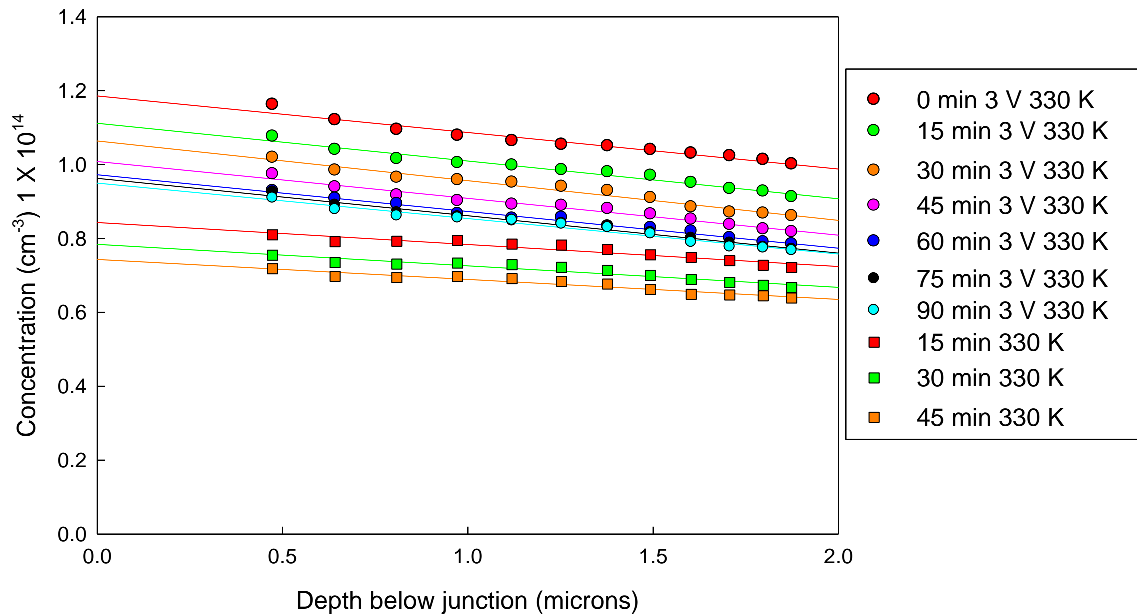


**Figure 4.6: Depth profiles of a 270 K alpha-particle irradiated sample subjected to 330 K isothermal annealing, first under a reverse bias of -3 V for 90 minutes and then later without any applied bias.**

Hereafter, annealing of the sample was continued without an applied bias under the same temperature conditions. The concentration decreased further with each annealing to a new set concentration. Further investigation of the effect of bias during the annealing of the E' will be done in future work (see Section 5.2)

The reduction of the annealing rate under reverse bias was observed experimentally and the reduction of the annealing rate was assumed to be due to a charge state of the defect. It was therefore expected that a depth profile should show a step in the profile after annealing at the point where the defect crosses the Fermi-level. This was clearly not observed, therefore it is believed that the reduction in annealing rate is due to a different mechanism.

## 4.2.7 Activation energy & apparent capture cross-section ("DLTS finger print")

In article 3 the activation energies of the two defects were identified using two techniques, namely subtraction of transient and the use of manual input of regularization parameters. The activation energy of the E-centre and E' was found to be 0.370 ± 0.005 eV and 0.375 ± 0.005 eV respectively. The apparent capture cross-section was found to be approximately $6.2\times10^{-15}$ cm$^2$ for the E-centre and $7.9\times10^{-15}$ cm$^2$ for the E'.

### 4.2.8 True capture cross-section

The capture cross-section was obtained for the combination of the two defects and each defect individually using the subtraction of transients method. There are some interesting features to be seen in peak height versus the filling pulse duration in Figure 4.7 and 4.9. The first is that it follows the general sigmoid function one expects to see for point defects. The second is that there is a second, decreasing sigmoid decreasing for increasing pulse width for both defects. The Arrhenius plot of the first sigmoid for all three cases can be seen in Figure 4.9.

The true capture cross-section over the measured temperature range of 196 K to 212 K for the E-centre ranged from $6.2\times10^{-19}$ cm$^2$ to $9.6\times10^{-19}$ cm$^2$. However, it ranged from $4.4\times10^{-19}$ cm$^2$ to $1.1\times10^{-18}$ cm$^2$ for the E' and from $5.6\times10^{-19}$ cm$^2$ to $9.7\times10^{-19}$ cm$^2$ for the combined capture cross-sections over the same temperature range.

The capture cross-section at the high temperature limit for the E-centre was obtained to be in the range of $2.0\times10^{-16}$ cm$^2$ to $2.5\times10^{-16}$ cm$^2$. These values obtained are comparable to the results obtained by Markevich (2006) of $9.2\times10^{-17}$ cm$^2$ for the V-Sb complex. The high temperature capture cross section of the E', however, was obtained to be in the range from $1\times10^{-14}$ cm$^2$ to $1\times10^{-12}$ cm$^2$. Interestingly enough, when observing the capture cross-section when the measured peak contained both the E-centre and E' it was found to lie in the range $4.5\times10^{-16}$ cm$^2$ to $1.5\times10^{-15}$ cm$^2$.

The capture barrier heights for the E-centre, E' and the two defects combined were measured to be 0.043 eV, 0.092 eV and 0.053 eV respectively. Comparing the value obtained for the E-centre to that obtained by Markevich (2006) of 0.083 eV, there are two possible reasons behind the difference. The first is that they measured directly after irradiation, which means the peak that was observed consisted of both E-centre and E' which increased their measured barrier height and the second may be that they used different biasing conditions.

The probability that a trap captures a free carrier is described by the capture cross-section and depends on the physical identity of the trap. Since the value is as high as $10^{-16}$ cm$^2$ for the E-centre and $10^{-13}$ cm$^2$ for the E' it suggests that there is Coulomb attraction between the carriers and their respective traps. The second sigmoid function that describes the decrease in the peak height with increasing filling pulse width is still under investigation. It could have been the result of the capture of a second electron by a negative-U process. Further experimentation will be done in the near future to investigate this decrease in the capture cross-section.

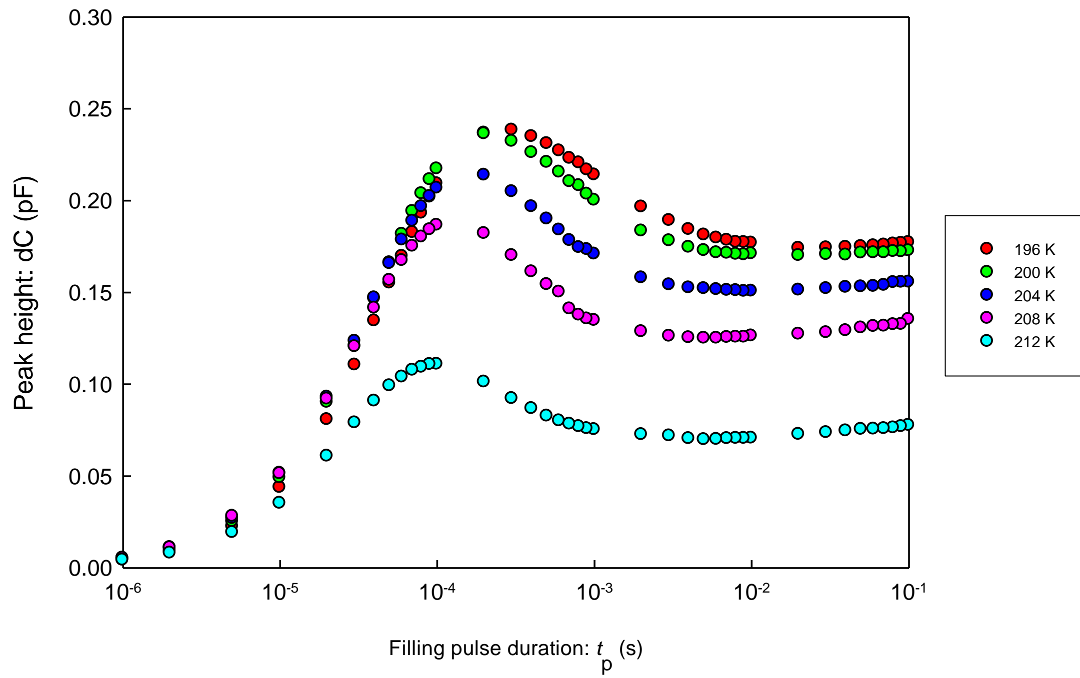


**Figure 4.7 Peak height versus the pulse width (filling pulse duration) at different temperatures of a sample irradiated at 273 K and then annealed at 330 K for 1 hour.**

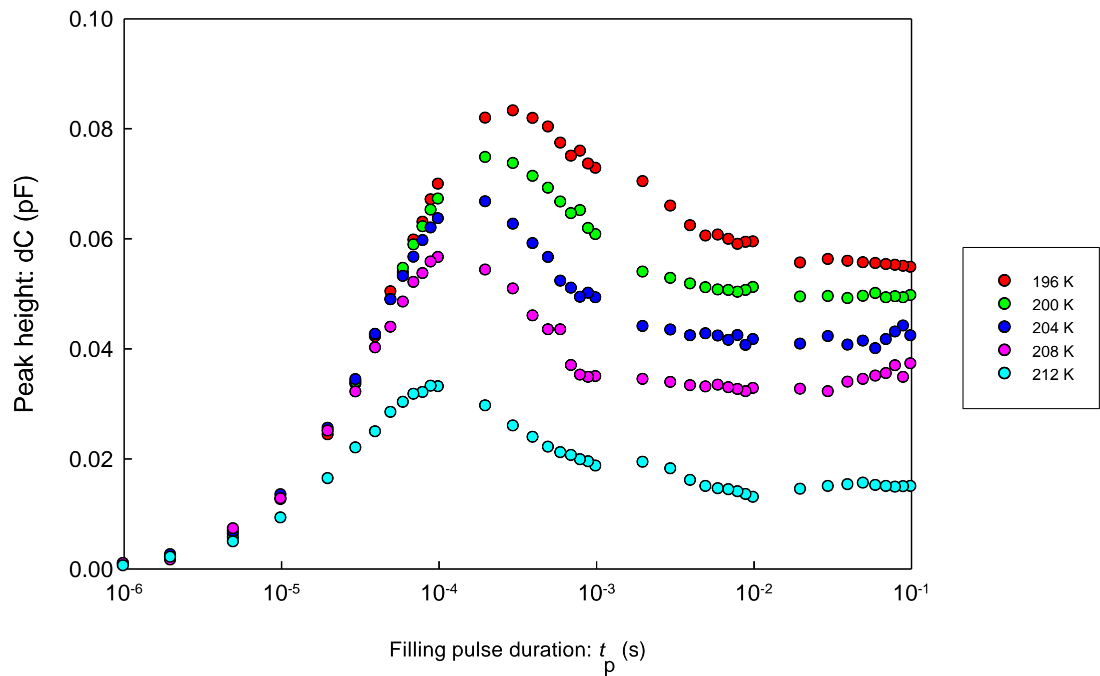


**Figure 4.8 Peak height versus the pulse width (filling pulse duration) at different temperatures of the E' obtained through the subtraction of transient method.**

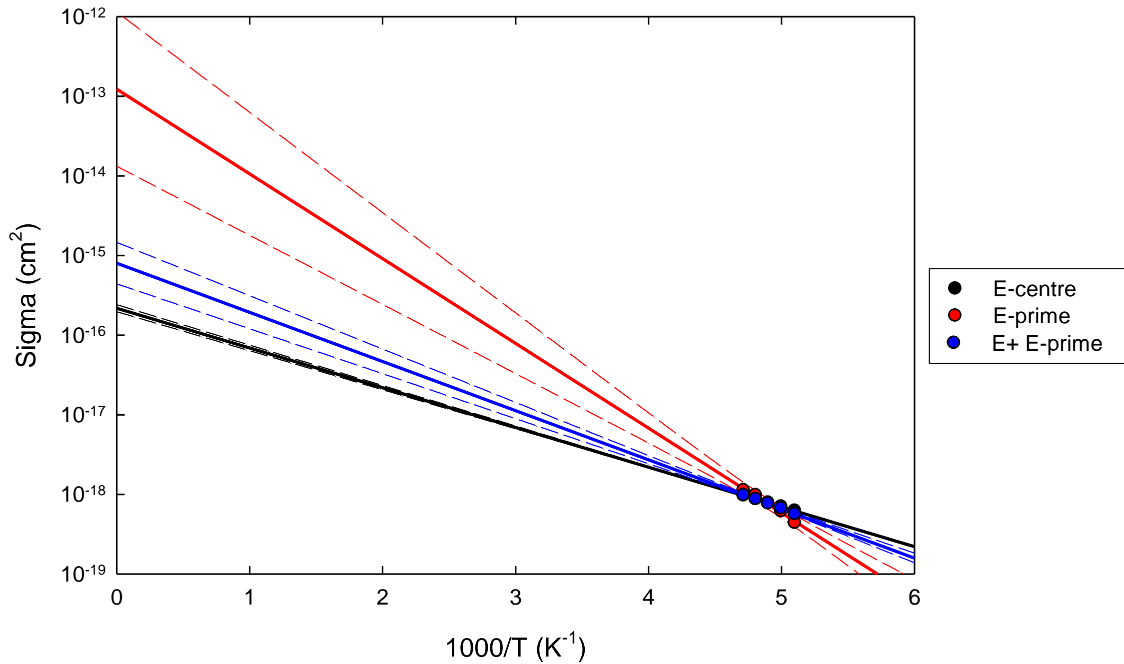


**Figure 4.9: Arrhenius obtained for the capture cross-section of the E-centre, E' and the combination of the defects. Dashed lines represent the 95% confidence intervals for each true capture cross-section.**

## 4.2.9 E' in Si

In Article 2 an isochronal annealing study was performed on samples with three different dopants, P, Sb and As, leading to three different E-centres. The P-vacancy showed signs of a second defect masked behind its emission rate which may be its E' related defect. The other two defects showed no E' related defects. Possible reasons might be that they are low temperature related defects that anneal at temperatures lower than room temperature or the nature of these traps act differently in Si when compared to Ge. Further investigations of the P-vacancy related E' will need to be carried out.

# Article 1

# Investigation of the introduction and annealing behavior of the donor-vacancy complex in alpha-particle irradiated germanium

Abraham W. Barnard, Walter E. Meyer, F. Danie Auret, Phuti N.M. Ngoepe and Sergio M.M. Coelho

Published in Proceedings of SAIP 2015

# Investigation of the introduction and annealing behaviour of the donar-vacancy complex in alpha-particle irradiated germanium

**Abraham W. Barnard, Walter E. Meyer and F. Danie Auret**

Department of Physics, University of Pretoria, Private bag X20, Hatfield 0028, Pretoria

E-mail: u10688112@tuks.co.za

**Abstract**. The annealing behaviour of the donor vacancy complex (E-centre) in Ge has been investigated by high resolution (Laplace) deep level transient spectroscopy (L-DLTS). In this study Sb-doped Ge was used and the defect was introduced by irradiating the Ge sample with alpha particles from an Am-241 source. The Sb-vacancy complex has an activation energy of 0.37 eV ($E_{0.37}$) for electron emission as determined by L-DLTS. The E-centre in Ge has been observed to anneal out in a two stage process. In the first stage the defect concentration decreases rapidly when the sample is heated to approximately 320 K, and then remains relatively constant with annealing temperature. In the second final stage, at a temperature of approximately 370 K, the defect concentration decreases quite rapidly until the defect finally anneals out completely. A possible hypothesis is that the E-centre observed is in fact two different defects corresponding to the fast and slow annealing components. However, in this study, we found that both the slow and the fast annealing components of the E-centre have the same L-DLTS signatures (activation energy and apparent capture cross-section) as well as the same true capture cross-section. In effect, both the fast and the slowly annealing components of the E-centre seem to be the same defect. We investigated this phenomenon by investigating different irradiation and annealing procedures and suggest that the fast annealing component of the E-centre can be explained by Ge self-interstitials, released from other radiation induced defects recombining with the vacancy in the E-centre.

## 1. Introduction

Germanium shares unique properties with silicon in which both have 4 valence electrons that results in the formation of tetrahedral crystal lattice. This dramatically changes the electrical properties when substitution atoms are introduced [1]. It is mainly used in a highly pure form as a detector material and is not extensively used in devices due to the overwhelming success of silicon in applied fields. This material has however gained a lot of interest recently as a semiconductor material due to improved epitaxial growth techniques for electronic and opto-electronic applications. When compared to Si, Ge is a possible candidate for fast switching transistors or complimentary metal-oxide-semiconductor (CMOS) devices due to its higher hole and electron mobility [4].

The donor vacancy pairs (E-centre) formed by introducing vacancies into the antimony doped germanium crystal lattice through alpha or electron radiation has been identified to be trap with an activation energy of 0.37 eV, which will be indicated as $E_{0.37.}$ The rate of $E_{0.37}$ introduction depends on the concentration of the Sb in the material [3]. When high concentrations of Sb are present, the $E_{0.37}$ peak dominates and becomes the sole observed peak with other defects being secondary that grow over time. Defects within germanium are removed by low annealing temperatures between 625 K and 675 K with the E-centre annealing out by dissociation and diffusion of the vacancy. Annealing with a reverse bias delays or prevents annealing of the E-centre in Ge which is a contrast to the annealing of the E centre in Si which has a bias enhancement [2].

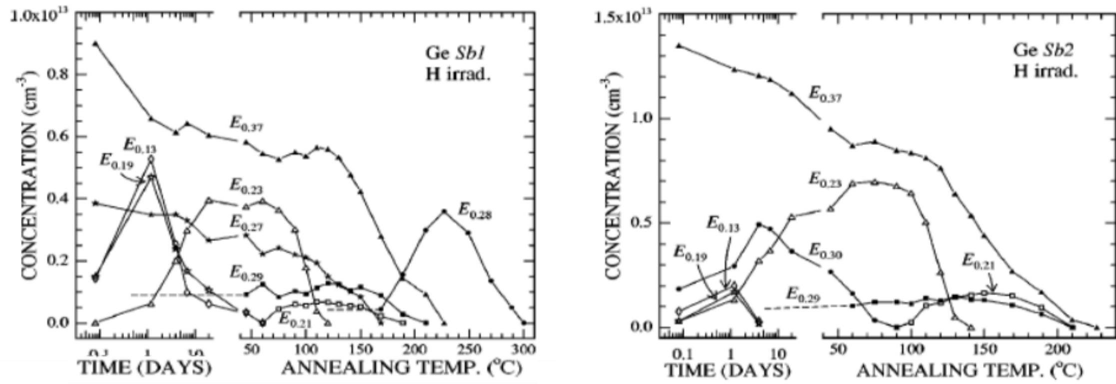


**Figure 1.** Isothermal annealing at room temperature followed by isochronal annealing at intervals of 15 minutes for two germanium samples Sb1 and Sb2 after exposure to proton radiation [2].

The $E_{0.37}$ observed by J. Fage-Pedersen and A. Nylandsted Larsen in figure 1 showed a reduction in concentration when exposed to room temperature and a further reduction once exposed to temperatures greater than 400 K. It was found that a major fraction of $E_{0.37}$ anneals at approximately 450 K. Over a large temperature span, thermally activated diffusion or association would not proceed. Thus if the $E_{0.37}$ peaks don't contain large contributions from other defects there has to be some kind of unstable source created during the irradiation that release mobile species at room temperature that consumes the E-centre [3].

## 2. Experimental details

The Ge supplied by Umicore used in this study was bulk grown (100) n-type germanium. Multiple samples of approximately 6 mm by 3 mm were first degreased with trichloroethylene, isopropanol and methanol for 5 minutes each then etched in a mixture of $H_2O_2$:$H_2O$ with a ratio of 1:5 for 1 minute and dried with nitrogen. Immediately after cleaning a layer of 80 nm AuSb was deposited on the backside forming the ohmic contacts through resistive evaporation. After formation of the ohmic contacts, the samples were rinsed of with isopropanol for 5 minutes and dried off with nitrogen before being annealed at 650 K for 10 minutes in an environment flushed with argon at a rate of 0.1 litres per minute. The samples were cleaned with isopropanol for 5 minutes again and etched with the same mixture of $H_2O_2$:$H_2O$ for 1 minute before being dried off with nitrogen. Gold circular dots, 100 nm thick, with a diameter of approximately 0.6 mm were grown at a rate of 0.1 nm per second through resistive evaporation on the front of the samples.

Three doping densities were deployed and are denoted as GeSb1, GeSb2 and GeSb3 with the first two approximated to contain $1 \times 10^{15}$ cm$^{-3}$ Sb and the third measured to have $2.6 \times 10^{15}$ cm$^{-3}$. One contact on GeSb1 was exposed to Am-241 in intervals of 30 minutes and annealed at 330 K for 60 minutes after each exposure. L-DLTS was performed at 195 K after each exposure and annealing, up to a resultant exposure of 180 minutes. The second sample (GeSb2) underwent the same procedure but was exposed in intervals of 40 minutes with the third exposure being 50 minutes. Three other contacts on GeSb1 were exposed for the full length of 180 minutes then annealed at 330K for 60 minutes with a L-DLTS spectrum taken at 195K. Another contact on GeSb2 and a contact on GeSb3 were exposed at intervals of 30 minutes with a Laplace transient recorded after each exposure.

In this paper we have studied the introduction and annealing kinetics of two defects that have a similar energy level which has previously been identified as the E-centre.

## 3. Experimental results

The energy level $E_{0.37}$ may represent at least two defects with very similar energy levels that cannot be distinguished through conventional DLTS methods due to the resolution not being high enough. For convenience sake we will denote the first reduction as the removal of the $E'_{0.37}$ and

the second reduction as the removal of the E-centre ($E_{0.37}$) that was observed by many. This peak was identified to lie approximately at 195 K on the conventional DLTS spectrum, thus we used L-DLTS at this temperature for higher resolution [5]. However even using this high resolution technique, it was not possible to distinguish between the two traps.

### 3.1. Introduction kinetics of $E_{0.37}$

The introduction rate of the $E_{0.37}$ was determined by introducing both defects through alpha radiation as seen in figure 2 and removing only the $E'_{0.37}$ from the two germanium samples by means of low temperature annealing. The introduction of $E_{0.37}$ was tested by introducing both defects for the full exposure time period on multiple points on the GeSb1 sample. After removing the $E'_{0.37}$ defect it was found that the introduction of the $E_{0.37}$ was linear and did not depend on whether the $E'_{0.37}$ was annealed out during or after the irradiation. This is shown clearly in figure 2 where the concentration after annealing (red dots) showed a linear relationship with irradiation time, irrespective of the annealing occurring in one step after irradiation or in shorter steps between irradiations. The introduction kinetics for $E_{0.37}$ was observed to be linear which suggests that is was of a first order introduction which is consistent with vacancies captured by Sb.

### 3.2. Introduction kinetics of $E'_{0.37}$

The combined introduction rate of $E'_{0.37}$ and $E_{0.37}$ through alpha particle radiation was determined to be that of a quadratic function. This was determined by introducing both defects into the crystals at intervals of 30 minutes and then modelling their combined introduction rate against the equation.

$$Nt = At^{B}$$

where *Nt* is the trap concentration and t is the total exposure time to alpha radiation. In figure 3 the best fit with the equation, GeSb2 was found to have $A = 6.67 \times 10^{9}$ with $B = 2.04$ and GeSb3 was found to have $A = 1.02 \times 10^{10}$ with $B = 2.02$. This suggests an introduction rate for the simultaneous introduction of both defects to be that of a quadratic nature. Since it was earlier determined that the introduction kinetics of the $E_{0.37}$ was that of a linear nature, it can easily be seen that the introduction kinetics of the $E'_{0.37}$ is that of a second order process.

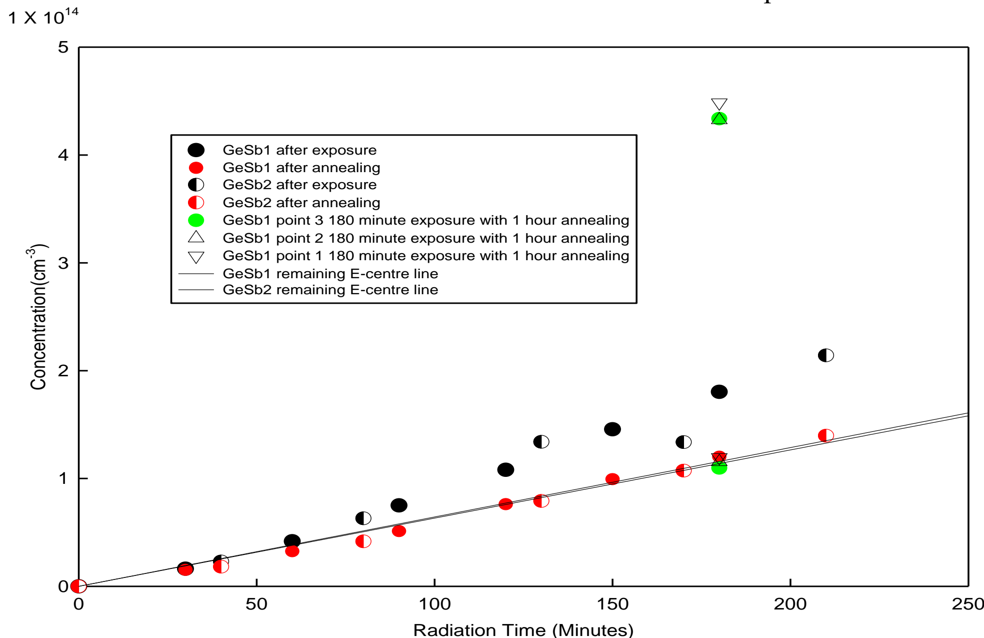


**Figure 2.** GeSb1 exposed to alpha radiation at 30 minute intervals with 60 minutes 330 K annealing after each exposure. GeSb2 exposed to alpha radiation at 40 minute intervals with same annealing procedure

with the third exposure being 50 minutes. Three GeSb1 points exposed to alphas for 180 minutes then annealed at 330 K for 60 minutes.

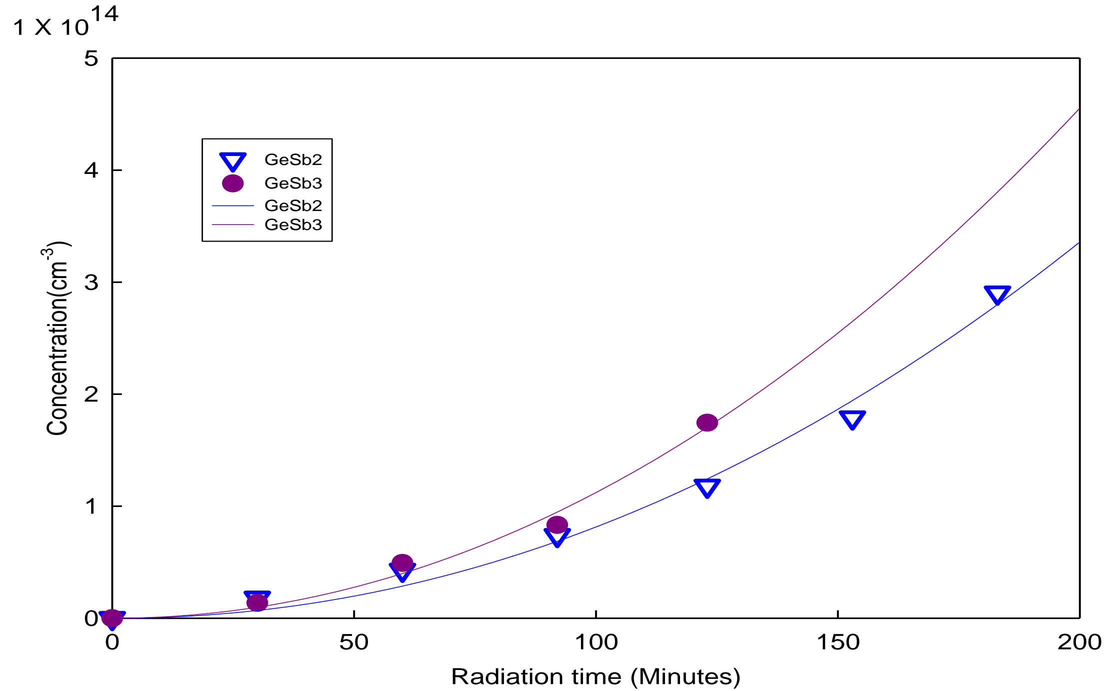


**Figure 3.** The concentration of the simultaneous introduction of $E'_{0.37}$ and $E_{0.37}$ in the samples GeSb2 and GeSb3 which were exposed to AM-241 at intervals of 30 minutes.

3.3. Annealing behaviour of $E_{0.37}$ and $E'_{0.37}$

This annealing behaviour of the $E'_{0.37}$ peak that is observed through Laplace DLTS was reconfirmed by exposing one of the germanium samples to alpha radiation and immediately doing isothermal annealing measurements on it. It was found that the annealing behaviour at room temperature (300K) was described as exponential decay to a constant concentration. This is consistent with first order decay of the first component with a second component remaining. This annealing behaviour was also confirmed in figure 4 at temperatures of 315 K and 330 K where exponential decay with greater decay constants were observed. We will refer to the component that anneals out in this first stage as the $E'_{0.37}$ defect. Annealing at 330 K for 60 minutes has been found to guarantee the removal of the $E'_{0.37}$ for experimental purposes. Only once the sample was exposed to temperatures greater than 400 K which is seen in isochronal annealing's in figure 5, did the rest of the $E_{0.37}$ peak that is observed in Laplace DLTS anneal away.

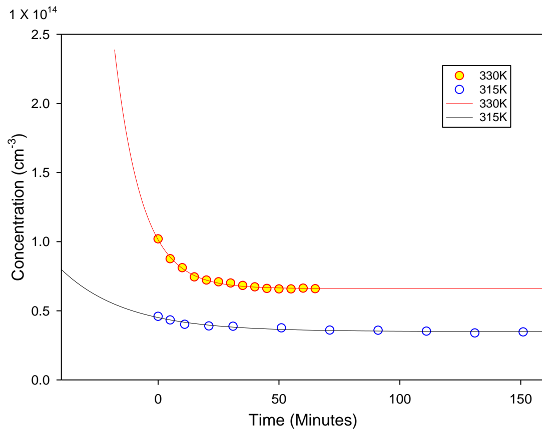


**Figure 4.** Isothermal annealing of the $E'_{0.37}$ defect at 315 K and 330 K.

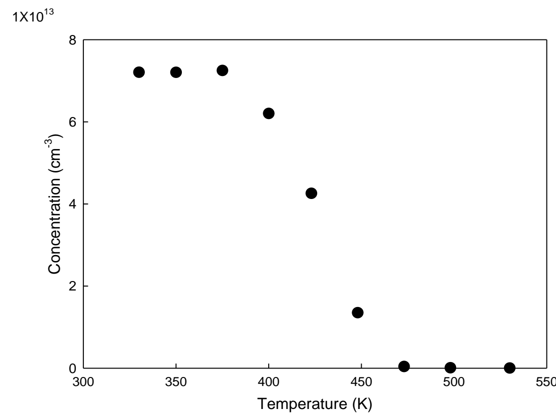


**Figure 5.** Isochronal annealing of the $E_{0.37}$ defect at time intervals of 15 minutes at 25 K increments.

## 4. Conclusion

It was found that the two defects $E'_{0.37}$ and $E_{0.37}$ cannot be distinguished through DLTS or through high resolution techniques such as L-DLTS. The introduction kinetics of the $E_{0.37}$ was found to be linear and the introduction kinetics of the $E'_{0.37}$ was found to be quadratic. The annealing of both the $E_{0.37}$ and $E'_{0.37}$ through isochronal annealing was found to exhibit exponential decay. The $E'_{0.37}$ anneals out first at temperatures as low as room temperature with the $E_{0.37}$ which experiences annealing at temperatures greater than 400K. Since the introduction rate of the $E_{0.37}$ is linear it is consistent with the theory of vacancies captured by Sb. The quadratic nature of the $E'_{0.37}$ suggests the reaction of newly introduced defects with previously introduced defects through radiation. A possible theory that will still need to be investigated through density functional theory would be that there may be a self-interstitial captured by the E centre defect which is then seen as the $E'_{0.37}$ defect.

## References

[1] S.M. Sze, Physics of Semiconductor devices, Wiley & Sons, Canada, 1981.
[2] J.Fage-Pederson, A. Nylandsted Larsen, Irradiation-induced defects in Ge studied by transient spectroscopies, Physical Review B, **62** 15 (2000) 10116.
[3] A. Mesli, L. Dobaczewski, K. Bonde Nielsen, V.L. Kolkovsky, M. Christian Petersen, and A. Nylandsted Larsen, Low-temperature irradiation-induced defects in germanium: In situ analysis, Physical Review B, **78** (2008) 165202.
[4] R. Hull, J.C. Bean (Eds.), Germanium Silicon, Physics Materials, Semiconductor and Semi-metals, vol. 56, Academic, San Diego, 1999.
[5] A.R. Peaker, Laplace deep level transient spectroscopy: Embodiment and evolution, Pysica B: Condensed Matter, **407** 15 (2012) 3026

Article 2

# Investigation of the isochronal annealing profiles of the E-centres in n-type silicon through Laplace deep-level transient spectroscopy

Abraham W. Barnard, Walter E. Meyer and F. Danie Auret

Submitted to Proceedings of ICACS 2016 Elsevier

# Investigation of the isochronal annealing profiles of the E-centres in n-type silicon through Laplace deep-level transient spectroscopy

**Abraham W. Barnard, Walter E. Meyer and F. Danie Auret**

Department of Physics, University of Pretoria, Private bag X20, Hatfield 0028, Pretoria

E-mail: u10688112@tuks.co.za

**Abstract**. The vacancy-dopant complex in silicon, often referred to as the E-center, is a well-known defect. In this study, we investigated vacancy complexes with three common dopants namely phosphorous, antimony and arsenic by measuring isochronal annealing profiles of all three in n-type silicon. Si samples doped with P and combinations of P with Sb and As were exposed to alpha radiation from an Am-241 source. By making use of high-resolution Laplace deep-level transient spectroscopy (Laplace-DLTS), we distinguished the different E-centres from each other, and measure their annealing rates individually. We found that phosphorous-vacancy, arsenic-vacancy and antimony-vacancy start annealing at temperatures 390 K, 415 K and 450 K respectively. A previously unobserved defect related to the phosphorous dopant was observed to start annealing at 340 K.

## 1. Introduction

Silicon (Si) is a common semiconductor material used in solid state devices in the microelectronics industry. The crystal structure of Si is commonly referred to as the diamond structure, which may be described as two interpenetrating face centred cubic lattices [1]. When pure silicon is doped with group V elements such as phosphorus (P), arsenic (As) or antimony (Sb) it results in the formation of n-type semiconductor material. Group V elements contribute excess of free electrons resulting in an increase in the conductivity of intrinsic semiconductors. The E-centers are combinations of vacancies and dopants and have been found to have energy levels of 0.40 eV, 0.435 eV and 0.45 eV for Sb-vacancy, As-vacancy and P-vacancy respectively [2].

Conventional-DLTS involves the investigation of capacitance transients measured at varying temperature. In this technique the transient is analyzed by an electronic system sensitive to a given emission rate, referred to as the rate window. During the temperature variation that the sample undergoes, the emission rate of carriers from a defect will vary. When the emission rate is equal to the rate window, a peak in the spectrum is obtained. Laplace-DLTS is an isothermal extension of conventional-DLTS that is known for its high resolution in determining emission rates of carriers from defects. Here, the emission rates are obtained from the inverse Laplace transformation of capacitance transients that are captured and averaged at fixed temperatures [3].

Isochronal annealing is a thermal annealing technique for removal of radiation induced defects. During this process the sample undergoes repeated thermal annealing for a fixed time with temperature being increased at constant intervals. This technique can be used for identification of defects or determining activation energies which indicate te mechanism according to which the defect anneals, i.e. recombination, complex dissociation, migration or complex formation [4].

## 2. Experimental details

P-doped epitaxial Si with a free carrier concentration of $1.1 \times 10^{16}$ cm$^{-3}$ and a thickness of 6 µm was used. This wafer was commercially grown using chemical vapour deposition on an n$^{++}$ substrate. The wafer was then cleaved into 4 pieces with the first piece being used as a control. The second piece was implanted with As and the third with Sb to concentrations of approximately $1\times10^{16}$ cm$^{-3}$ for each dopant. The fourth piece was doped with both As and Sb to yield approximate concentrations of $1\times10^{16}$ cm$^{-3}$ of each dopant. By performing a set of implantations at different energies, a uniform profile of dopants for the first 1.2 µm below the surface was achieved. The 3 implanted samples were then annealed at 950 °C for 30 minutes in a nitrogen flushed environment. This allowed for activation of the dopants and removal of disorder due to implantation.

The samples cut from these wafers were degreased by dipping them in trichloroethylene, isopropanol and methanol for 5 minutes each. Etching was done directly afterwards with hydrofluoric acid (40%) for 1 minute before drying the sample with nitrogen gas and mounting it for evaporation. Ohmic contacts of Au-Sb (0.6% Sb), 100 nm thick were deposited on the back surface of the Si at a rate of 0.1 nm per second by means of resistive evaporation. The samples were degreased and etched again before the deposition of 100 nm palladium Schottky contacts on the front surface of the Si. The samples were irradiated by an Am-241 source with a fluence rate of $7.1\times10^{6}$ cm$^{-2}$s$^{-1}$. The P-doped sample was exposed for 24 hours. The samples doped with P and a combination of either As or Sb were exposed for 2 days while the sample doped with all 3 dopants was exposed for 3 days. Isochronal annealing was done at intervals of 10 K from 300 K to 600 K for either 15 or 30 minute annealing intervals. The annealing was done by placing the samples on a silver heating plate in an argon environment which fluctuated by approximately 0.15 K during the mounting of the sample. The samples were rapidly cooled down to 300 K after each annealing period. L-DLTS was performed after each annealing at 225 K to observe the 3 vacancy dopant complexes as well as the di-vacancy.

## 3. Experimental results

### 3.1. Isochronal annealing behaviour of P-doped Si

The first sample which was only doped with P was exposed to alpha radiation for 24 hours. Laplace-DLTS which was done at 225 K only revealed a single spectrum peak which suggested only a single defect present in this temperature region after irradiation. However with low noise measurements (i.e average noise <0.1 fF) and increasing the resolution through manual input of regularization parameters this peak would occasionally split into two different peaks identified as due to the di-vacancy and the P-vacancy. The emission rates of these two peaks were always less than a factor 4 apart resulting in uncertainty in true concentrations present of the two defects.

Isochronal annealing was done every 10 K from 300 K to 600 K for periods of 30 minutes. The annealing profile as seen in Figure 1, however, suggested the presence of 3 defects within the single peak observed. The first defect starts annealing around 340 K and seems to be almost completely annealed out at 380 K before the second defect starts annealing at 390 K. The spectrum shows that the defect remained at a relative stable concentration before dropping again at 570 K as the third defect started annealing out. The second defect has been identified to be the P-vacancy defect with the third defect known to be the di-vacancy. However, the first defect has not been identified or been seen before and may be the result of a new defect due to alpha irradiation.

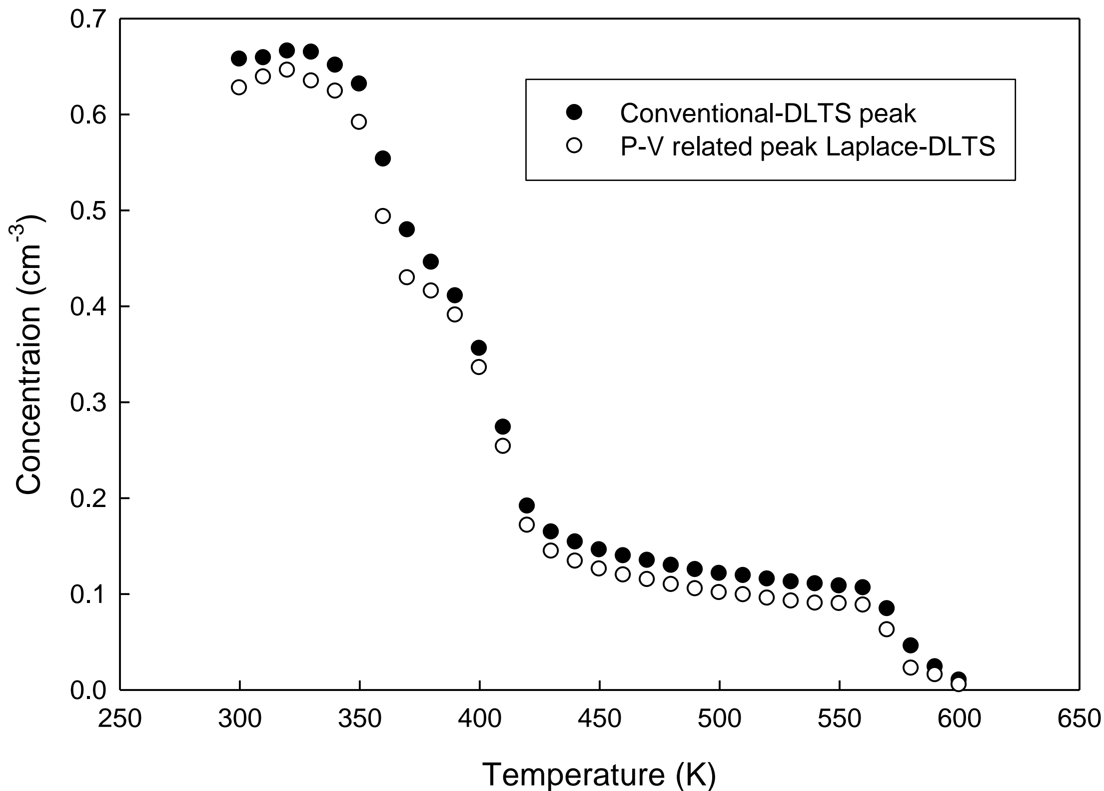


**Figure 1.** Isochronal annealing behavior of defects in P-doped Si after 24 hours exposure to alpha radiation. The sample was annealed for 30 minutes every 10 K interval.

3.2. Isochronal annealing behaviour of Si dual doped with P and Sb

Laplace DLTS done at 225 K on Si dual doped with P and Sb after being irradiated with alpha particles at room temperature for 48 hours revealed two distinguishable peaks as seen in Figure 3. The left hand side peak has been identified to be due to both the P-vacancy and di-vacancy which was observed in the P-doped Si. Using the same conditions used with the P-doped Si resulted in a new peak on the left of the original, unchanged peak. Since the emission rate of two peaks was a factor greater than 4 apart the concentration of Sb-vacancy present was easily determined. Isochronal annealing on the sample was done from 300 K to 600 K at intervals of 10 K for 15 minute periods. The conventional-DLTS profile as seen in Figure 4 could only distinguish the three defects that were seen in the P-doped Si as there was no indication of where the Sb-vacancy started to anneal. From the Laplace-DLTS spectrums we obtained the same profile for the left peak as in Figure 1. However, the right hand side peak gave the annealing profile of the Sb-vacancy which started to anneal at 450 K.

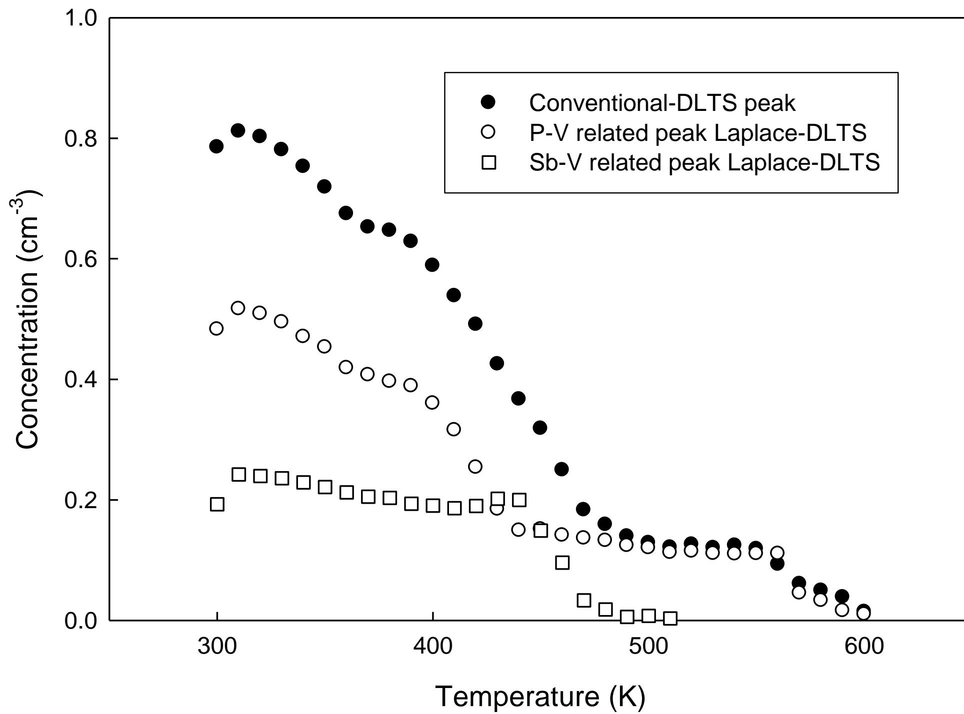


**Figure 2.** Isochronal annealing behavior of Si dual doped with P and Sb after 48 hours exposure to alpha radiation. This is the comparison between conventional and Laplace-DLTS of 15 minute annealing's at 10 K intervals of the samples defects.

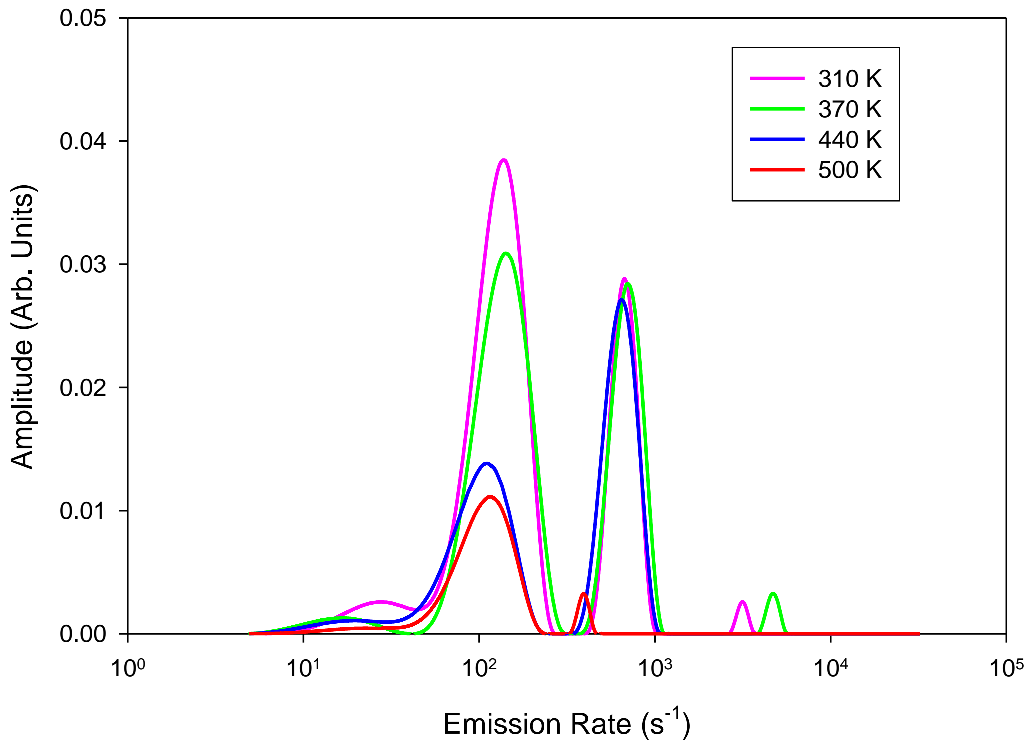


**Figure 3.** Laplace-DLTS spectrum showing the isochronal annealing behaviour of the defects in Si dual doped with P and Sb. Annealing was done every 10 K from 300K to 600K at 15 minute intervals. For clarification purposes only key spectrums are shown where a defect has been annealed out. The peak on

the left is related to the P-vacancy complex combined with the di vacancy and the right side peak is related to the Sb-vacancy complex.

### 3.3. Isochronal annealing behaviour of Si dual doped with P and Sb

The Laplace-DLTS spectrum generated from Si doped with P and As at 225 K were less than a factor 4 apart making it impossible to determine independent defect concentrations. The single peak could be split into 3 individual peaks using the conditions as previously mentioned however the rates and heights varied with each repeated measurement. The dual doped sample was exposed 48 hours to alpha radiation and annealed for 15 min in steps of 10 K. The profile as seen in Figure 4 shows only hints of the new defect seen in the previous samples at 350 K. The P-vacancy started to anneal at 390 K however the As-vacancy's annealing profile intertwines with the P-vacancy profile making it impossible to determine it in this manner. The next sample was annealed at 405 K for 4 hours to remove the P-vacancy before isochronal annealing was done from 405K onwards for 15 minute intervals. This left an uncertainty since the decrease in concentration seems to already occur at 415 K as seen in Figure 4.

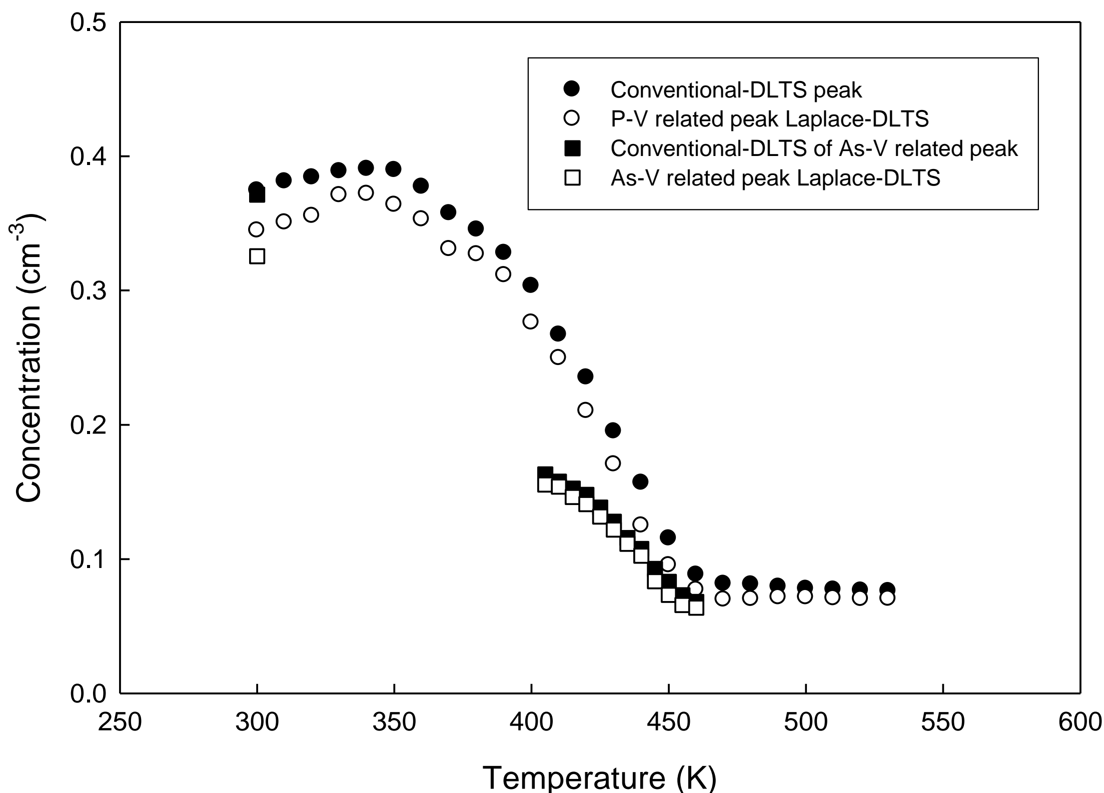


**Figure 4.** Isochronal annealing behavior of defects Si dual doped with P and Sb after 48 hours exposure to alpha radiation. The first sample was annealed for 15 minutes at 10 K intervals from 300 K to 530 K. The second sample was annealed at 405 K for 5 hours then annealed for 15 minutes at 5 K intervals from 410 K to 460 K.

## 4. Conclusion

We were able to successfully distinguish between the P-vacancy complex and the Sb-vacancy complex using Laplace DLTS. Identification of the defects became increasingly difficult through

Laplace-DLTS when the number of defects present with similar emission rates increased. Laplace-DLTS was unable to clearly distinguish emission rates for the sample doped with all 3 dopants as it resulted in a single linear isochronal profile for all 3 E-centres with no distinguishable features. The 3 E-centres P-vacancy, As-vacancy and Sb-vacancy started to anneal out at temperatures 390 K, 415 K and 450 K respectively. The di-vacancy was found to start annealing at 570 K. A new defect that is related to the P-vacancy complex was found to start annealing at 340 K. This defect was observed for the P-doped sample and the samples dual doped with P and either As or Sb. The annealing of any E-centre had no effect on the concentration of the other E-centres present in the lattice.

**References**

[1] Dimitrijev S 2006 *Principles Of Semiconduter Devices* (New York: Oxfors University Press)
[2] Auret FD, Peaker AR, Markevich VP, Dobaczewski L and Gwilliame RM 2006 Physica B: Condensed Matter **376-377** 73More references
[3] Dobaczewski L, Kaczor P, Hawkins ID and Peaker AR 1994 *J. Appl. Phys.* **76** 194
[4] Lanoo M and Bourgoin J 1981 *Point Defects in Semiconductors II* (Springer-Verlag) 247

# Article 3

# Properties of a previously unobserved donor-related electrically active defect in Ge induced by alpha-particle irradiation

Abraham W. Barnard, Walter E. Meyer and F. Danie Auret

Published in Proceedings of ICACS 2016

# Properties of a previously unobserved donor-related electrically active defect in Ge, introduced by alpha-particle irradiation

**Abraham W. Barnard, Walter E. Meyer and F. Danie Auret**

Department of Physics, University of Pretoria, Private bag X20, Hatfield 0028, Pretoria, South Africa

E-mail: u10688112@tuks.co.za

**Abstract**. Alpha particle irradiation was used to study the radiation-induced defects in n-type germanium (Ge). Investigation of the well-known antimony (Sb)-vacancy complex (commonly known as the E-center) in Ge, with an activation energy of 0.37 eV ($E_{0.37}$), has led to the discovery of another defect with a DLTS signature virtually indistinguishable from the E-center, but with different annealing characteristics. We shall refer to this new defect as the E-prime. Although the two defects are easily distinguishable by annealing, the DLTS signal produced by the E-center and E-prime were not distinguishable through conventional deep level transient spectroscopy (DLTS). Separation of the two peaks was only possible through the use of low noise equipment in conjunction with high resolution Laplace-DLTS. The activation energy of the Sb-vacancy and the E-prime was determined to be 0.370 ± 0.005 eV and 0.375 ± 0.005 e. Depth profiles showed uniform distribution of both defects below the Schottky junction.

## 1. Introduction

Sb doped Ge crystals exposed to either proton or electron radiation contain a prominent deep level trap due to the Sb-vacancy complex. Fage-Pederson and Larsen [1] studied the annealing behavior of this defect and found it to anneal out in two stages. The first reduction of the concentration occurs at room temperature (300 K) with the second reduction at temperatures of greater than 400 K. Fage-Pederson and Larsen attributed the first reduction to mobile species released at room temperature from an unstable source consuming some of the E-center. In this paper we show that careful measurements by Laplace DLTS can distinguish the defect annealing out at room temperature from the defect annealing out at 400 K. We therefore believe that there are two different defects with very similar DLTS signatures involved. In this paper we refer to the defect annealing out at low temperature as the E-prime, while the component annealing out at high temperature, which has up to now usually been studied, we will call the E-center, as is traditional. In a previous study we have shown that the introduction rate of the E-prime depends on the concentration of the E-center, which indicates that the two defects may be structurally related [2].

Deep-level transient spectroscopy (DLTS) is a tool used to experimentally observe electrically active defects in semiconductors. This technique measures the capacitance of a Schottky diode in order to detect the emission of carriers from defects in the diode's depletion region and is used for the identification of defects. Conventional DLTS measures capacitance transients as a function of temperature using a box-car averaging technique, which is sensitive to a specific emission rate window. When the emission rate is equal to the rate window, a peak is obtained [3]. However, this peak is broad and it is not possible to distinguish two defects with closely spaced emission rates. Laplace DLTS enhances the resolution of conventional DLTS and is known as a high resolution technique. Laplace DLTS involves measuring many capacitance transients at a set temperature and averaging them. An inverse Laplace transform is then performed on the average capacitance transient to deconvolute the transient to individual exponential decays. By using L-DLTS it is often possible to deconvolute a single peak observed by means of conventional DLTS into a number of peaks with different emission rates [4].

Laplace-DLTS is based on the assumption that a transient obtained in conventional-DLTS may contain multiple emission spectrums. With this in mind the capacitance transient obtained from a Laplace-DLTS measurement will be the sum of multiple transients for multiple emission spectrums. In the case of this paper the two defect emission rates were at the limit of what can be distinguished by Laplace-DLTS [5].

The defects were separated by means of annealing by assuming that the measured transient is the resultant of both transients. Directly after irradiation, a resultant capacitance transient, due to both defects, was recorded. The sample was then annealed to remove the low-temperature annealing defect, and a transient due to only the high temperature annealing defect was recorded. The two transients were then subtracted and the difference between these two transients would represent the transient emitted by the defect that was annealed. This allows for the measurement of individual emission rates without interference of other emission rates. In this paper, this method of defect analysis will be referred to as the subtraction of transients method.

## 2. Experimental details

The semiconductor material used in this study was (111) bulk grown n-type Ge supplied by Umicore. The doping density of the substrate has been determined as approximately $2 \times 10^{15}$ $cm^{-3}$ by CV measurements [6]. Multiple samples of 3 mm by 3 mm were degreased using trichloroethylene, isopropanol and methanol for 5 minutes each. Etching was done directly afterwards using a mixture of $H_2O_2$:$H_2O$ with a ratio of 1:5 for 1 minute for removal of the oxide layer where after the sample was dried with nitrogen. Immediately after the etching process the samples were mounted onto a sample holder and a layer of 150 nm of Au-Sb (0.5% Sb) was resistively deposited on the back surface under a vacuum of $1 \times 10^{-6}$ mbar at a rate of 0.1 nm per second. This was followed by a 10 min annealing at 650 K in an argon flushed environment. The same cleaning and etching process was used before resistive deposition of the 100 nm palladium Schottky barrier diodes (SBDs), 0.6 mm in diameter, through a metal mask under a vacuum of $5 \times 10^{-7}$ mbar at a rate of 0.1 nm per second.

Alpha particle irradiation with an energy of approximately 5.4 MeV from an $^{241}$Am source was used to irradiate the sample with a fluence rate of $7.1\times10^{6}$ $cm^2$ $s^{-1}$ and introduce the dominant Sb-vacancy trap. The samples were exposed to this source at 270 K for 2 hours under zero bias in a vacuum of $2 \times 10^{-3}$ mbar to prevent condensation and any loss of the E-prime defect due to annealing. Laplace DLTS was used to determine the Arrhenius plots and depth profiles by two different methods. The first method was done through subtraction of transients: The Laplace DLTS transients of the samples were first measured giving a summation Arrhenius and depth profile of the two defects. The E-prime defect was then annealed out at 330 K for 1 hour. The transients were measured again to give the Arrhenius and depth profile of only the Sb-vacancy defect. The transients of just the Sb-vacancy were subtracted from the corresponding transients containing both defects to give a transient that represents only the E-prime defect which allowed the determination of the Arrhenius and depth profiles of the E-prime defect alone.

The second method was through splitting of the peak by means of Laplace DLTS: By using low noise cables that were kept as short as possible and taking the average of 10 000 transients, it was possible to obtain a signal to noise ratio better than 1000 to 1. Manual input of the regularization parameters to the Laplace inversion routine allowed the peak to be split into two peaks with emission rates approximately a factor two apart. Laplace DLTS was done at a sampling rate of 97 kHz, with 6000 samples, averaged 10 000 times with a reverse bias of -2 V and filling pulse level, $V_p$, set to 0 V.

## 3. Experimental results

The spectrum obtained from Laplace DLTS after irradiating the sample at 270 K for 2 hours can be seen in Figure 1 (d). After the samples were annealed at 330 K for 1 hour the emission spectrum for the Sb-vacancy complex emission (b) was observed. In comparison to the emission rate

originally obtained, the peak decreased in height and shifted towards the right after annealing. The shifting of the peak after annealing shows that there is a second defect with a similar but lower emission rate (i.e. to the left of the peak). This causes a resultant emission rate of both defects when present in the material. Subtracting the capacitance transients from each other produced a new transient with an emission rate (c) shifted towards the left. This emission rate is related to the E-prime complex. The transient obtained after irradiation (d) was used in conjunction with manual input of regularization parameters resulting in two unique peaks with emission rates similar to that obtained using the subtraction of transient method.

The regularization parameter determines how easily the inversion algorithm will split a broad single peak into two (or more) single peaks. Manual regularization parameters were used to allow the inversion routine to take into consideration the possibility of 2 or more closely spaced peaks. Upper and lower limits of the regularization parameters were observed during the calculations of the emission rates. Values above the upper limit would result in a single peak with no distinct features. Just below the upper limit the peaks partially start splitting. Below the lower limit there are multiple false peaks that were not repeatable between subsequent measurements. Between the upper and lower limits there was a large range where the same emission rates were repeatedly obtained from both defects, under a range of DLTS conditions. The Sb-vacancy and E-prime emission peaks observed by means of this method of peak splitting deviated by approximately 3% from the emission rates obtained with the subtraction of transient method. Splitting the peaks by means of inverse Laplace transform was observed to be limited to observing the emission rates, and did not provide reliable amplitudes.

Arrhenius plots for both defects were measured multiple times in the region of 188 K and 212 K. The measurements were done in 3 K intervals using both manual regularization parameters and the subtraction of transient method. Due to the nature of Laplace DLTS, it was not deemed reliable to obtain reliable emission rates from the peak splitting method when the peaks were very close together. This effect is seen in Figure 2 at 4.65/1000 $K^{-1}$ and 5.41/1000 $K^{-1}$ for the subtraction of transient method. The average energy obtained after 5 successive measurements for the Sb-vacancy was $0.370 \pm 0.005$ eV while the average activation energy for the E-prime was $0.375 \pm 0.005$ eV.

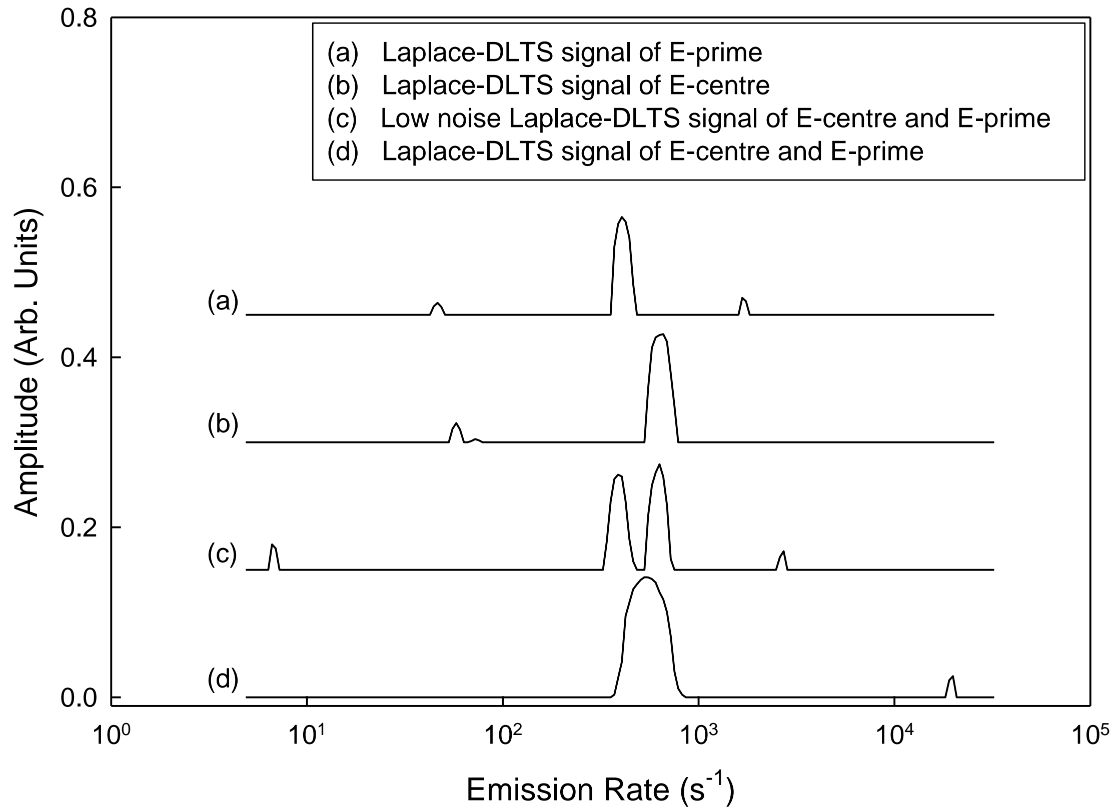


**Figure 1.** Laplace-DLTS spectra recorded at 203 K from a sample exposed at 270 K to alpha particles from an $^{241}$Am source for 2 hours. The Laplace-DLTS spectrum (d) is the general signal seen from measurements. Spectrum (c) is the same signal with manual regularization parameters combined with low noise measurements. The spectrum (b) was obtained after 1 hour annealing at 330 K which reveals only the Sb-vacancy peak. The spectrum (a) represents the E-prime and is obtained by subtracting the capacitance transient of (b) from the capacitance transient of (d).

DLTS probes depths of up to 2 μm below the junction of the Schottky diode. The alpha particles from the $Am^{241}$ source have energies of up to 5.4 MeV and easily penetrates depths much greater than this. SRIM simulations for these alpha particles show penetration depths of up to approximately 17 μm beneath the junction for Ge. It was therefore reasonable to assume a uniform distribution of vacancies introduced during irradiation. The samples used were uniformly doped with Sb, resulting in the expectation of uniform vacancy dopant pair distributions after irradiation. Depth profiles were obtained after irradiation at 270 K. The combined introduction of Sb-vacancy and E-prime was found to be uniformly distributed beneath the junction. The samples were annealed at 330 K for 1 hour to remove the E-prime defects. Depth profiles of the Sb-vacancy concentration was uniformly distributed beneath the junction as seen in Figure 3. As previously, the difference in capacitance transients was used to obtain the E-prime concentration depth profile. The E-prime was also uniformly distributed beneath the junction. The summation of the Sb-vacancy and E-prime depth profile concentrations resulted in the measurement of the combined measured concentration depth profile of both defects. This uniform distribution of both defects strongly suggests that their complex formations is the result of alpha particle irradiation.

It was not possible to experimentally obtain depth profiles of both defects using manual regularization parameters, as the error in the amplitudes of the peaks was too large.

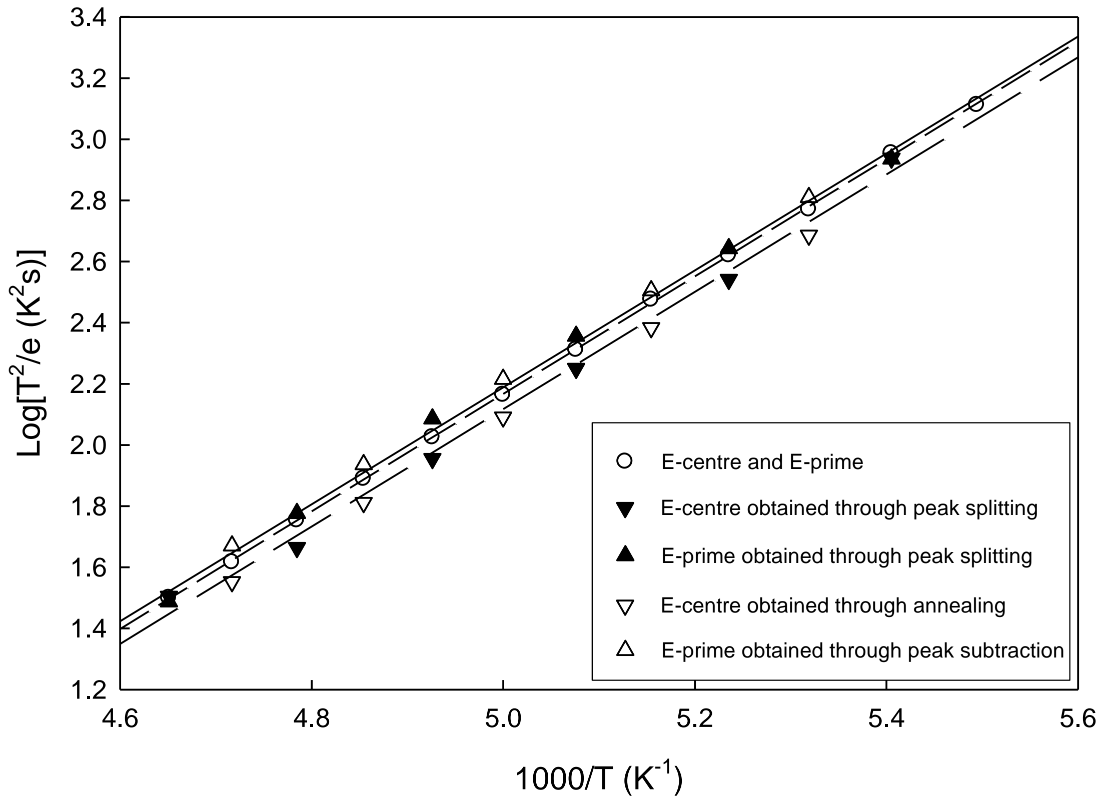


**Figure 2.** Arrhenius plots of traps introduced in n-type Ge by high energy alpha radiation from an $^{241}$Am source. The Sb-vacancy is represented by upside down triangles with the E-prime being represented by upright triangles. Solid symbols represent data obtained using the peak splitting method while empty symbols represent data from the subtraction of transient method. Every second data point has been omitted from both methods for the Sb-vacancy and E-prime for clarity due to the overlapping of data points. The Arrhenius plots obtained for the defects are represented by the best fit lines through the data. The short dashed line represents the plot obtained with both defects present in the sample. The line with longer dashes represents the Sb-vacancy complex and the solid line the E-prime complex.

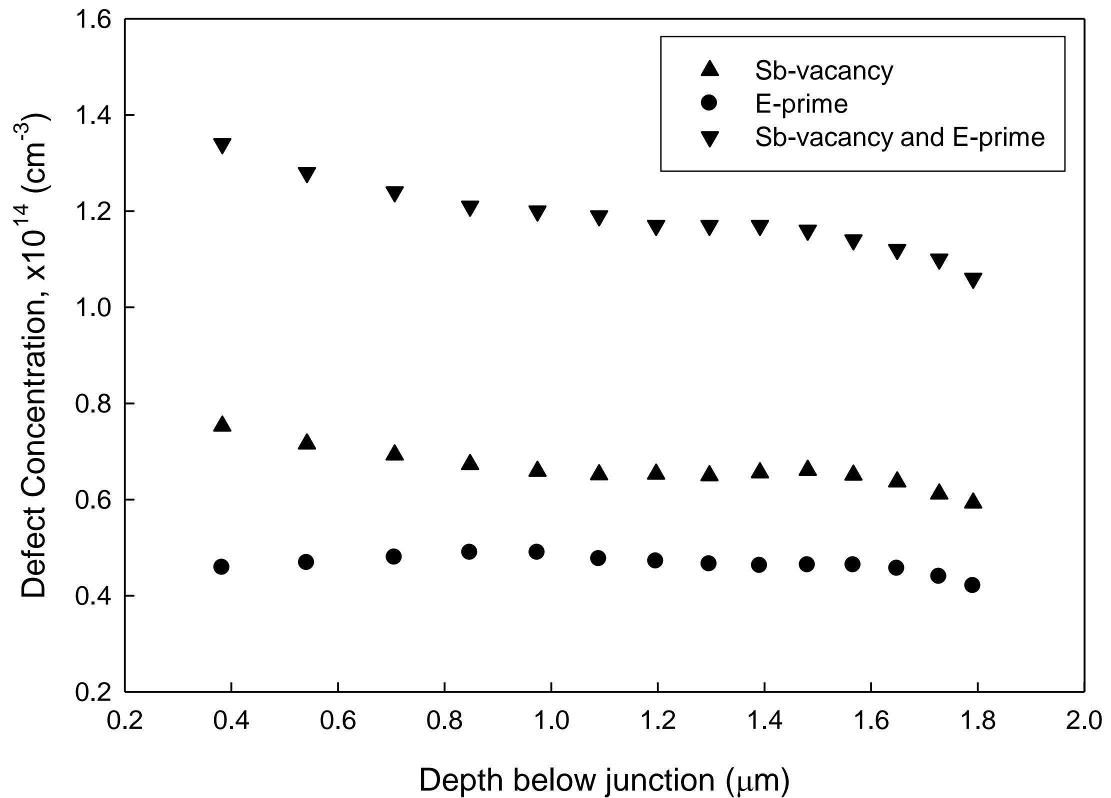


**Figure 3.** Depth profiles determined from L-DLTS of the combination of Sb-vacancy and E-prime after exposure to 1 hour alpha particle irradiation (upside down triangles). Depth profiles of the Sb-vacancy after 1 hour annealing at 330 K (upright triangles). E-prime depth profiles determined through subtraction of corresponding transients (circles).

## 4. Conclusion

We provide strong evidence that the room-temperature annealing component of the defect traditionally referred to as the E-center in Ge is a distinct defect. Using low-noise Laplace DLTS and manual tuning of the regularization parameter to split the peak due to the E-center into two peaks associated with the high and low temperature annealing components of the defect. The presence of two discrete emission components was further confirmed by annealing and subtraction studies that allowed the transients of the defects to be studied individually. Depth profiles using the subtraction of transient method revealed a uniform distribution of Sb-vacancy and E-prime defects beneath the junction. The subtraction of transient method and manual input of regularization parameters methods both yielded distinct activation energies for the defects: 0.370 ± 0.005 eV for the Sb-vacancy and 0.375 ± 0.005 eV for the E-prime. The uniform depth profiles suggests both defects are the result of alpha-particle radiation exposure. In a previous study, it was shown that the E-prime concentration induced by radiation was proportional to the concentration of the E-centres, therefore we expect the E-prime to be structurally related to the E-center [2]. We suggest the introduction is highly dependent on the concentration of Sb-vacancy already present in the system.

A possible structure for the E-prime would be the traditional Sb-vacancy with a close Ge self-interstitial. The proximity of the self-interstitial would explain why the defect anneals out so easily. While the fact that the Ge self-interstitial causes a small perturbation to the potential well due to the Sb-vacancy, explaining why the defects have similar emission.

**References**

[1] J. Fage-Pederson, A.N. Larsen, A. Mesli, Physical Review B 62.15 (2000) 10116-10125
[2] A.W. Barnard, W.E. Meyer, F.D. Auret, P.N.M. Ngoepe, S.M.M. Coelho, The Proceedings of the 60th Annual Conference of the South African Institute of Physics (SAIP2015) 8 – 13
[3] D.V. Lang, Journal of Applied Physics. 45.7 (1974) 3023
[4] L. Dobaczewski, P.Kaczor, I.D. Hawkins, A.R. Peaker, Journal of Applied Physics 76.1 (1994) 194
[5] A.A. Istratov, O.F. Vyvenko, H. Hieslmair, E.R. Weber, Measurement Science and Technology 9 (1998) 477
[6] S.M. Sze, N.G. Kwok K, Physics of Semiconductor Devices 3$^{Rd}$ Edition, (John Wiley & Sons Incorporated, 2006)

**Acknowledgements:**
This work is based on research supported by the National Research Foundation of South Africa, Grant Number 98961.

# Article 4

# Annealing of the Sb-vacancy and a closely related radiation induced defect in n-type germanium

Abraham W. Barnard, Walter E. Meyer and F. Danie Auret

Submitted to Proceedings of SACPM 2017 Elsevier

# Annealing of the Sb-vacancy and a closely related radiation induced defect in n-type germanium

**Abraham W. Barnard, Walter E. Meyer and F. Danie Auret**

Department of Physics, University of Pretoria, Private bag X20, Hatfield 0028, Pretoria, South Africa

E-mail: u10688112@tuks.co.za

**Abstract**. Deep level transient spectroscopy was used to study the defects induced by alpha-particle irradiation from an $Am^{241}$ source in antimony doped n-type germanium. Previous investigations of the well know Sb-vacancy defect have led to the discovery of a second defect with very similar emission properties, referred to as the E'. Although both defects have similar emission rates, they have very different annealing properties. In this study we further investigated these properties of the E' in Sb doped samples irradiated at 270 K with alpha particles from an $Am^{241}$ source. Laplace deep level transient spectroscopy was used to determine the concentration of each defect. An isothermal annealing study of the E' was carried out in the temperature range 300 K to 325 K in 5 K increments, while the Sb-vacancy was annealed out at 390 K onwards, long after the E' was completely annealed out. The annealing activation energy was determined through isothermal annealing profiles for both the Sb-Vacancy and the E' as 1.05 eV and 0.73 eV respectively with a prefactor of $2.05\times10^{9}$ $s^{-1}$ and $2.7\times10^{8}$ $s^{-1}$.

## 1. Introduction

Germanium (Ge) predicted in 1869 by Dmitri Mendeleev and discovered in 1886 by Clemens Winkler is known as the gateway material for semiconductor transistor and integrated circuit development. This was quickly overthrown by Si due to the excellent properties of $SiO_2$ which acts as an insulator for the formation of gates in MOSFETS. Ge does not easily form this oxide layer on its surface causing fabrication of technology required for Ge to be more complicated [1]. As semiconductor, Ge is mainly used as a detector material, highly sensitive to ionizing radiation, X-rays and gamma rays. The performance of the device is highly influenced by the fluence and time it is exposed to radiation [2].

The Sb-vacancy ($E_{0.37}$) is one of the fundamental point defects in Ge and is known to occur in large concentrations in Sb doped Ge after exposure to high energy particles (alpha particles, neutrons, electrons, etc.) [3]. The second defect currently identified as the E' has a similar energy level to that of the $E_{0.37}$ but has been observed to have different annealing properties. The E' has been found to experience annealing from temperatures as low as room temperature (300 K) while the $E_{0.37}$ starts annealing around 390 K. The introduction rate of the E' was found to be that of second order while $E_{0.37}$ was that of a first order. The E' is therefore dependent on the concentration of E' already present within the crystal lattice [4]. A possible theory that exists is that the E' consists of an $E_{0.37}$ with a Ge self-interstitial which gives the possibility of recombination during annealing.

Isothermal annealing is a technique that thermally removes radiation induced defects. During this process the sample undergoes thermal annealing at a set temperature for a fixed periods of time. This technique is used to determine both the period required to anneal a defect to a certain concentration at a set temperature and determining the activation energy for annealing. This activation energy will identify the mechanism according to which the defect anneals, i.e. complex dissociation, migration, recombination or complex formation during annealing [5,6].

## 2. Experimental details

The Ge wafer with <111> crystal orientation supplied by Umicore was determined to be doped uniformly with Sb with a concentration of $2\times10^{15}$ cm$^{-3}$. This wafer was cut into many smaller samples of 3 mm by 6 mm. The samples were degreased with trichloroethylene, isopropanol and methanol for 5 minutes each. They were then wet etched in a solution of hydrogen peroxide ($H_2O_2$) and deionized water in 1:5 ratio for 1 minute before being blown dry with nitrogen. The samples were mounted on a mounting plate and placed in a vacuum of $1\times10^{-6}$ mbar before resistively evaporating AuSb (0.6% Sb) ohmic on the back surface of the wafer. Thermal deposition occurred at a rate of 1 Å/s for a total thickness of approximately 1000 Å. After deposition the samples were annealed at 623 K to activate the ohmic contact. As preparation for the Schottky contacts, the samples were degreased and wet etched with the same chemicals and conditions as previously mentioned. The samples were mounted behind a metal contact mask and placed under a vacuum of $1\times10^{-6}$ mbar before depositing Pd Schottky barrier diodes (SBD) of 0.6 mm in diameter. Thermal deposition was done at a rate of 1 Å/s for a total thickness of approximately 1000 Å.

The samples were irradiated for 60 minutes with an $Am^{241}$ source at 270 K under a vacuum of $1\times10^{-3}$ mbar. Laplace DLTS with a sampling rate of 97 kHz, with 4000 samples, averaged 6000 times was performed at 203 K under a reverse bias of -2 V and filling pulse level of 0 V to observe the Sb-vacancy and E'. Both defects have similar emission rates, almost indistinguishable from each other except through annealing. The experiment was split into two parts: Firstly, the samples underwent isothermal annealing at temperatures ranging from 305 K to 325 K until stable concentrations were obtained. Then the annealed samples were subjected to another isothermal annealing process at temperatures ranging from 410 K to 435 K until approximately zero concentrations were reached.

## 3. Experimental results

The L-DLTS emission spectrum obtained was a single peak representing the concentration of both defects being observed. The peak can be observed to anneal out in two stages (see Figure 1), first annealing to a set concentration at 315 K and then to a relative zero concentration at 415 K. During isothermal annealing of a single defect, an exponential decay would be observed in the defect concentration $N_T$. This can be described as a first order annealing process and is written as:

$$N_T(t) = N_T(0)e^{-c(T)t} \quad (1)$$

where $N_T(0)$ is the initial concentration of the defect and $c(T)$ is the decay rate constant for a given temperature [6]. Since the Sb-vacancy and E' have indistinguishable L-DLTS signals, the initial concentration observed after irradiation at 270 K is that of the summation of the two defects. Taking this into consideration the concentration observed can be written as:

$$N_T(t) = N_{T1}(0)e^{-c_1(T)t} + N_{T2}(0)e^{-c_2(T)t} \quad (2)$$

where $N_{T1}(0)$ and $N_{T2}(0)$ represents the initial concentration of the Sb-vacancy and E' respectively with $c_1(T)$ and $c_2(T)$ their constant decay rates for set temperatures. The E' undergoes annealing at much lower temperatures than the Sb-vacancy (approximately 100 K difference for observable annealing), that the decay rate constant of the Sb-vacancy can be approximated to be zero ($c_1(T)$ = 0) at these temperatures. This simplifies Equation 2 to:

$$N_T(t) = N_{T1}(0) + N_{T2}(0)e^{-c_2(T)t} \quad (3)$$

Here only the concentration of the E' will change as a function of time in the observed temperature range.

The isothermal annealing of the E' was done across the temperature range 300 K to 325 K in 5 K steps. Each individual profile was made using 15 minute annealing steps. Since the sample anneals to a non-zero concentration in this temperature range, plotting the natural logarithm of the normalized concentration for a linear fit was not feasible. This is due to the error in approximating the set concentration of Sb-vacancy that was introduced into the system after irradiation. This problem was overcome by the use of the non-linear least-squares equation fitter supplied with SigmaPlot. A further advantage of this technique is that it correctly weighs the errors in the experimental data. For determining the decay rate constant for a set temperature of the E', the 'single, 3 parameter' exponential decay function was used, which is equivalent to Equation 3. The annealing activation energy was determined to be approximately 0.73 eV with a prefactor of $2.7\times10^{8}$ $s^{-1}$ for the E' (see Figure 3).

The samples used in the previous experiment were used again for the next annealing procedure where the annealing of the Sb-vacancy complex was investigated. These profiles were done over the temperature range of 410 K to 435 K in 5 K steps. 15 minute annealing intervals were used. Data was used only after the first annealing step to ensure that any remaining E' did not affect the annealing rate. Since it was just a single defect being observed, the natural logarithm of the normalized concentration of the isothermal annealing profiles as a function of time would give a linear profile (see Figure 2). The activation energy was determined to be approximately 1.05 eV with a prefactor of $2.05\times10^{9}$ $s^{-1}$.

.

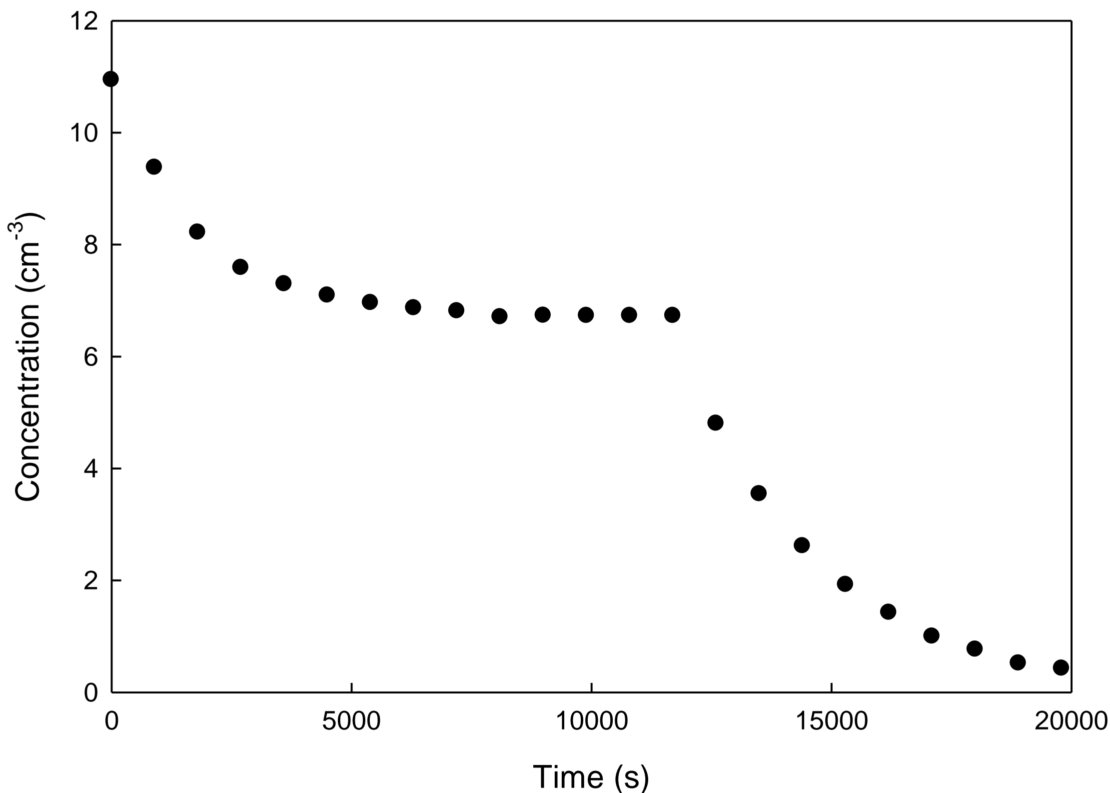


**Figure 1.** Annealing of a sample irradiated at 270 K for 60 minutes with an $Am^{241}$ source. The sample underwent successive isothermal annealing at 315 K till a relatively stable concentration was reached. It then underwent another successive isothermal annealing at 415 K till a relatively "Zero" concentration was achieved.

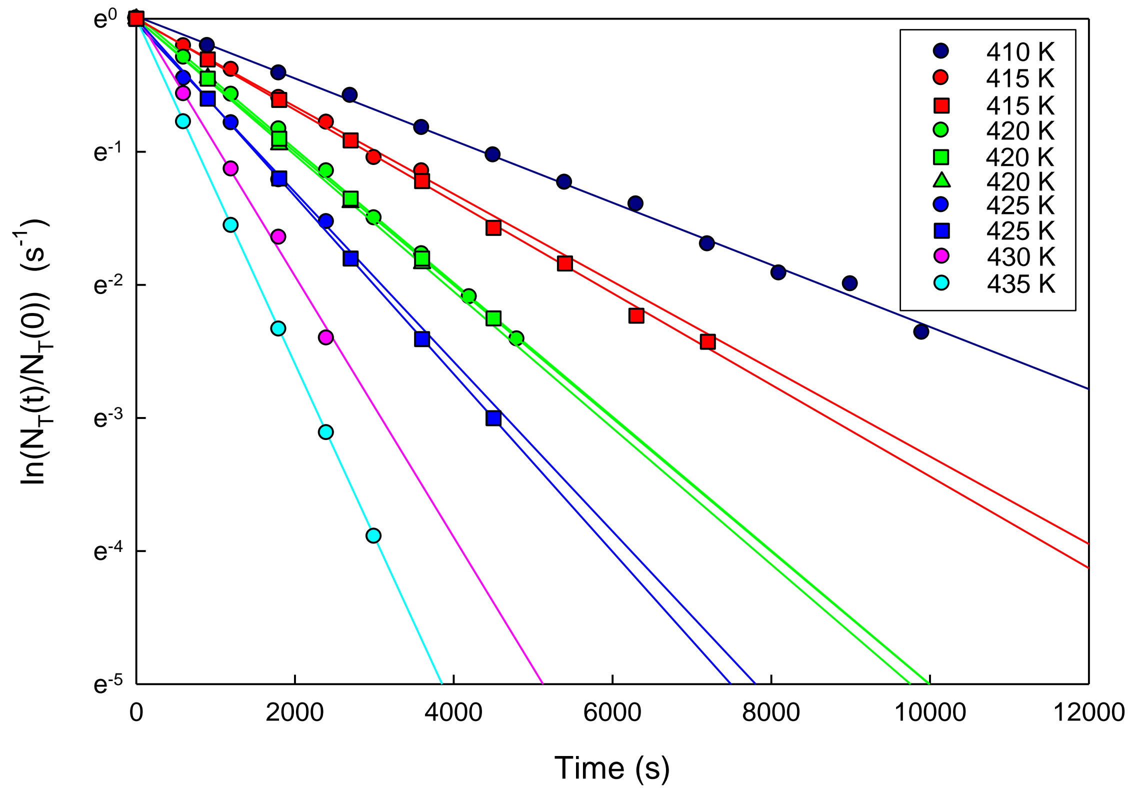


**Figure 2.** Semi-logarithmic plot of the normalized isothermal concentration annealing profiles of the Sb-vacancy at different temperatures.

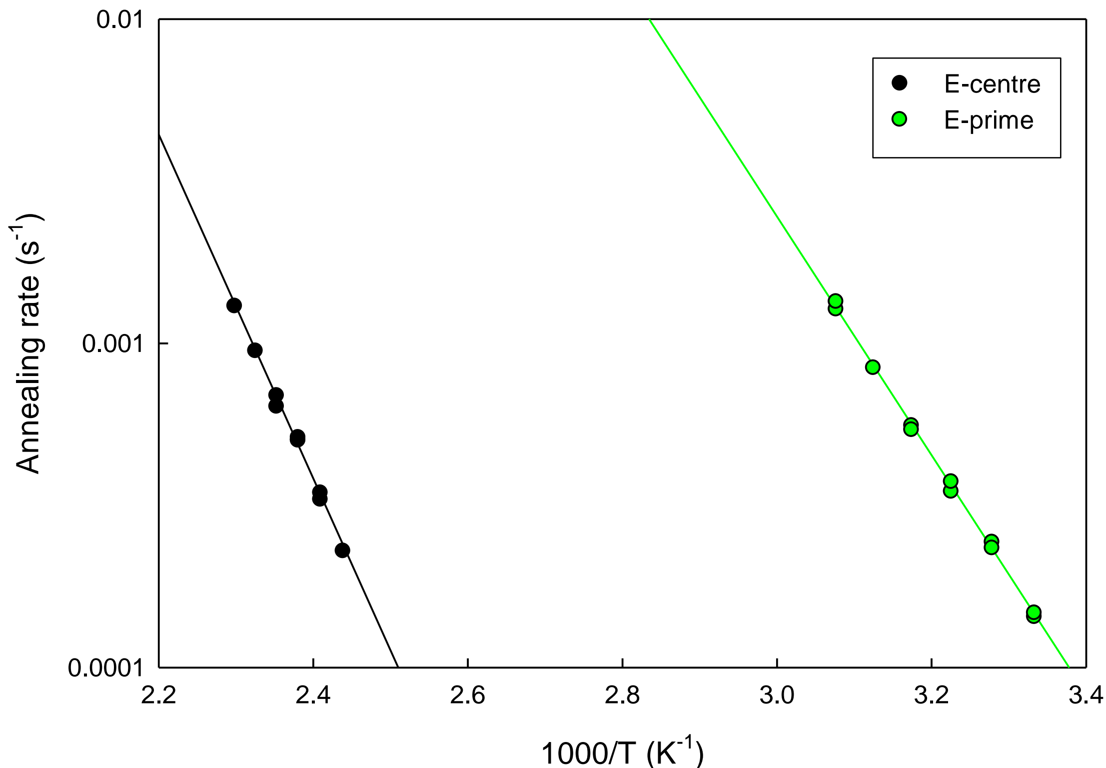


**Figure 3.** Arrhenius of the annealing activation energy of the Sb-vacancy and E’ obtained from multiple isothermal annealing profiles.

## 4. Summary and conclusion

The annealing activation energies for the Sb-vacancy and E’ were 1.05 eV and 0.73 eV respectively with a prefactor of $2.05\times10^{9}$ $s^{-1}$ and $2.7\times10^{8}$ $s^{-1}$. The frequency factor of the two defects indicate the annealing processes were of similar nature, however the lower frequency factor of the E’ indicates that the process according to which it anneals occurs with a significantly lower attempt frequency. The prefactor of the Sb-vacancy suggests that the defects anneals by dissociation of the vacancy. A possible theory to explain this is that the E’ is a Ge interstitial close to the Sb-vacancy point defect that would allow the defect to anneal out with lower energy, but with a lower attempt frequency.

## 5. Acknowledgments

This work is based up on research supported by the National Research Foundation (NRF). Any opinion findings and conclusions or recommendations expressed in this material are those of the author(s) and therefore the NRF does not accept any liability regard there to. The Laplace DLTS software and hardware used here was received from L. Dobaczeweski (Institute of physics, Polish Academy of Science) and A. R. Peaker (Center for Electronic Materials Devices and Nano-structures, University of Manchester.

**References**

[1] Claeys, C. and Simoen, E. (2011). *Germanium-Based Technologies*. 1st ed. Amsterdam: Elsevier Science, pp.1-5.

[2] Schlesinger, T. (1995). *Semiconductors for room temperature nuclear detector applications*. 1st ed. San Diego [u.a.]: Acad. Press, pp.23-25.

[3] Fage-Pedersen, J., Larsen, A. and Mesli, A. (2000). Irradiation-induced defects in Ge studied by transient spectroscopies. *Physical Review B*, 62(15), pp.10116-10125.

[4] Barnard, A., Meyer, W., Auret, F., Ngoepe, P. and Coelho, S. (2015). Investigation of the introduction and annealing behaviour of the donor-vacancy complex in alpha-particle irradiated germanium. *Proceedings of SAIP2015*.

[5] Sumino, K. (1990). *Defect control in semiconductors*. 1st ed. Amsterdam: North-Holland, pp.1423-1429.

[6] Bourgoin, J. and Lannoo, M. (1983). *Point Defects in Semiconductors II*. 1st ed. Berlin Heidelberg New York: Springer-Verlag, pp.247-270.

# 5 Conclusion

In this dissertation, it has been shown that the previously observed E centre defect in Ge consists of two distinct defects: one corresponding to the well categorized Sb-vacancy defect and the other to a defect that anneals out at room temperature is referred to as the E'. Special techniques have been developed to distinguish between the two defects and categorize their properties. In this chapter the results obtained in this dissertation are summarized and suggestions for future work are discussed.

The data obtained in this dissertation is summarized in Table 5.1.

## 5.1 Summary

It was shown that the defect traditionally identified as the E-centre consists of two distinct defects with similar emission rates almost indistinguishable from each other even through L-DLTS. The properties of the defects that best distinguish them are the introduction and annealing kinetics. The peak observed in both conventional and L-DLTS annealed in two stages. The first annealing stage was observed at temperatures as low as 300 K and was referred to as the E' defect. The second annealing stage was observed from 390 K onwards and was identified to be the defect which is commonly referred to as the E-centre. The annealing activation energies of the two defects were consistent with the observed temperature ranges. However, as similar frequency factor was obtained for both defects, indicating that their annealing mechanisms were of similar nature, and consistent with annealing by means of dissociation. This agrees with the theory that the E-centre is a Sb-vacancy pair and the vacancy anneals out by means of dissociation. A possible theory we suggest is that the E' is of similar nature but with the addition of a Ge interstitial.

The E-centre was found to be introduced linearly as a function of time under a constant fluence of alpha-particle irradiation. However, the E' was found to be introduced quadratically as a function of time under the same constant fluence. The E-centre introduction kinetics is consistent with the formation of Sb-vacancy complexes, while the introduction kinetics of the E' suggest that the formation of the E' is influenced by the presence of another radiation induced defect. However, it is still uncertain which introduction kinetics the E' follows. The extremes of the introduction profile will need to be tested to see if the E' uses the E-centre as a catalyst or if a third unobservable defect is involved during irradiation and consumed by the E' during annealing. The profiles obtained in Article 1 suggest the E' uses the E-centre as a catalyst during

irradiation, which contradicts the theory of the E’ being a Sb-vacancy complex with a Ge interstitial as no E-centre was consumed during the annealing of the E’.

**Table 5.1: Summary of electrical properties obtained through experimentation.**

| | E-centre | E’ | E-centre + E’ |
|---|---|---|---|
| $\boldsymbol{Annealing\ range\ (K)}$ | $\gtrapprox 390\ \mathrm{K}$ | $\gtrapprox 300\ \mathrm{K}$ | |
| $\boldsymbol{Introduction\ kinetics}$ | $Linear$ | $Quadratic$ | $Quadratic$ |
| $\boldsymbol{Depth\ profile}$ | $Uniform$ | $Uniform$ | $Uniform$ |
| $\boldsymbol{Effect\ of\ bias\ annealing}$ | $Decrease\ in\ annealing\ rate$ | $Decrease\ in\ annealing\ rate$ | |
| $\boldsymbol{Enthalpy\ \Delta E_{ne}\ (eV)}$ | $0.370 \pm 0.005$ | $0.375 \pm 0.005$ | |
| $\boldsymbol{Apparent\ capture\ cross\ section\ \sigma_a\ (cm^2)}$ | $7.9 \times 10^{-15}$ | $6.2 \times 10^{-15}$ | |
| $\boldsymbol{True\ capture\ cross-section\ at\ T \rightarrow\ \sigma_{n0}\ (cm^2)}$ | $2.0 \times 10^{-16} \rightarrow 2.5 \times 10^{-16}$ | $1.3 \times 10^{-14} \rightarrow 1.0 \times 10^{-12}$ | $4.5 \times 10^{-16} \rightarrow 1.5 \times 10^{-15}$ |
| $\boldsymbol{True\ capture\ cross\ section\ from\ 196\ K\ to\ 212\ K\ \sigma_n\ (cm^2)}$ | $6.2 \times 10^{-19} \rightarrow 9.6 \times 10^{-19}$ | $4.4 \times 10^{-19} \rightarrow 1.1 \times 10^{-18}$ | $5.6 \times 10^{-19} \rightarrow 9.7 \times 10^{-19}$ |
| $\boldsymbol{Capture\ barrier\ height\ (eV)}$ | 0.043 | 0.092 | 0.053 |
| $\boldsymbol{Annealing\ activation\ energy\ \Delta E_a\ (eV)}$ | 1.05 | 0.73 | |
| $\boldsymbol{Annealing\ frequency\ factor\ c_0\ (s^{-1})}$ | $2.05 \times 10^{9}$ | $2.70 \times 10^{8}$ | |

Although the E-centre and E' were found to have almost indistinguishable positions in the band gap, their true capture cross-sections varied enough to distinguish them from each other. The true capture cross-sections suggest that both defects have a Coulomb potential and are therefore are likely to be donors.

After irradiation, the depth profiles of the E-centre and E' were found to be approximately constant with depth beneath the junction. However, during experimentation it was observed that the E' experienced reduced annealing when the diode was placed under a reverse bias. The reduction of the annealing rate under reverse was assumed to be due to a charge state of the defect. The isothermal annealing profile under a reverse bias was expected to produce a step where the defect crosses the Fermi-level. This was not observed, suggesting it might be due to different mechanisms. Further experimentation with different applied biases during annealing is required to fully understand this phenomena.

## 5.2 Future research

There is still a significant amount of work that needs to be done to fully characterize the electrical properties of the Sb-vacancy related E' in Ge.

- The activation annealing energy of the E' needs to be fully researched using subtraction of transient method with the isothermal annealing profiles.
- The effect of bias on annealing of the Sb-vancay and its relative E' needs further investigation. The defects need to be annealed under different biases with depth profiles done before and after the annealing to see which region under the junction is affected by this effect. The bias dependent annealing should also be investigated further through isochronal and isotermal annealing, and the effect on activation energy of the annealing needs to be investigated.
- The effect of bias on the introduction of the Sb-vacancy and its relative E' in Ge needs to be investigated. Depth profiles need to be done to see if the introduction rate is influenced by bias.
- The introduction profile for the E' needs to be investigated by means of low temperature (273 K) irradiation.
- The presence of a similar defect in Si, and its relationship with the Sb-vacancy related E' in Ge should be investigated.
- The reduction in the DLTS signal after long filling pulse lenghts for both the E and E' should be investigated. This experiment will have to be repeated on different equipment to eliminate possible effects due to overshoot and investigate the posibility of negative-U effects.

# 6 REFERENCES

Barron, A. and Smith, C. (2008). *Crystal structure*. 1st ed. [ebook] p.11. Available at: http://cnx.org/contents/6Q1RYWaw@10/Crystal-Structure [Accessed 16 Oct. 2016].

Bauerlein, R. (1962). *Radiation Damage in Solids (D. S. Billington, ed)*. 1st ed. New York: Academic Press, p.358.

Bourgoin, J. and Lannoo, M. (1983). *Point Defects in Semiconductors II Experimental Aspects*. 1st ed. Berlin: Springer-Verlag, pp.247-268.

Claeys, C. and Simoen, E. (2007). *Germanium-based technologies*. 1st ed. Amsterdam: Elsevier, pp.1-5.

de Juan, F., Cortijo, A. and Vozmediano, M. (2010). Dislocations and torsion in graphene and related systems. *Nuclear Physics B*, 828(3), pp.625-637.

Dobaczewski, L., Kaczor, P., Hawkins, I. and Peaker, A. (1994). Laplace transform deep-level transient spectroscopic studies of defects in semiconductors. *Journal of Applied Physics*, 76(1), pp.194-198.

Dobaczewski, L., Peaker, A. and Bonde Nielsen, K. (2004). Laplace-transform deep-level spectroscopy: The technique and its applications to the study of point defects in semiconductors. *Journal of Applied Physics*, 96(9), pp.4689-4728.

Fage-Pedersen, J., Larsen, A. and Mesli, A. (2000). Irradiation-induced defects in Ge studied by transient spectroscopies. *Physical Review B*, 62(15), pp.10116-10125.

Hartmut, F. and Sadrozinski, W. (2007). *Extraction of Doping Density Distributions from C-V Curves*. 1st ed. [ebook] California Santa Cruz, Santa Cruz: SCIPP. Available at: http://scipp.ucsc.edu/papers/07_06.pdf [Accessed 17 Oct. 2016].

Holmström, E., Nordlund, K. and Kuronen, A. (2010). Threshold defect production in germanium determined by density functional theory molecular dynamics simulations. *Physica Scripta*, 81(3), p.035601.

Iniewski, K. (2011). *Radiation effects in semiconductors*. 1st ed. Boca Raton: CRC Press, pp.3-6.

Kinchin, G. and Pease, R. (1955). The Displacement of Atoms in Solids by Radiation. *Reports on Progress in Physics*, 18(1), pp.1-51.

Kopeliovich, D. (2012). *Imperfections of crystal structure [SubsTech]*. [online] Substech.com. Available at: http://www.substech.com/dokuwiki/doku.php?id=imperfections_of_crystal_structure [Accessed 12 Aug. 2016].

Kosyachenko, L. (2015). *Solar Cells - New Approaches and Reviews*. 1st ed. InTech, pp.199-220.

Laidler, K. (1987). *Chemical kinetics*. 3rd ed. Harper & Row, p.42.

Lang, D. (1974). Deep-level transient spectroscopy: A new method to characterize traps in semiconductors. *Journal of Applied Physics*, 45(7), pp.3023-3032.

Lang, D. (1979). *Thermally stimulated relaxation in solids*. 1st ed. Berlin: Springer Verlag, p.93.

Lannoo, M. and Bourgoin, J. (1981). *Point Defects in Semiconductors I Theoretical Aspects*. 1st ed. Berlin: Springer-Verlag, pp.1-4.

Markevich, A.V. et al. "Phonon-Assisted Changes In Charge States Of Deep Level Defects In Germanium". *Physica B: Condensed Matter* 376-377 (2006): 61-65. Web.

Mayer, J. (1970). *"Ion implantation in semiconductors, silicon and germanium"*. 1st ed. New York: Academic Press, pp.65-73.

Meroli, S. (2012). Radiation damage for silicon detectors. [Blog] *Science at Cern*. Available at: http://meroli.web.cern.ch/meroli/lecture_radiation_damage_silicon_detector.html [Accessed 15 Oct. 2016].

Mikelsen, M., Monakhov, E., Alfieri, G., Avset, B. and Svensson, B. (2005). Kinetics of divacancy annealing and divacancy-oxygen formation in oxygen-enriched high-purity silicon. *Physical Review B*, 72(19).

Montanari, S. (2005). Fabrication and characterization of planar Gunn diodes for Monolithic Microwave Integrated Circuits. Ph.D. Research Center Juelich.

Moore, W. (1987). *Physical chemistry*. 1st ed. Harlow (Essex, GB): Longman Scientific and technical, pp.546-555.

Moskalyk, R. (2004). Review of germanium processing worldwide. *Minerals Engineering*, 17(3), pp.393-402.

Nishinaga, T. (2015). *Handbook of crystal growth*. 2nd ed. Amsterdam, the Netherlands: Elsevier, p.21.

Nyamhere, C. (2009). *Characterization of process and radiation induced defects in Si and Ge using conventional deep level transient spectroscopy (DLTS) and Laplace-DLTS*. 1st ed. Pretoria.

Palmer, D. (2014). *Properties of Diamond, Silicon and Germanium*. [online] Semiconductors.co.uk. Available at: http://www.semiconductors.co.uk/propiviv5431.htm [Accessed 9 Sep. 2016].

Patterson, J. and Bailey, B. (2010). *Solid-state physics*. 1st ed. Berlin: Springer.

Poole, C. (2004). *Encyclopedic dictionary of condensed matter physics*. 1st ed. Amsterdam: Elsevier.

Rhoderick, E. and Williams, R. (1988). *Metal-semiconductor contacts*. 1st ed. Oxford [England]: Clarendon Press.

Rosso, D. (2016). *Global Semiconductor Sales Top $335 Billion in 2015*. [online] Semiconductor Industry Association. Available at: http://www.semiconductors.org/news/2016/02/01/global_sales_report_2015/global_semiconductor_sales_top_335_billion_in_2015// [Accessed 8 Sep. 2016].

Scheel, H., Capper, P. and Rudolph, P. (2011). *Crystal growth technology*. 1st ed. Weinheim: John Wiley & Sons, pp.177-179.

Schroder, D. (2006). *Semiconductor material and device characterization*. 3rd ed. New York: Wiley, pp.127-131.

Shockley, W. and Read, W. (1952). Statistics of the Recombinations of Holes and Electrons. *Physical Review*, 87(5), pp.835-842.

SigmaPlot. (1996). Systat Software Inc.

Sigmund, P. (2006). *Particle Penetration and Radiation Effects*. 1st ed. Berlin: Springer-Verlag.

Silvaco (2014). *Simulations of Deep-Level Transient Spectroscopy for 4H-SiC*. [online] Available at: http://www.silvaco.com/tech_lib_TCAD/simulationstandard/2014/apr_may_jun/a2/a2.html [Accessed 9 Oct. 2016].

Stewart, D. (1996). *Silicon - expert written, user friendly element information*. [online] Chemicool.com. Available at: http://www.chemicool.com/elements/silicon.html [Accessed 12 Oct. 2016].

Streetman, B. (1990). *Solid State Electronic Devices*. 1st ed. Englewood Cliffs (New Jersey): Prentice-Hall, pp.149-160.

Sze, S. and Kwong, K. (2006). *Semiconductor devices, physics and technology*. 3rd ed. New York: Wiley, pp.134-196.

Williams, D. and Carter, C. (2009). *Transmission Electron Microscopy*. 1st ed. New York: Springer, pp.419-439.

Winkler, C. (1886). Discovery of a New Element *Nature*, 33(853), pp.418-418.

Wei, J. (2015). Deep Level Transient Spectroscopy Using HF2LI Lock-in Amplifier. [Blog] *Zhinst*. Available at: http://www.zhinst.com/blogs/jamesw/deep-level-transient-spectroscopy/ [Accessed 18 Aug. 2016].

Ziegler, J., Biersack, J. and Littmark, U. (1983). The Stopping and Range of Ions in Matter. New York: Pergamon.

Zhao, J., Schlesinger, T. and Milnes, A. (1987). Determination of carrier capture cross sections of traps by deep level transient spectroscopy of semiconductors. *Journal of Applied Physics*, 62(7), pp.2865-2870.

Zohta, Y. and Watanabe, M. (1982). On the determination of the spatial distribution of deep centers in semiconducting thin films from capacitance transient spectroscopy. *Journal of Applied Physics*, 53(3), pp.1809-1811.